Microcantilever-based studies of bio/chemical systems

Jensenius, Henriette

Publication date:
2002

Document Version
Publisher's PDF, also known as Version of record

Microcantilever-based studies of bio/chemical systems

Ph. D. Thesis

Henriette Jensenius [1]

15 March 2002

[1]Mikroelektronik Centret, Technical University of Denmark, Building 345 east, 2800 Lyngby, Denmark.

Preface

The present thesis is written as part of the requirements to be fulfilled in order to obtain the Ph. D. degree at the Technical University of Denmark. The work has been carried out at the Microelectronics Center (MIC) in the period January 1999 to February 2002.

The Ph. D. Project has been carried out as part of the Bioprobe project under the supervision of project leader Dr. Anja Boisen and co-supervised by Dr. François Grey, vicedirector of MIC.

The starting point of this work was a microcantilever chip with two cantilevers, each with an integrated piezoresistor: The Biosensor chip, developed by Anja Boisen [1] and Jacob Thaysen [2]. I made initial tests of the function of this chip using a laser to heat one of the two microcantilevers on the chip.

The next goal was to develop selective sensitivity of one of the microcantilevers on the chip. A technique was developed for coating only one of the two closely spaced cantilevers with a polymer. Humidity and the evaporating gases from droplets of different alcohols were measured. A model was developed that could explain the evaporation measurements quantitatively. Masters student Louise N. Christensen pursued the study of the polymer response and the performance of the chip under my supervision.

In a liquid environment, it was expected that the combination of piezoresistive readout and an integrated reference cantilever would have significant advantages compared to the conventional optical readout scheme. However, a solution had to be found for protecting the exposed gold leads on the body of the chip. An open flow system, where the flow was maintained by two pumps, was developed.

The first Biosensor experiments in the flow cell, done together with Rodolphe Marie, were the immobilisation of thiol modified single stranded DNA oligos onto a thin layer of gold evaporated onto one side of one of the cantilevers. Rodolphe continued this work investigating the immobilisation by fluorescence methods and obtained adsorption and desorption rate constants for the thiol modified oligos on the gold coated cantilever.

The possibilities within protein based detection were investigated. Work was done to develop a bacteria immunoassay - an E. coli sensor. Under my supervison, masters student Lars H. Veje worked on fluorescence verification of the biochemical system and development of the Biosensor experiments.

One of the critical points in a microcantilever based sensor is the behaviour of the bio molecules on the surface of the cantilever. The atomic force microscope (AFM) is an instrument exceptionally well suited for studying biomolecular behaviour on surfaces. The use of carbon nanotubes as probe tips in AFM investigations of single biomolecules was explored and is described in the second part of the thesis.

The AFM work was carried out at the University of Leiden, Institute of physics (LION), the Netherlands, while I was a visitor of Prof. Thomas Schmidt, Department of Biophysics, Huygens Laboratory and Dr. Ir. Tjerk Oosterkamp, Department of Interface Physics, Kamerlingh Onnes Laboratory.

Model biological samples were imaged in buffer in collaboration with Ph. D. students Dionne C. G. Klein and Matthew Osbourn. I then started to work on the assembly of carbon nanotube probes (CNTs) and pursued this work with Dr. Suzanne P. Jarvis in Tsukuba, Japan. While in Tsukuba, I investigated solvation layers using quartz tuning forks with CNT tips together with Dr. Masami Kageshima. On returning from Japan I imaged IgG antibodies. I obtained preliminary images of IgG on mica with a CNT and on gold with a conventional SiN probe.

Acknowledgements

I would like to thank

My supervisor Anja Boisen for her visionary project, developing the microelectromechanical biosensor, and for her supervision, co-supervisor Francois Grey for inspiration and Erik Thomsen for his support at the crucial initial writing stage.

My students Louise N. Christensen and Lars Helt Veje who contributed hard work to this thesis and have been a source of stimulation.

The Bioprobe group with a special thanks to the developers and processors of the unique Bioprobe without whom my work would not exist and to Rodolphe Marie for the collaboration on immobilisation of DNA oligos.

Ole Hansen for inspiring ideas and helpful discussions especially about the evaporation model. Claus Bo Vöge Christiansen for biochemistry discussions, the helpfulness of countless members of the former BCMS group and in general the stimulation of the interdisciplinary environment at MIC.

For inspiring interactions with our potential industrial collaborators.

The highly skilled and always helpful staffs of the black and white workshops who transformed many scribbles and half ideas into functioning devices. The staff of the administration, for much paperwork and technicalities barely touching down on my desk.

I would like to thank Thomas Schmidt, Tjerk Oosterkamp and the AFM team at the Leiden Institute of Physics for a warm welcome and a highly stimulating stay. Especially, Tjerk for also supporting my visit to Suzanne Jarvis in Tsukuba, Japan and Suzi and Masami Kageshima, for making my stay a very rewarding and big experience. Here, I wish to thank Anja again, for the full support for my Dutch adventure.

My friends, my family and my roommates, in the collective with the most beautiful view, for being around and putting up with my moods and my absence.

Martin.

Contents

Chapter 1

Introduction

Problems worthy
of attack
prove their worth
by hitting back

Grooks, Piet Hein

This thesis addresses challenges at the intersection between micro-, nano- and bio-technology.

The main topic is the development of a microscopic and ultra sensitive biosensor, which is cheap to produce, simple and low cost in use and a versatile platform for detection ranging from temperature and volatile gases to highly specific detection of bacteria and genes. Schematically, a microelectromechanical biosensor can be seen as a chemical reaction (for example the binding of molecules to a surface) generating a mechanical response (in this case a bending of the cantilever) that is recorded electrically (here by the change of resistance in a piezoresistor).

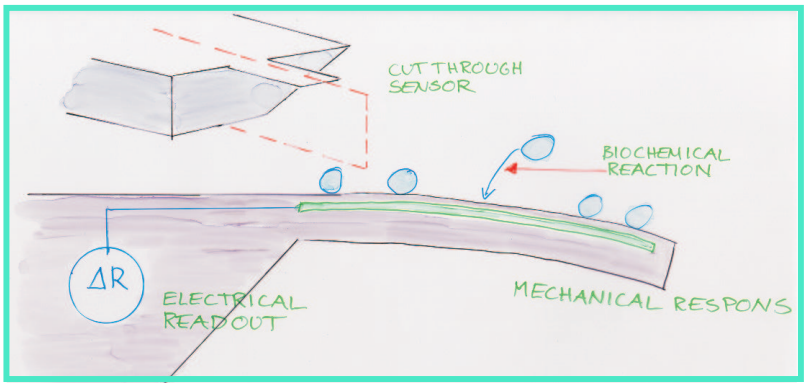

Figure 1.1: Schematic function of a microelectromechanical biosensor

In order to optimise the sensitivity of cantilever-based biosensors, ultimately a molecular scale understanding of the binding and ordering of the detector molecules on different surfaces is desired. The atomic force microscope (AFM) [3] is an ideal tool for such investigations because the molecules can be studied in varying buffers and on different surfaces. The second part of this thesis pursues nanomechanical developments in AFM and bioimaging with the AFM using carbon nanotube probes are investigated.

The two parts of this thesis further have in common that they exploit the mechanical properties of a very flexible, microscopic cantilever beam. At microscopic dimensions a silicon cantilever beam is both very soft and has high resonance frequencies. Typical dimensions of such a cantilever is a few hundred micrometers in length, 50-100 micrometers in width and the thickness can be less than a micrometer. The cantilever beams are most often fabricated in silicon or silicon nitride using lithographic and micro machining techniques originally developed for microelectronics [4].

The widespread interest and availability of microcantilevers is largely a consequence of their use for imaging with AFM. In AFM a very sharp tip at the end of the cantilever is scanned over a surface. The interaction between the tip and the surface is felt by the motion of the cantilever and a topographic image can be obtained. Utilising the surface of the cantilever itself as the functional element, the cantilever can be applied as a sensor and the collective effect of surface phenomena can be studied.

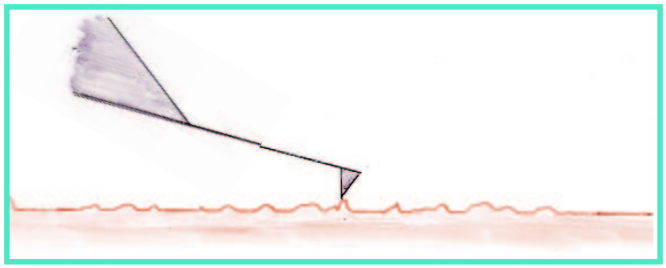

Figure 1.2: Principle of the AFM

When the cantilever is used as a sensor the mechanical system is greatly simplified, as there is no scanning involved, no tip fabrication is required, and no positioning relative to a surface is needed, the active surface being the cantilever itself.

1.1 Microcantilever based sensors

The step from imaging to exploiting the chemical sensor potential of the microcantilever came in 1994 where Gimzewski and colleagues from IBM, Rüschlikon,

published a paper on detection of the heat produced by the catalytic conversion of H_2 and O_2 to H_2O over a platinum coated cantilever surface [5]. The heat detection sensitivity was estimated to be in the pJ range. This was the beginning of a small avalanche of publications on different applications of microcantilever based sensors from laboratories on both sides of the Atlantic, notably from T. Thundat and coworkers at Oak Ridge National laboratories [6–9], J. R. Barnes and colleagues at Cambridge University [10, 11] and H-J Butt and R. Raiteri, then at the Max-Plank institute of Biophysics in Frankfurt [12, 13].

A Ph. D. thesis by A. Moulin, exploring the applications from temperature sensor to the differential detection of low density lipoproteins and an oxidised form of the same molecule, came out in 1998.

Rüdiger Berger and colleagues at IBM, Rüschlikon investigated many effects including work on alkane thiol adsorption on gold [14] and thermogravimetry using piezoresistive cantilevers [15]. Developments in the direction of multicantilever sensors followed [16].

At ETH in Zürich H. Baltes group has been working on a multifunctional sensor with integrated CMOS [17, 18]. D. R. Baselt et al. at Naval Research Laboratories have proposed a sensor base on piezoresistive readout with a magnetic enhancement mechanism [19].

M. D. Antonik et al., at Johns Hopkins University School of Medicine, showed that cells living, and dying, on a cantilever could be used as environmental detectors [20].

Recently, it has been reported that in gene detection it is possible to detect variations in hybridising DNA strands down to the single base-pair level [21, 22] and that antigens can be detected at clinically relevant levels [23].

1.1.1 Operation modes

Both as a sensor device and as an imaging tool the cantilever can be operated in basically two different ways: a 'static mode' where the static bending of the cantilever is observed and a dynamic mode where the quantities measured relate to the vibration properties, for example changes in the resonant frequency.

The first mode depends on the stress developed on the surface of the cantilever. If there is a difference in the stress developed on the two sides the cantilever will bend in such a way that the stresses are balanced by the bending.

A special case of differential stress development is the heat sensitivity of a bimetallic cantilever, where a difference in thermal expansion coefficient of two materials will cause the cantilever to bend [11].

Another example is the stress induced by the preferential adsorption of molecules on one side of the cantilever. The adsorption/binding of molecules to one side of the cantilever gives rise to a change in free energy [24–27], which is balanced by the stress in the cantilever. The static mode is preferred in liquid environments,

because it is not sensitive to the damping. The sensitivity is predicted to be 10^{-4} N/m [28].

In the dynamic mode, the resonant frequency is proportional to the square root of the spring constant k over the mass m: $f_0 \propto \sqrt{k/m}$. A mass change can thus be detected by a change in resonant frequency where $\Delta m \propto k(1/\sqrt{f_1^2} - 1/\sqrt{f_0^2})$, when the spring constant does not change. This principle was demonstrated using polystyrene beads to have sub ng resolution [29] also in liquid [30]. It was used to detect for example the adsorption of mercury with pg sensitivity [31] and dehydration of copper sulphate crystals [15]. Atto gram sensitivities are now expected in connection with bacteria detection [32]. The sharpness of the resonance peak, and thus the resolution of the determination of the resonance frequency, is given by the quality factor or Q-factor. Measuring variations in Q-factor, amplitude and phase lag, the damping of the cantilever motion can be studied. This can for example give information about the viscosity of the medium surrounding the cantilever [33].

1.1.2 Detection

Essential to any microcantilever based sensing is the detection of the mechanical response. The most wide spread detection technique, used in most commercial AFMs, is the optical leverage method: A laser beam is reflected of the end of the cantilever and the movement of the reflected beam is detected by a photosensitive device [34] (figure 1.3, a). In the microelectromechanical biosensor, the

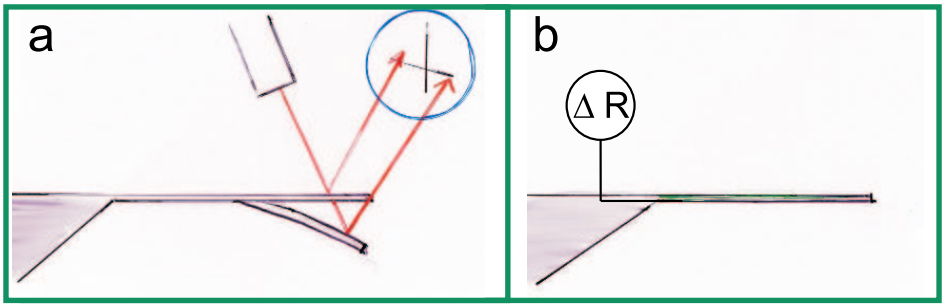

Figure 1.3: Two principles of detection of microcantilever deflection: Optical leverage (a), integrated piezoresitive readout (b)

stress change in a piezoresistor integrated in the microcantilevers, gives the signal (figure 1.3, b). This can be directly related to the change in surface stress on the cantilever [35]. Though intimately connected the relation between the surface stress and the surface energy is less straightforward [25] and it is complicated to distinguish the different contributions from molecular reactions on the surface, which include binding energy, electrostatic interactions, entropy change and intermolecular interactions. On the other hand, with the Biosensor we can directly

measure the change in surfaces stress, both the stress generated in bending and in stretching and thus in principle have a sensitive tool to interrogate these complex collective phenomena.

1.2 This project

1.2.1 Aims

The aims of this project are to explore and demonstrate different applications of the Biosensor and obtain understanding of the possibilities and limitations.

The applications start with laser power measurements in air and continue with the development of a chip sensitive to gasses.

A crucial step is to make the sensor liquid compatible, which means finding a way to protect electrical leads on the sensor and design a flow system so measurements can be made in changing solutions.

To arrive at a Biosensor the first task is to understand the necessary steps to make it functional and to choose systems to work with. For each system immobilisation, localisation and functionality were evaluated on a global scale.

Of course the ultimate goal is to reach the point where the stress development on the cantilever, due to specific adsorption of biomolecules, could be measured.

Finally, molecular scale understanding of the behaviour of biomolecules on surfaces could increase understanding of the Biosensor function.

1.2.2 Outline of the Thesis

The thesis consists of two parts: the first describes the development from the cantilever chip to a biosensor. The second part is about the use of carbon nanotubes (CNTs) as probes in atomic force microscopy.

Part I begins with an introduction to the Biosensor chip and the measurements of surface stress. The first applications of the sensor as an power meter are presented.

In chapter three the development of a gas sensor is described. The sensitivity towards vapour is obtained by coating one side of one of the cantilevers with a polymer film. Measurements are performed and the signals interpreted quantitatively using a simple model of the instantaneous alcohol concentration in the measurements chamber. The investigations are pursued towards high reproducibility and the effect of the use of a reference cantilever and on-chip Wheatstone bridge are illustrated. Dependencies of temperature and polymer film thickness are observed.

Chapter four follows the design of the liquid cell and flow system and the coating of the electrical leads of the chip.

Chapter five describes the work on the specific biosensor developments. The specific challenges are presented and the work on verification by fluorescence detection is described. Measurements on the immobilisation of short single strands of DNA on gold are presented and the preparatory steps for realising an E. coli immunosensor are described. Signals which could be from bacteria detection have been observed although only barely above noise threshhold.

Part II begins with an introduction to AFM and the crucial role of the probe tip. Carbon nanotubes are introduced and work on the assembly of carbon nanotube probe tips is presented in chapter eight.

In chapter nine bioimaging is performed, both with and without nanotube probes. With the nanotubes large intramolecular phase contrasts were observed in the imaging of IgG.

An alternative use of the carbon nanotube (CNT) as probe in the measurements of oscillatory forces at the solid liquid interface is briefly described in chapter ten.

Part I

Piezoresitive Micro-Cantilevers for Sensing

The development of the microelectromechanical chip into a microelectromechanical biosensor, can also be formulated in a few questions:

- Will the chip work as a sensing device?
- How to make liquid operation possible?
- What is needed to make it into a biochemically specific sensor?

This part of the thesis addresses these questions.

Chapter 2

The Biosensor chip

The Biosensor chip, which is at the basis of the work in this thesis, was first developed by Anja Boisen as an advanced device for atomic force microscopy [1]. It was further developed and tested by Jacob Thaysen [36]. Jacob Thaysen, Peter Rasmussen and others have since continued the work on optimisation for biosensor use. Here, the main principles of the sensor will be presented, summarising results from the theses of Thaysen [35] and Rasmussen [37], to which are referred for detailed discussions and technical investigations. An example of an application of the sensor in laser power measurements will be demonstrated and the applications we have been working with in the Bioprobe group will be briefly overviewed.

2.1 Principles of design and function

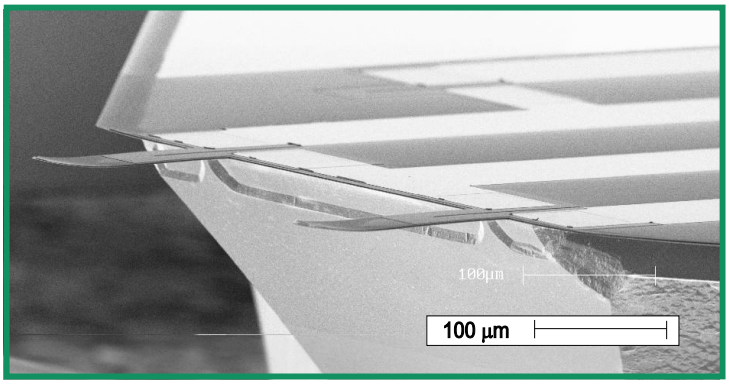

Figure 2.1: A SEM image showing a 3/4 view of the front of the Biosensor chip. In the foreground the two cantilevers with resistors on top. Behind them the bulk silicon body of the chip and the gold leads connecting the resistors.

Figure 2.1 is a scanning electron microscope (SEM) image of the front end of the Biosensor chip. As many of the applications that will be presented are not

'bio', the chip will also be called the cantilever chip or simply the sensor. One microscopic cantilever is seen in the foreground. The cantilever is 200 μm long, 50 μm wide and approximately 1-2 μm thick. A second, reference, cantilever is placed next to the first at a distance of 200 μm. The structures seen on the surface of the cantilevers are stress sensitive piezo resistors and on the body of the chip, one of two additional resistors can be seen. Gold leads connect all the resistors.

Three measurement principles based on microscopic cantilevers were described in the introduction: The thermal sensitivity of a bimorph structure, the detection of mass changes using the resonant frequency shift and the detection of stress changes due to strains in surface layers. The thermal conductance and the damping of an aqueous environment will reduce the sensitivities of the two first measuring principles, so the latter is expected to yield the highest sensitivity for the detection of biomolecules in a liquid.

The main transduction system of the Biosensor exploited in the present work is the reaction of the measurement cantilever beam due to a stress generating process on the surface of the cantilever.

2.1.1 Integrated readout

The classical way to detect bending of microscopic cantilevers is to use the optical leverage technique developed in connection with the atomic force microscope (AFM, chapters 1 and 7). This measurement principle is very sensitive – deflections down to a tenth of an Ångstrøm can be measured in this way. However, there are some drawbacks using the optical system: First of all an optical detection system requires sensitive alignment and it is inherently bulky, because part of the sensitivity relies on the distance between the bending cantilever and the detector. Also, certain constraints are placed on the properties of the cantilever that must be a good reflector for the laser beam. Further, the laser itself can contribute noise and drift to the system and interference effects are known to be troublesome. Finally, the optical system can be complicated to operate in some environments. For example in liquid, highly relevant for biological applications, changing refractive indices can generate apparent deflections and an opaque liquid diffuses the light. In a highly specialised environment such as ultra high vacuum it can be quite involved to install an optical detection system.

Though the sensitivity is not expected to be enhanced, these complications motivated the development of *active probes*, cantilevers with a built-in read-out mechanism.

In the literature, mainly three basic principles have been used in order to integrate the readout with the cantilever for AFM: capacitive [38], piezo-electric [39, 40] and piezo-resistive [41]. The piezo-resistive readout mechanism was chosen because of its versatility with respect to operating environments and AFM operating modes, the processing possibilities and because it had already proven

resolutions at the Ångstrøm level [1]. A cantilever with a piezo-resistive read-out can be operated with relative ease in liquids, ultra high vacuum and in dusty environments. The read-out from the cantilever depends on the stress induced in the resistors and the detection becomes a simple electrical measurement.

2.1.2 Encapsulated resistors

The piezoresistors are integrated in the cantilever as a thin layer of doped poly silicon on the top of the lever. Typical values for the resistors were 6 kΩ. Full encapsulation of the resistors in dielectric silicon oxide prevents leak currents, which also reduces temperature sensitivity. In order to make the Biosensor compatible for operation in liquid the cantilevers further have a top coating of silicon nitride as silicon oxide is a poor diffusion barrier especially for water and sodium. The

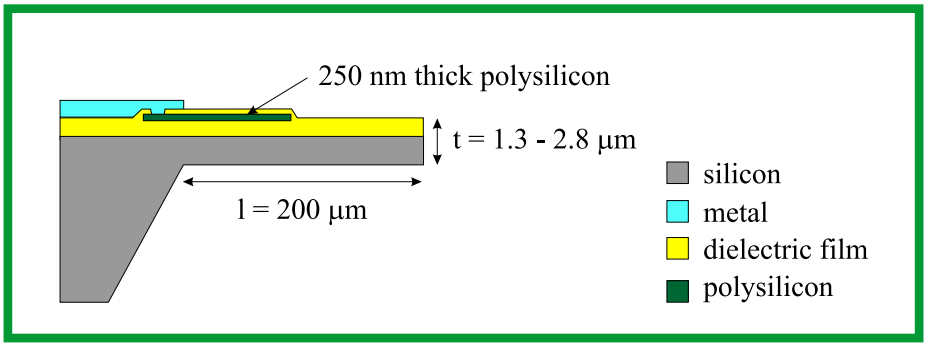

Figure 2.2: A cut through a cantilever showing the layered structure of the integrated and encapsulated resistor.

multilayered structure of the resulting cantilever is shown in figure 2.2. Great care must be taken in the design to balance the stresses of the different materials in the layers if one wants to obtain straight cantilevers [37]. In the present thesis several generations of cantilever sensors have been used each with slightly varying thicknesses of the layers resulting in differences in the sensitivities. This will be summarised in table 2.1.

In order to work in an electrolyte the electrical leads on the body of the chip must however also be protected. In section 4.1 we investigate some postprocessing steps for protection of the leads on the body of the chip. Currently, much work is been done on developing batch processes which would yield fully protected leads.

2.1.3 Integrated reference & on-chip Wheatstone bridge

An ubiquitous problem in sensitive measurements is the ambient noise and it has been pointed out that a reference cantilever can provide an important filtering of this background noise [16]. Systems providing such references with laser beam-detection have been developed by Hans Peter Lang and coworkers using a

multiplexing scheme [42]. In the case of piezoresistors, heating of the resistors when a voltage is applied is an additional concern which can be compensated by a thermally symmetric design [1, 2].

The Biosensor was constructed with a second cantilever that can be used as a reference placed close to the measuring cantilever. Two additional resistors, equivalent to the ones on the cantilevers, were placed on the body of the chip. This way the resistors pairwise have similar environments.

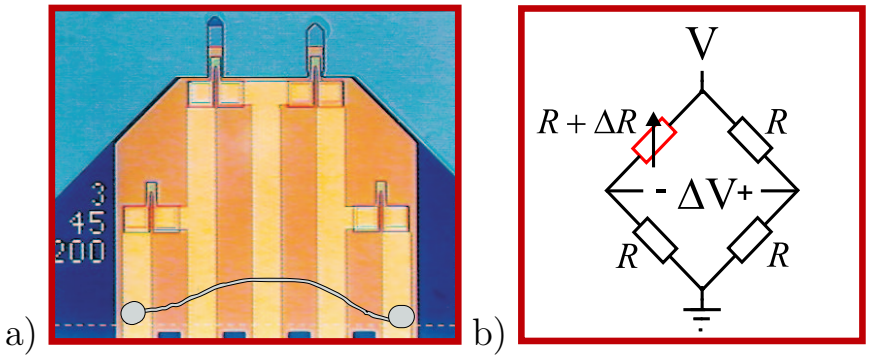

Figure 2.3: a) Optical top view of the Biosensor chip with an added on-chip wire bond and b) A sketch of the Wheatstone bridge arrangement

Figure 2.3 shows the top view of the front of the sensor in an optical micrograph. The resistors can bee seen on the cantilevers and on the body of the chip behind them. Square connection pads on each side of the resistors are seen connected to gold leads.

The picture shows one of the first generation of sensors originally developed for atomic force microscopy (the 'AFM chips'). They are optimised for deflection sensing, with the resistors only covering the back third of the cantilever [43], a tip integrated on the front of the sensing lever (to the left) [2, 37] and the reference lever being of a slightly squatter design, to avoid contact with the scanned sample while retaining the similar mechanical and thermal characteristics [1, 2].

When the chip is mounted the resistors can be connected in a Wheatstone bridge configuration (figure 2.3.b). A measurement of the voltage change over the bridge, ΔV, is then a direct measure of the change of the resistance on the measurement cantilever relative to the reference, ΔR. If $\Delta R \ll R$ the output voltage ΔV is given by

$$\Delta V = \frac{1}{4} V \frac{\Delta R}{R}, \tag{2.1-0}$$

where V is the voltage over the bridge. Unless otherwise stated we have used a bridge supply voltage of 4V. With this potential the signal to noise ratio is close to optimal [37].

This construction is highly thermally symmetric which effectively compensates resistor selfheating effects and makes it possible to cancel thermal drift as

well as fluctuations due to changes in air/liquid currents and other sources of noise which act on scales larger than the separation between the two cantilevers.

Cantilevers with piezo resistive readout are now commercially available[1]. However the resistors are not encapsulated and an external bridge must be set up. Besides the noise reduction due to the reference cantilever, it has been shown that the drift of the sensor is decreased two orders of magnitude with the on-chip bridge [2, 36].

2.1.4 Stressing a piezo resistor

When a piezoresistor is strained the resistance, R, of the piezoresistor changes. The relative resistance change, $\Delta R/R$, can be written as a function of the strain ϵ:

$$\Delta R/R = \kappa_{\parallel}\epsilon_{\parallel} + \kappa_{\perp}\epsilon_{\perp}, \tag{2.1-0}$$

where $\parallel$ and $\perp$ denote the longitudinal and transversal directions and the κ's are the respective material specific gauge factors. In the case of silicon the piezoresistive effect can be orders of magnitude larger than in metals for example. The gauge factors depend on the direction of the current relative to the strain and they have opposite signs in the two different directions. The resistors on the cantilevers are dimensioned so there is little contribution from the part of the resistor, at the top of the cantilever, which is subjected to transverse strain during bending.

The gauge factor resulting from the combined effects of transverse and longitudinal strains, κ, is determined experimentally for each batch of sensors. To measure the gauge factor a force is applied to the end of the cantilever, by deflecting it a known distance with a point probe, while the resistance change is measured (figure 2.4).

For a deflection z, the effective κ is found from the slope of the curve using the relation between the end point deflection of the cantilever and the relative change in resistance [35]:

$$\frac{\Delta R}{R} = \kappa \frac{3(1-\lambda/2l)h_{NR}}{l^2} z, \tag{2.1-0}$$

where l is the length of the cantilever and λ/l is the relative length of the piezoresistor. h_{NR} is the distance between the neutral axis and the middle of the resistor (figure 2.5). The neutral axis is defined as the plane parallel to the cantilever surface where no stress is felt when the cantilever is bent. The position of the neutral axis, for example relative to the bottom of the cantilever, h_{NB}, can be calculated from [44]

$$h_{NB} = \frac{\sum_i E_i t_i h_{iB}}{\sum_i E_i t_i}, \tag{2.1-0}$$

[1]Piezolever, Park Scientific Instruments, Sunnyvale, CA, USA

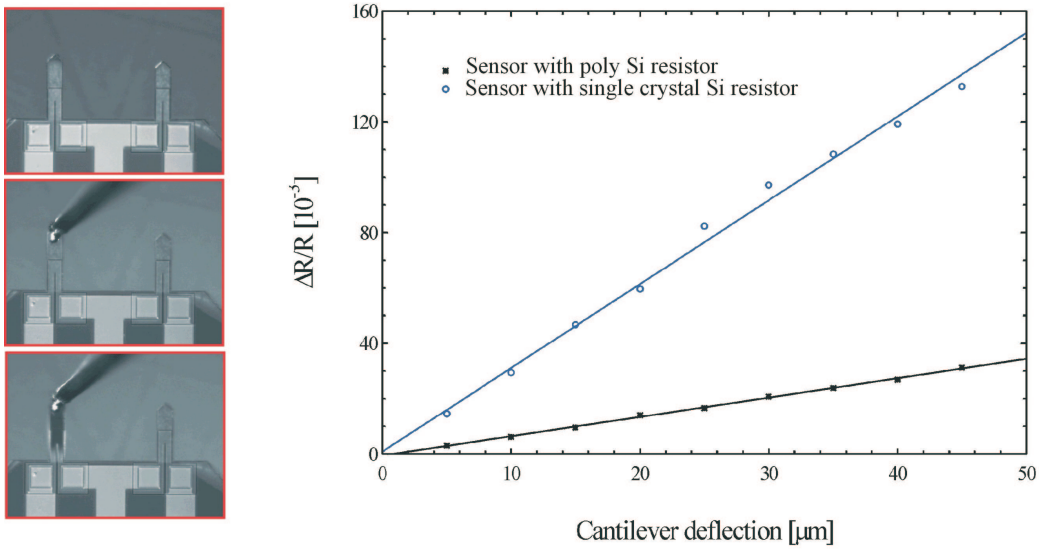

Figure 2.4: Relative resistance change as a function of deflection. The three pictures on the left show the cantilever being deflected by a fine point on a micromanipulator. The sensitivities for both sensors with single and poly crystalline piezoresistors are shown [2].

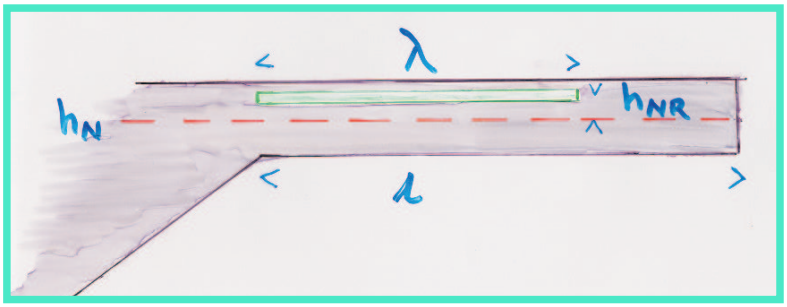

Figure 2.5: Cross section of a cantilever of length l with a resistor of length λ at a distance h_{NR} from the neutral axis.

where E_i are the Young's modula of the different cantilever layers, t_i the thickness of the layer and h_{iB} the position of the middle of the layer, also relative to the bottom of the cantilever. In a one layer cantilever the neutral axis would be in the middle of the cantilever.

For the poly silicon p^{++} piezoresistors used in the Biosensor the dimensionless κ is found to be 25.

The strain in the resistor, ϵ, is related to the stress, σ, by

$$\epsilon = \frac{\sigma}{E}, \tag{2.1-0}$$

where E is the Young's modulus. Eqs. 2.1.4 and 2.1.4 relate the stress in the

resistor to the resistance change

$$\frac{\Delta R}{R} = \kappa \frac{\sigma}{E}. \tag{2.1-0}$$

In terms of the voltage change over the bridge, ΔV, we get for the stress change in the resistor σ from eqs. 2.1.3 and 2.1.4

$$\Delta V = \frac{V}{4} \frac{\kappa}{E} \sigma. \tag{2.1-0}$$

2.1.5 Detecting a surface stress

We will use the stress sensitivity of the resistor to study changes on the cantilever surface and especially stress changes in films on the cantilever surface.

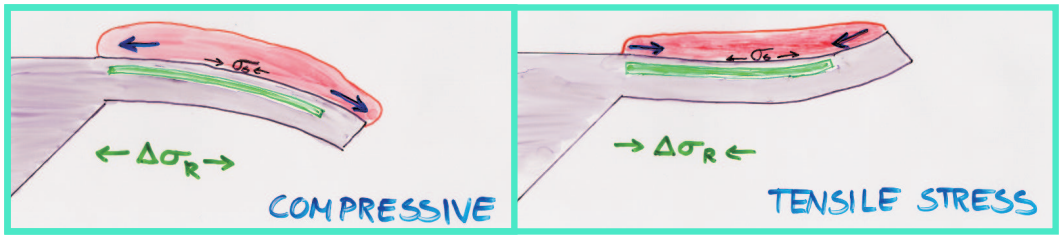

Figure 2.6: Stress in a film on a cantilever. As the film expands the cantilever is bent down giving rise to a tensile stress in the resistor. The resulting stress in the film is compressive as its expansion is hindered and balanced by the bending of the beam. Conversely, for a contracting film the cantilever bends up and the resulting stress in the film is tensile.

Figure 2.6.a shows a cantilever with an expanding film on the top surface. The cantilever bends downwards and expands until the stress thus created in the cantilever balances the stress in the film. The stress in the film, σ_F, is compressive as the expansion is hindered by the supporting cantilever ($\sigma_F < 0$). The resulting stress on the upper side of the cantilever is tensile. The stress in the film extrapolated to an infinitely thin film is the surface stress, $\sigma_s = \sigma_F t_F$, where t_F is the thickness of the film. The opposite case of a contracting film, giving rise to a tensile surface stress, is illustrated in figure 2.6.b.

In the steady state both the net force and the net moment around the neutral axis must be zero and from this it is possible to obtain a relation between the stress in the resistor, σ, and the surface stress σ_s [35, 45]. The detailed relation between a surface stress on one side of our composite cantilevers and the resistance change caused by the strain in the resistor is complex because of the relation between the different materials in the cantilevers. A detailed model for a multilayer cantilever is developed in [35]. Here, we look at the result in the simplified case of a cantilever consisting of only one layer of material of thickness t and an infinitely thin resistor placed at one of the cantilever surfaces (figure 2.7). A surface stress

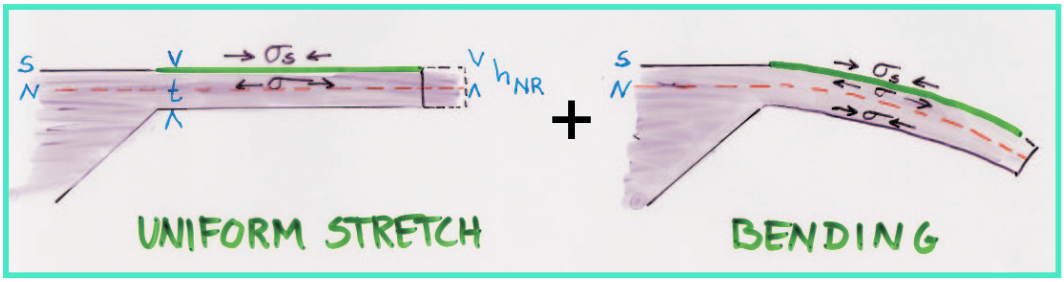

Figure 2.7: A 1-layer cantilever model. The applied surface stress σ_s, the resulting stress in the resistor σ and the neutral axis are indicated.

σ_s applied to the surface S of the cantilever is described by the relation [35]:

$$(\frac{\Delta R}{R})_{1-layer} = -\kappa(\frac{1}{Et} + \frac{3h_{NS}^2(1-\frac{h_{SR}}{h_{NS}})}{Et(t/2)^2})\sigma_s, \qquad (2.1\text{-}0)$$

where h_{NS} is the distance from the neutral axis to the surface S, at which the stress is applied, and h_{SR} is the distance from S to the resistor. The two terms between the brackets illustrate that the stress in the resistor consists of a contribution from the pure stretching/compression of the resistor (the first term) and a contribution due to the bending of the cantilever (the second term). If the stress is applied to the surface where the resistor is placed $h_{SR} = 0$ and equation 2.1.5 becomes

$$(\frac{\Delta R}{R})_{1-layer} = -\kappa(\frac{1}{Et} + \frac{3}{Et})\sigma_s = -\kappa\frac{4}{Et}\sigma_s. \qquad (2.1\text{-}0)$$

In this example the bending and the pure stretch/compression work together. If the applied stress and the resistor are on opposites sides of the neutral axis the bending and the pure stretch/compression work in opposite directions: $h_{SR}/h_{NS} = 2$. This changes the sign of the bending term and equation (2.1.5) becomes $\Delta R/R_{1-layer} = \kappa(2/Et)\sigma_s$, that is a factor two less sensitive than when they work together (equation 2.1.5).

Even from the simplified relations above it can be appreciated that the sensitivity is enhanced through a large gauge factor and a thin, soft cantilever. When using the bending, the ability to place the resistor (and the applied stress) far away from the neutral axis is another sensitive parameter. Note in particular, that the sensitivity is independent of the length and width of the cantilever.

If one imagines a cantilever made of only one thin layer, which is a resistor material, $h_{SR} = h_{NS}$ and there would be no bending contribution. On the other hand, equal strains σ_s applied to both the front and the back of the cantilever would work in the same direction thus also adding up to half the sensitivity of the bending enhanced measurement. However, this sensitivity it might be possible to increase because, no longer depending on establishing a distance to the neutral axis, the cantilever could be thinned by at least a factor of two.

One should keep in mind that the bending part of the signals measured, ΔV, are due to the differential stress change on one side of the cantilever relative to the other side. This is measured relative to the differential stress changes on the reference cantilever. When the measuring cantilever is coated with a film, the back sides of the cantilevers are the same so we need to consider only what happens on the two front sides. If the bare surface of the reference cantilever can be considered inert, the voltage change ΔV is a direct measure of the surface stress change due to changes in the film on the measurement cantilever.

When we in the following talk about 'the stress' we will mean the surface stress of the *film* on the cantilever and use the terms tensile and compressive as defined in figure 2.6.

2.2 On sensitivity, noise and optimisation

Throughout the present thesis three generations of cantilever sensors, developed within our group, have been used; from the very first functioning AFM imaging chip (figures 2.1 and 2.3) to later generation sensors, developed specifically to meet some of the challenges we encountered in the applications to bio-sensing in liquids.

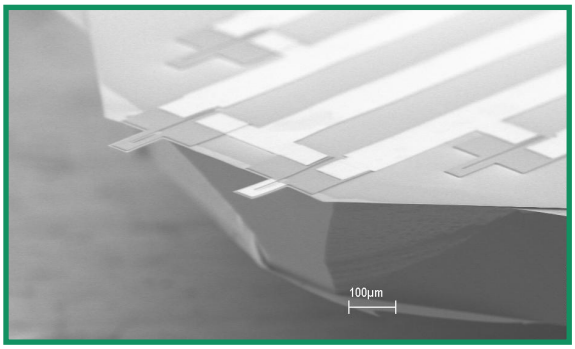

Figure 2.8: SEM image of a second generation Biosensor chip. Note that the resistors cover the whole length of the cantilever and that the cantilevers have the same dimensions. Also the connector pads to the unprotected gold leads have been pulled back from the edge of the chip to facilitate the protective coating procedures. Finally, one can see that in this case the sensing cantilever has been coated with gold (light colour).

For example figure 2.8 shows a so-called FagPakke sensor designed with identical cantilever geometries and resistors covering the whole length of the cantilever to enhance the sensitivity. The connector pads and the gold leads are pulled back from the edge of the substrate so it becomes easier to apply the post processing protective coatings for work in liquids. This sensor also comes with a gold coating of the top surface of the measuring cantilever, a feature used for the adsorption of

	AFM	Poly5	FagPakke 1 2
Multilayer structure — thickness in μm			
Top Coat (SiN)	0.12	0.12	0.08
Dielectric (SiO)	0.095	0.1	0.1
Resistor (Poly Si p^{++})	0.36	0.3	0.176
Dielectric (SiO)	1.0	1.0	0.72
Base (Poly Si)	0.5 5	0.2	0.23
Total	2.075 6.575	1.720	1.306
Neutral axis and sensitivities			
h_{NB} [μm] (bottom – neutral axis)	1.050 3.055	0.945	0.671
$\Delta R/R(\sigma_s)^{-1}$ $[(\mathrm{N/m})^{-1}] \cdot 10^{-4}$	-2.64 -1.2	-2.95	-3.77 -3.57
$\sigma_{s,min}$ (theoretical) $[\mathrm{N/m}] \cdot 10^{-3}$	7.4 17	6.6	4.59 5.7
$\Delta\sigma_s/\Delta V$ [(N/m)/V] (Supply voltage $V = 4$ V)	3783 8617	3387	2652 2801

Table 2.1: Cantilever properties. Sensitivities calculated from the detailed model in [35] by Peter Rasmussen.

sulphur containing molecules. Finally, the materials in the cantilever have been optimised.

The details of the structures of the three different types of senors employed are summarised in table 2.1. The 'AFM chips' were produced by a method which left the thickness on the Si base of the cantilever rather uncertain. While a thickness around 0.5-1 μm is expected, it can also be 5 μm thick. It is instructive to see that this changes the surface stress sensitivity by a bit more than a factor of two.

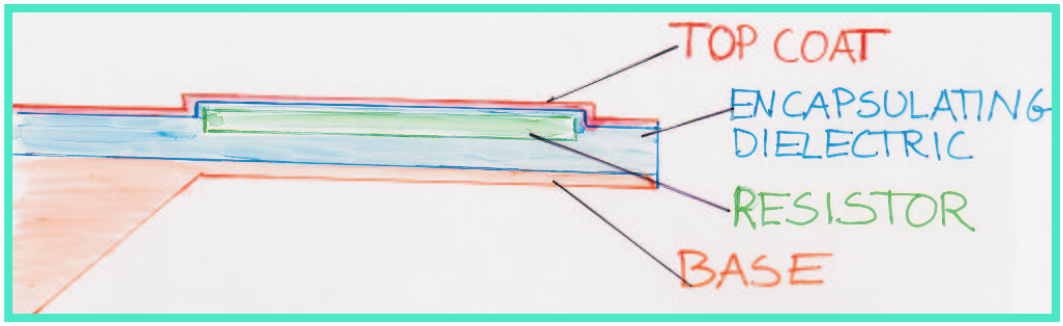

Figure 2.9: Sketch of cantilever layers in table 2.1

	Young's modulus (E) GPa	Thermal Expansion (α) 10^{-6} K^{-1}	Thermal Conductivity (β) W/m K
SiN (Low stress)	250	0.8	19
SiO	70	0.55	1.4
(Poly) Si	180	2.33	157

Table 2.2: Material Properties

2.2.1 The sensitivity

The deflection sensitivity was determined directly as described in section 2.1.4, and from this the gauge factor of the piezoresistor was found. Using the gauge factor, the Young's modula and thicknesses of the material layers in the cantilever, the surface stress sensitivity $\sigma^{-1}\Delta R/R$ was determined from a five layer version of equation 2.1.5 [35]. The position of the neutral axis can be calculated from the stiffness, thickness and position of each layer (equation 2.1.4). The position of the neutral axis relative to the base of the cantilever, h_{NB}, and sensitivities for the different types of cantilevers are listed in table 2.1. Especially the Young's modulus of SiN can however be associated with quite some uncertainty. Here a value for low stress SiN is used. However, depending on the processing, variations up to 30 % are not unexpected.

2.2.2 Noise in the piezoresistors

The minimum detectable signal of the piezo-resistive cantilever based sensor is limited by the noise level of the measurement. The general theory of the noise in piezoresistive cantilevers and the optimisation of the signal to noise ratio in real devices are extensively studied in [35, 43]. Part of the noise is intrinsic to the piezoresistors. It consists of three terms: 1) Vibrational noise due to the thermal vibrations of the cantilever, which depends on the temperature, the length of the resistor, the relative length of the cantilever and resistor, the stiffness of the cantilever material and the measurement bandwidth. 2) The Johnson noise which is due to thermal fluctuations of the charge carriers in the resistor and depends linearly on the resistance and the measurement bandwidth. Finally, 3) the so called $1/f$ or Hooge noise, which can be described by a model where the noise is inversely proportional to the frequency and the number of carriers in the resistor. The $1/f$ noise is thought to originate from scattering off lattice impurities in the resistor as it has been found to be sensitive to the annealing of the doped resistor [35].

The resulting total internal noise can be evaluated in terms of the noise in deflection [37] or in surface stress [35] and in both cases the $1/f$ noise turns out to be dominant for frequencies below 10 kHz for a 3 V supply voltage [46]. The vibrational noise is more than an order of magnitude smaller than any of the

other terms. In the case of the deflection an optimum resistor length can be determined. In the case of the surface stress the total noise continues to decrease with resistor lengths beyond 500μm [35].

The total internal noise contribution from the resistors in the sensors we used, was calculated from the noise expressions in [35] to give a theoretical lower limit of the detectable surface stress, $\sigma_{s,min}$. The values of $\sigma_{s,min}$ are also found in table 2.1.

2.2.3 Optimisation

The performance of the Biosensor can be enhanced, especially with respect to the use as a surface stress sensitive device. First, in the case of the detection of an endpoint deflection it can be shown that the greatest sensitivity is obtained for a resistor close to the clamping of the lever. Further optimised for noise, the optimal resistor length for a deflection sensitive AFM sensor is 1/3 of the cantilever length [43]. The surface stress on the other hand is a local property: the signal from the change of resistance is independent of where on the cantilever the stress change occurs (equation 2.1.5). In a sensor optimised for surface stress detection the resistor would therefore cover the whole cantilever, in order to pick up as much signal as possible (e.g. the FagPakke sensor figure 2.8).

The signal to noise level of the resistor can be increased using single crystalline silicon and optimised processing parameters regarding doping level, annealing and absolute dimensions of the resistors. Also, the dimensions of the cantilever and material properties such as the gauge factor and defects in the resistor can be tuned and optimised, an ongoing effort within the Bioprobe group.

We saw above that the dominant noise term was the $1/f$ noise. Using a lock-in amplifier the measurement can be centered around a high frequency. Thus, recently members of the project found that the value of the $1/f$ contribution to the noise can be decreased by more than a factor of 10 [47].

Fully optimised, the difference in the minimum detectable surface stress change between the piezo-resistive and an optical readout scheme, due to intrinsic noise, can be calculated to be a factor of ten in favour of the optical readout [35]. The probes used in this thesis could be 50 times less sensitive than this[2]. Except for the case of highly specialised laboratory work it is the hope that this difference is more than compensated by the potential ease of operation of the piezo-resistive detection.

2.3 Applications

The first chemical sensor applications of micromechanical cantilevers exploited the bending of the lever due to the bimorph effect upon heating [5, 10]. This can

[2]Peter Rasmussen, private communication.

be used for example to study the wave length dependent absorption by a thin sample film on the cantilever or the heat produced during a chemical reaction — in [5] for example the catalytic reaction of the conversion of H_2 and O_2 to H_2O over a Pt surface could be followed and in [48] phase transitions of alkanes were studied. The cantilever sensors are potentially sensitive down to fJ [11] and it was speculated that with the combination of high sensitivity and small detector size it could be used to follow heat production processes in single biological cells [10].

The first test of the function of the cantilever chip as a sensor was using it as a laser powermeter.

2.3.1 The Laser Powermeter

The argon laser system at MIC is used for lithography to obtain structures beyond the linewidth limit of the optical lithography which at MIC has a limit of 1 μm. By direct writing with the laser, a silicon oxide mask can be defined on a hydrogen-passivated silicon surface. However, fluctuations in the power of the laser and hysteresis in the external control limit the precision of the process. Because of its sensitivity the cantilever sensor could be used for continuous online monitoring of a small fraction of the laser beam.

The layered structure of the cantilevers in the sensor (figure 2.2) make them inherently bimorph. That is, a heating of one of the cantilever beams would produce a signal caused by the difference in thermal expansion of the cantilever materials. The signal we measure is due to the temperature difference between the two cantilevers.

We investigated the performance of the cantilever sensor ('AFM chip') by heating the measurement cantilever with the argon laser (at 488 nm) focused to a spot diameter of about 1 μm on the tip of the cantilever (figure 2.11). The power of the laser was controlled by an external controller and the beam was positioned using high resolution motorstages and a CCD camera.

In figure 2.10.a a timeseries of the output from the Wheatstone bridge of the sensor is shown where the power has been increased in discrete steps and then decreased again by nominally the symmetric power changes. The drops to zero after stabilisation at each power level are due to blocking during measurement with an independent power meter. At zero power it is seen that the noise level of the cantilever sensor is very low (< 0.1 mV) and the fluctuations at higher power are due to the laser. Furthermore, a hysteresis is notable in the laser power when comparing the hight of the steps during increase and decrease of the laser power. When the sensor output was plotted against the independently measured power we saw a linear increase of the output from the sensor as the power of the laser was increased (figure 2.10.b). From the slope of the curve in figure 2.10.b we get a sensitivity of 2.5 mV/mW which for this cantilever is between 9.5 and 22 (N/m)/mW (table 2.1, 'AFM chip'). The data contains the measurements from

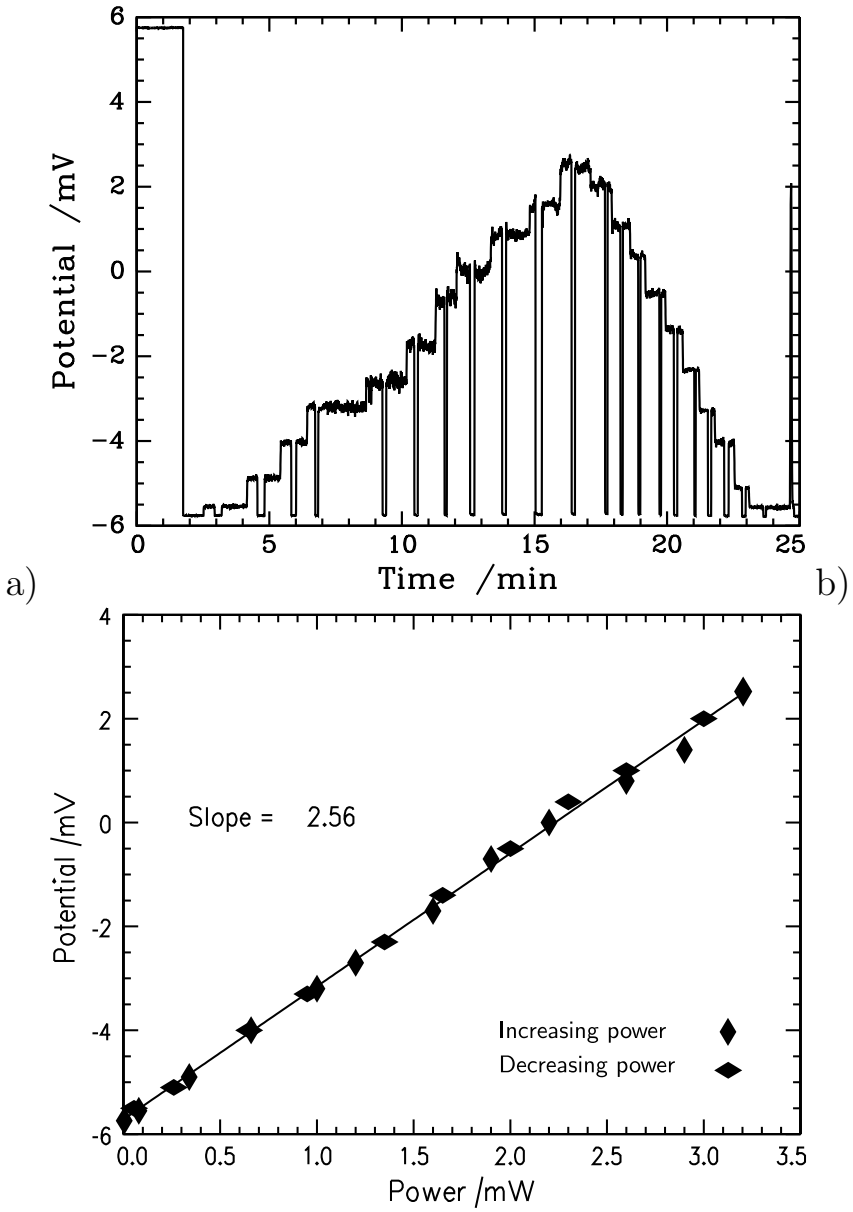

Figure 2.10: a) Wheatstone bridge output as function of time. The dips to zero are caused by blocking during an independent measurement of the power. b) Wheatstone bridge output as function of the laser power measured in a).

both increasing and decreasing laser power and it is seen that the measurement is completely reversible.

We can estimate the expected power sensitivity of the cantilever sensor using a simple 2-layer model for the end point heating of a cantilever, where the body of the chip is assumed a perfect heat sink [11]. For a cantilever of length l, width

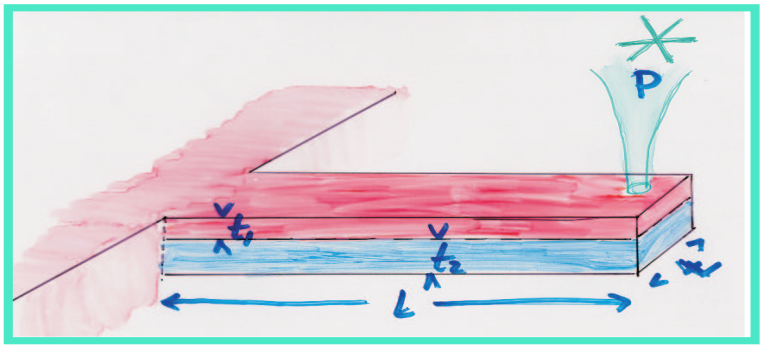

Figure 2.11: Two layer model of an AFM sensor type cantilever (table 2.1), of length l, width w and thickness $t = t_1 + t_2$. The end is heated with a focused laser beam. The body of the chip is considered a perfect heat sink and the temperature to vary linearly along the length of the beam.

w and thickness $t = t_1 + t_2$ (figure 2.11) we get[3]:

$$\Delta\sigma_s = 2(\alpha_1 - \alpha_2)\frac{E}{3(1-\nu)}\frac{t^3 l}{t_2^2 A(\beta_1 t_1 + \beta_2 t_2)w}P. \qquad (2.3\text{-}0)$$

α_i are the thermal expansion coefficients of the two materials, β_i are the thermal conductivities, P is the power and E and ν are respectively the Young's modulus and Poisson's ratio of the cantilever. A is a device parameter given by [11]:

$$A = 4 + 6\frac{t_1}{t_2} + 4(\frac{t_1}{t_2})^2 + \frac{E_1}{E_2}(\frac{t_1}{t_2})^3 + \frac{E_2}{E_1}\frac{t_1}{t_2}. \qquad (2.3\text{-}0)$$

The sensor used here is an AFM chip (table 2.1) and we will approximate the structure of the cantilever with a silicon layer of thickness $t_1 = 0.5\mu$m on a silicon oxide layer, $t_2 = 1\mu$m. With the material parameters of table 2.2 and $E = (E_{Si}t_1 + E_{SiO}t_2)/t = 110$ GPa we find $\Delta\sigma_s/P = 3.2 \cdot 10^3$ (N/m)/W, a factor three lower than the measured value 9.75 (N/m)/mW. This is a reasonable agreement considering the simplified assumptions of the model and the uncertainty connected to the structure of the AFM cantilevers. A sensitivity of 6.24(N/m)/mW was measured for a different sensor from the same batch. The assumption of a perfect heat sink at the base of the cantilever is also an idealisation that probably underestimates the temperature, especially in the region close to the base where the sensing resistor is placed.

The temperature at the heated end of the cantilever, at maximum power, can be estimate from [11] $\Delta T = lP/w(\beta_1 t_1 + \beta_2 t_2)$, where ΔT is the temperature

[3]The relation in [11] is for the deflection. The corresponding surface stress is found using the Stoney's formula, which describes the bending resulting from a stress difference $\Delta\sigma$ in terms of the resulting radius of curvature, R: $\Delta\sigma = Et^2/6R(1-\nu)$, where E is Youngs modulus, t is the thickness of the cantilever and ν is Poisson's ratio. In terms of the deflection of the cantilever, Δz, it becomes $\Delta z = (3l^2(1-\nu)/Et^2)\Delta\sigma_s$, where l the cantilever length comes in as a parameter which can enhance the signal in deflection measurements.

relative to ambient. With the model used above we get $\Delta T = 150$K. The corresponding stress change would be 9.3 N/m if we assume uniform temperature, which is close to the measured value of approximately 9 N/m.

The resistor is heated during the experiment and both the resistance and the gauge factor may change independently of the bimorph stress. The resistors are, however, designed to have low temperature variations and these are expected to vary quadratically with temperature [2]. The highly linear response suggests that the primary effect is the stress development.

The minimum detectable surface stress change for this cantilever is approximately 1 mN/m which corresponds to a minimum detectable power of 100 nW. The cantilever used here was not optimised for temperature sensitivity. The thermal sensitivity can be increased by using materials with large differences in thermal expansion. A sensitivity of 0.1 nW was estimated for a cantilever with a thick aluminum layer on a silicon cantilever [5].

It could be interesting to use the cantilever in connection with the laser setup as it only will require a small fraction of the power from the laser to monitor the variations with the cantilever and trigger online corrections to the laser controller. Another application exploiting the heat sensitivity is to study the heat developments due to for example chemical reactions on the cantilever surface [5].

2.3.2 Overview of applications of the Biosensor.

A number of people in the Bioprobe group are working on testing the sensor in different physical, chemical, molecular and micro biological applications all based on static deflection of the cantilever.

The sensor was first developed for AFM imaging and has been characterised and tested in scanning imaging [36, 46]. The sensor has also been used with success in a UHV setup were it performed well also at low temperatures (77K)[4].

Following the success of the laser power measurements the next step was to use a sensitised cantilever for gas detection (Chapter 3). Inspired by cantilever sensor work using optical readout [16] we coated a cantilever with a polymer and studied the absorption of the vapours of water and different alcohols. In the case of alcohol we found that the behaviour of the polymer could be described by a model of the absolute alcohol concentration. Besides a sensitive tool for characterising the polymer with respect to different environments the correspondence with the concentration model allowed us to determine a sensitivity better than 10 ppm for the detection of alcohols.

Experiments studying the adsorption of alkane thiols[5] on a gold surface were performed by Allan G. Hansen [49]. As when using optical read-out [14], a

[4]Klaus Hasselbach, Grenoble, privat communication.

[5]An alkane thiol is a carbohydrate chain with a sulphur group. In this case the sulphur was at the end of the chains.

gold layer was evaporated on the measurement cantilever and it was subjected to the vapours of alkane thiols of different lengths. The measurements were nicely described by a simple Langmuir adsorption model. The adsorption rates and saturation values were heavily dependent on the pretreatment of the gold surfaces.

A major challenge is the application of the Biosensor in liquid. In order to investigate the performance in aqueous solutions protections of the electrical leads were developed and flow experiments designed (chapter 4). The absorption of ethanol from water by a polymer was demonstrated and the heat sensitivity of a gold coated cantilever was measured [50, 51]. The adsorption of thiol modified short single stranded DNA strands on gold was studied with the Biosensor (chapter 5 and [52]). Experiments were also performed to detect the hybridisation of the complementary strand onto the thiol immobilised probe [44]. Finally, work has been carried out investigating applications in protein detection and an immunoassay for bacteria detection (chapter 5).

The development of the Biosensor chipis also continuing in the group. Most recently sensor systems have been developed with cantilevers integrated in a μfluid channel system, thus realising the potential of probing many molecules in parallel and μTAS compatibility [45].

2.4 Summary

We have described a highly versatile sensor for compact and direct measurement of minute changes in surface stress on a microcantilever. Both a readout and a reference cantilever are integrated on the sensor chip and from a simple measurement of the voltage change one gets the surface stress change on the measurement cantilever relative to the change on the reference. A concrete example of a heat measurement and a brief overview of our applications of the sensor were given.

Chapter 3

The Nose – Gas measurements

We describe the development of an alcohol vapour sensor using the cantilever sensor presented in the previous chapter. The cantilever is sensitised with a polymer layer and subjected to vapours of evaporating droplets of different kinds of alcohol. The measured signal is interpreted using an evaporation model for the droplet. It is seen that the initial reaction to a good approximation is directly proportional to the alcohol concentration in the measurement chamber. The sensitivity of the alcohol sensor is seen to be better than 10 ppm. Part of this work was published in APL, May 2000 [53] and in Ultramicroscopy in August 2000 [50].

3.1 Introduction

Mikrocantilevers have been used as gas sensors for example by detecting the heat production on the cantilevers surfaces due to chemical reactions [5, 48, 54], direct adsorption of mercury [6] or alkanethiols [13, 14] or absorption in polymers [16, 55].

Measurements on gases, by cantilever based sensors, detect either absorbtion or adsorption via a change in mass or in stress or the development of heat due to a chemical reaction on the cantilever surface.

3.2 Experimental

Sensor preparation

Before performing any measurements, the Biosensor chip was mounted with super glue on a ceramic substrate, which was patterned with gold leads, and wedge bonded (figure 3.1)[1]. The Wheatstone bridge was established with an on-chip bond. Electrical contact to the chip was obtained either by direct soldering to

[1]Wedge bonder: MicroSwiss, Kuliche and Soffa Industires Inc., model no 4123.

the gold leads on the ceramic or by using a specially designed contact and holder. The bridge was normally not completely balanced and this gave rise to an off-set

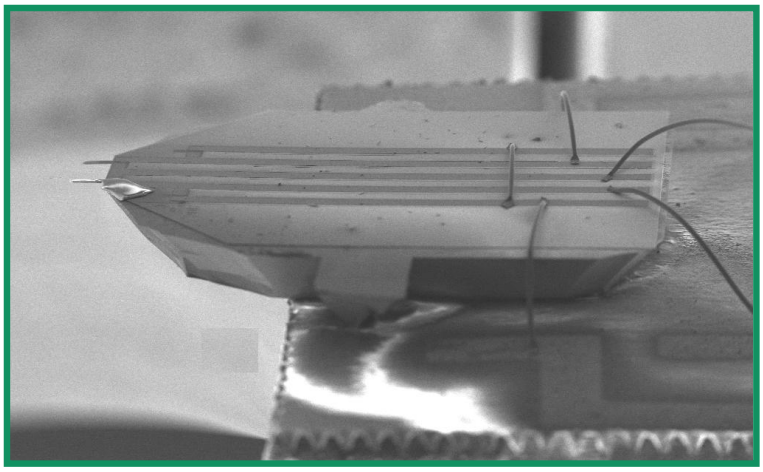

Figure 3.1: Scanning electron micrograph of the sensor mounted on a ceramic substrate and wedge bonded with aluminum wires. A polymer coating can be seen on the cantilever in the foreground.

of up to a few mV at a bridge supply voltage of 4 V.

In order to render the cantilever sensitive to vapours, one side of one of the two, closely spaced, cantilevers on the sensor was coated with a polymer, which we knew to swell when exposed to a humid environment. We used a UV sensitive photoresist[2] that was available from the cleanroom at MIC. The coating was performed manually with a glass capillary 'paintbrush' and a micromanipulator. The glass capillary had a protective polymer coating which made it easy to handle and it was coupled to teflon micro tubing connected to a syringe as sketched in figure 3.2[3]. The flow of the resist was manipulated with the syringe and, controlling the viscosity of the resist with acetone, a resist layer with a thickness of less than 5 μm could be obtained. However, also significantly thicker films, up to $\sim 50\mu$m, were used. Figure 3.3 shows a scanning electron micrograph of a sensor after coating. In **a** one can see that the polymer also covers part of the substrate and in **b** a side view of the cantilever shows that only one side of the cantilever is coated and that the thickness of the layer is 4 μm.

Coating the cantilever with the polymer induced a stress change on the cantilever. This decreased the off-set of the bridge by approximately 10%, corresponding to a tensile stress in the polymer. It did not otherwise affect the electrical properties of the integrated measurement system. The coated sensor was protected from daylight at all times.

[2]AZ 5200 E, Hoechst Celanese Corp., Chatham, NJ 07928, USA
[3]MIKROLAB AARHUS A/S, Axel Kiers Vej 34, 8270 Hœjbjerg Århus, Denmark

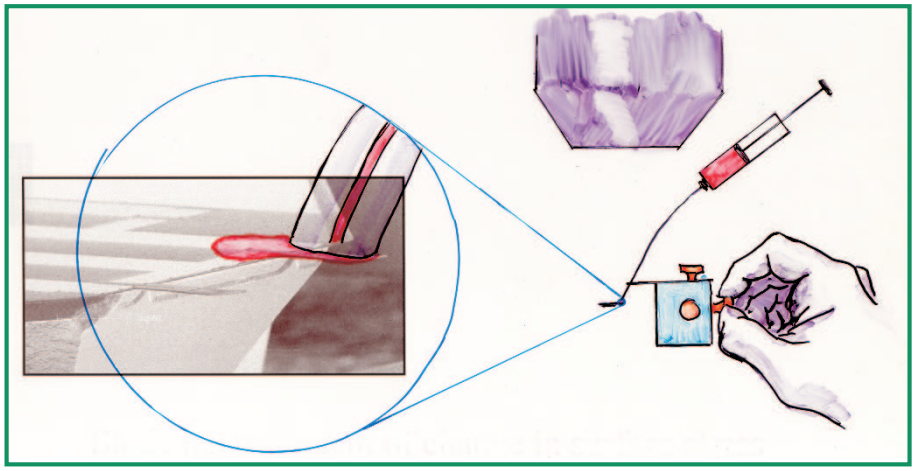

Figure 3.2: Sketch of cantilever coating. A syringe, with resist, was connected to a flexible glass capillary. The capillary, mounted in a micromanipulator, was used as a kind of brush to 'paint' the resist onto a cantilever, under view of a microscope.

Flow system

The measurement chamber was a 30 l plexiglass hood (approximately $30 \times 30 \times 35$ cm) placed on a plexiglass plate, the whole thing placed on a vibration isolation table. There was an inlet at the top of the hood for a controllable flow of nitrogen and at the bottom for electrical connections and alcohol inlet. For the measurements presented here we used a nitrogen flow, Q_0, of 10 l/min. The nitrogen inlet was covered with thin paper to diffuse the inflow. An equilibrium was established between the nitrogen inflow and the gas escaping through small random leaks between the hood and plate. A slight overpressure was thus maintained in the chamber

The Reynolds number is a dimensionless measure of the degree of turbulence in a flow defined as $R = \frac{\rho}{\eta} v d$, where ρ is the density, η the viscosity and v the velocity of the air and d a characteristic length of the system. Using the tabled values for air: $\rho = 1.293$ kg/m^3 and $\eta = 16.7 \cdot 10^{-6}$ Ns/m^2 [56], a typical length d of 30 cm and a velocity $v = Q_0/d^2$ we get $R \approx 40$ for the flow chamber in figure 3.4. Even though this does not by far indicate fully developed turbulent mixing, in combination with the diffusion of the flow at the inlet, the mixing in the chamber should be good.

The absolute humidity in the chamber was monitored by a conventional, capacity based, humidity sensor. The temperature was stable within approximately 1°C over an hour.

A variable voltage supply[4] was put over the Wheatstone bridge, normally at a supply voltage of 4 V, and the linearity with applied power verified for each sensor before the experiments. The output from the Wheatstone bridge was feed

[4]Iso-tech IPS 2303D, or equivalent.

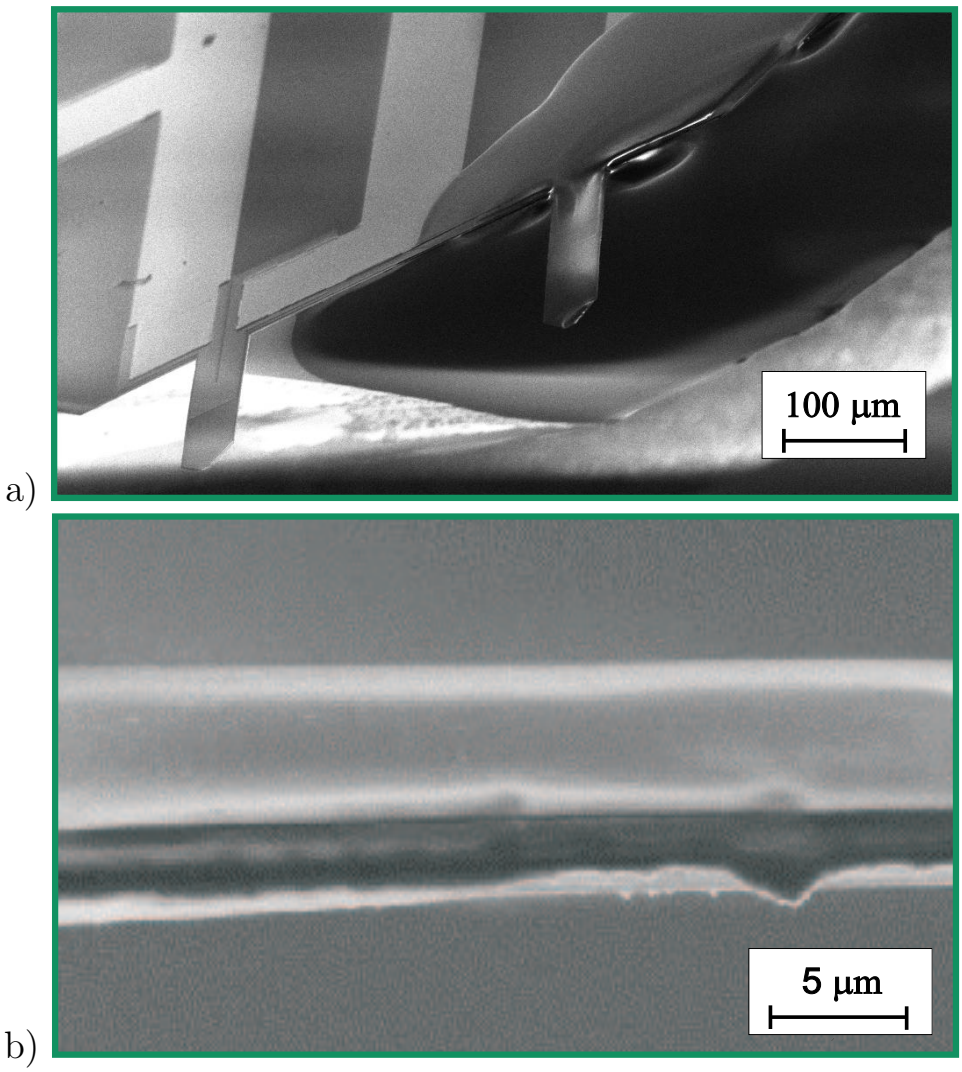

Figure 3.3: **a** Scanning electron micrograph of the sensor where one side of one of the two cantilevers and part of the substrate have been coated with a thin polymer layer. **b** Side view of the cantilever with a polymer layer on top. The thickness of the polymer is $\sim 5\mu$m.

directly to a Keithley 2000 multimeter[5] and collected via a GPIB card by a Labview program on a PC. The typical noise level was 10 μV ptp. Varying the flow rate over a factor 20 we did not observe any difference in the noise.

3.3 Humidity measurements

Changes in humidity have previously been measured using microcantilevers, both by the dynamic detection of mass change [15] and by static deflection due to

[5]Filter: moving average over 10 points, integration time 20 ms.

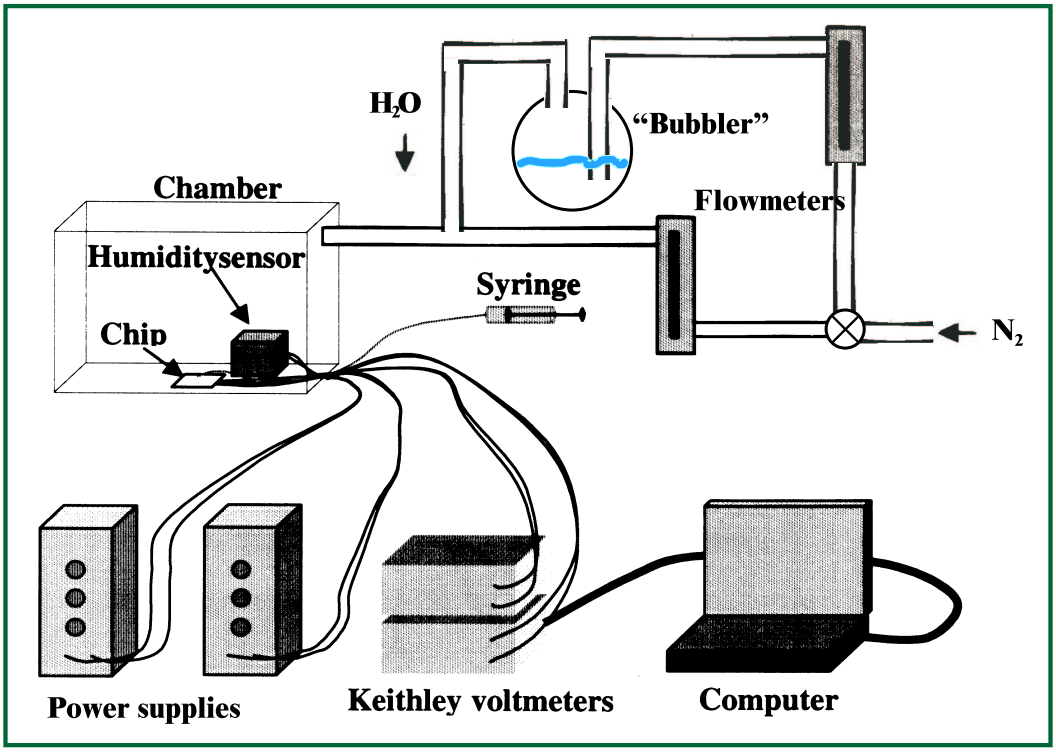

Figure 3.4: Set-up for gas absorption measurements

stress changes [57]. The sensitive element was in the first case a crystal (copper-sulphate-pentahydrate) deposited on the tip of a commercial piezoresistive cantilever. The cantilever was heated using the piezoresistor and the mass loss due to dehydration was measured from the change in resonant frequency, with a detection limit in the picogram range [15]. In the second experiment water absorption by native silicon oxide on a silicon cantilever was observed. One side of the cantilever was sealed with an evaporated layer of gold. An array of cantilevers were used and reference measurements were obtained by multiplexing between coated and non-coated levers.

Here we test the sensitivity of a polymer-coated Biosensor chip towards humidity. On one hand, it is a preliminary test of application on the other a characterisation that will be helpful to the alcohol detection experiments to come.

Experiment

The resist, with which we had coated the cantilever, is know to swell when absorbing water. This means that a compressive stress should be created in the polymer and the cantilever should bend away from the polymer - away from the side where the resistor is embedded - and generate an increase in the voltage output from the Wheatstone bridge (figure 2.6.a and equation 2.1.5).

The humidity of the inflowing nitrogen was varied between 2% and 65% by sending part of the flow through a bubbler with water. The voltage change over the Wheatstone bridge was measured together with the independent absolute humidity measurement.

Results

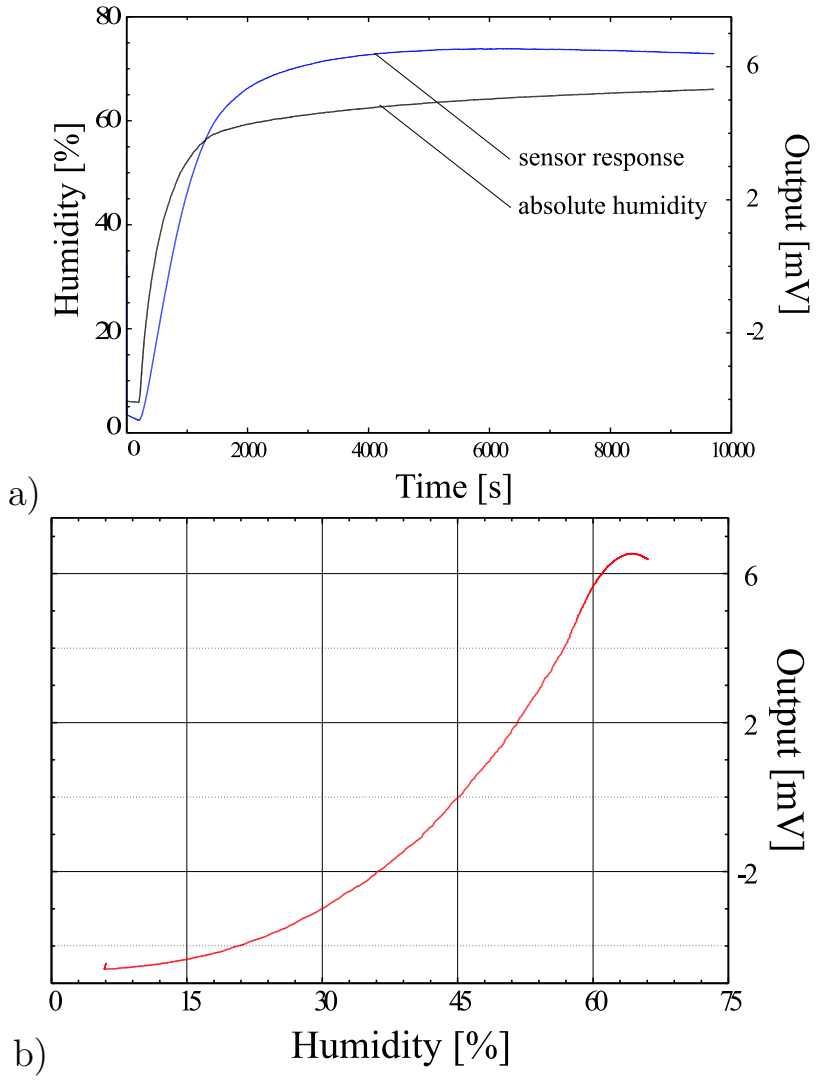

Figure 3.5: Humidity measurements with the sensor. One cantilever is coated with polymer. **a)** The time variation of the humidity and the voltage readout from the sensor. **b)** The measurements from **a)** plotted as sensor response as function of humidity.

Figure 3.5 shows the response of the polymer-sensitised Biosensor chip towards humidity variations. The polymer coating was approximately 10 μm thick. A voltage increase is seen, in agreement with the expected swelling of the polymer.

At the highest humidities there seems to be a saturation which could be due to a stress release, plastic deformation of the polymer. The data for the humidity increase from 60 to 65% were collected over $\sim$ 1.5 hours, so the 'relaxation' could also be due to drift in for example the temperature of the system. The maximum signal of 11 mV translates to the significant surface stress of 43 N/m corresponding to a 4.3 MPa compressive stress in the polymer[6], for an estimated polymer thickness of 10 μm. There is a notable delay in the response of the sensor and the response is non-linear for large variations in the humidity (figure 3.5.b). This could be because it takes some time for the water to reach equilibrium conditions in the polymer and for the stress to develop.

The polymer functionalised cantilever works as a sensor of water vapours. The response is not linear, probably due to relaxations in the polymer on timescales longer than the humidity variation. It is seen that the humidity should be controlled in sensing measurements using this resist.

3.4 Alcohol Measurements

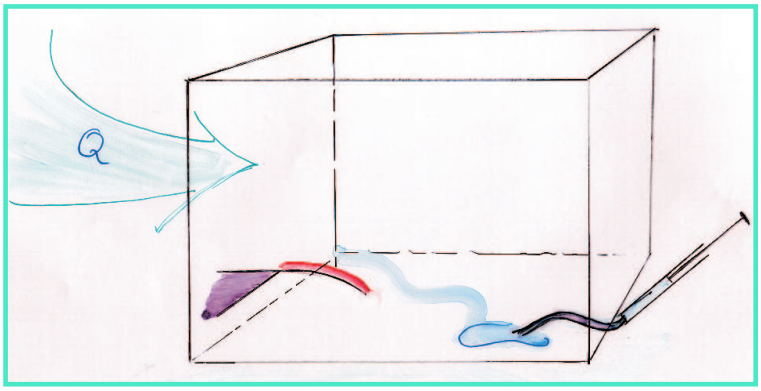

Figure 3.6: Principle of the alcohol measurements: A droplet of alcohol is lead into a chamber (30 l) through which there is a flow of nitrogen gas (Q). The response of the sensor to the evaporating droplet is observed.

We measured the response of the resist-coated cantilever to different amounts of the same alcohol and to the same amount of three different alcohols. As we have seen above, the polymer coating is sensitive to water vapour and as the humidity sensitivity was lowest at low humidities (figure 3.5), so humidity levels were kept low and constant, with a dry nitrogen flow: in all experiments, $3 \pm 0.5\%$. Liquid alcohol was led onto a ceramic substrate in the chamber approximately 2 cm from the sensor using a syringe and Teflon tubing. The cantilever response was recorded over time as the output voltage from the Wheatstone bridge. In figure 3.7.a the measured time response, due to the stress change in the polymer film,

[6]Using the conversion factor for the Poly5 type chip from table 2.1

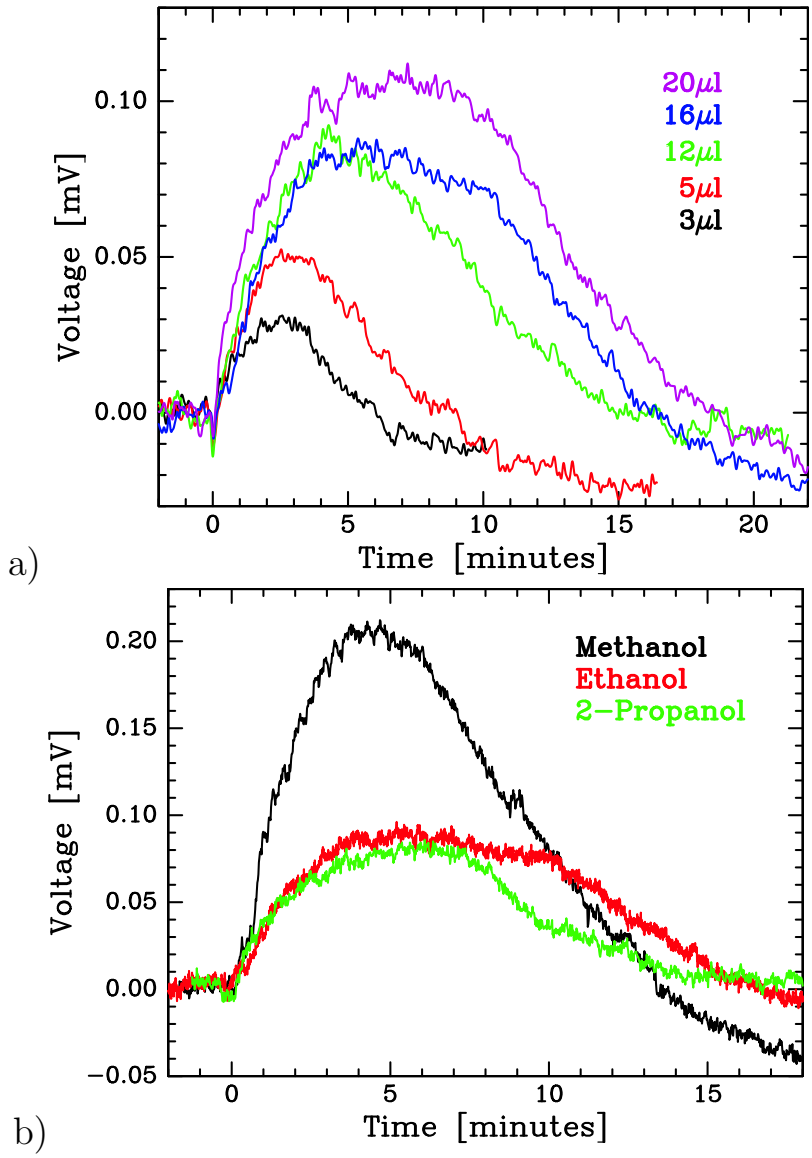

Figure 3.7: The response of the sensor with, one resist-coated cantilever, subjected to **a)** the evaporation of between 3 and 20 μl ethanol and **b)** 16 μl of three different alcohols. All curves are shifted so the injection of alcohol is at time zero and zero mV.

is plotted for five different amounts of ethanol (3, 5, 12, 15 and 20 μl) injected at time zero. The offset is for each measurement adjusted to zero at the time of alcohol injection.

As the amount of ethanol is increased, the maximum of the cantilever signal increases and the time it takes for the signal to reach its maximum value also increases. A change of the signal of 0.1 mV corresponds to a surface stress change of 0.4 N/m (table 2.1). The response of the cantilever towards alcohol was reproducible to better than 10% as measured from the difference in the maximum

peak height. Most of this variation is expected to be due to the manual control of the injection of the alcohol.

When injecting 16 μl of different alcohols, figure 3.7.b, different cantilever responses are observed, as also reported by Lang and co-workers [42]. Measurements are presented on 16 μl of methanol, ethanol and propanol. Methanol, which has the lowest molecular mass and the highest vapour pressure, gave rise to the fastest and largest cantilever response. The response to ethanol and propanol are similar and the maximum response was about half that of methanol.

Note, the signals have been inverted compared to the previous temperature and humidity measurements. This means that the stress in the resistor is compressive. It is not clear why this should be the case. The back sides of the cantilevers are the same so we need to consider only what is going on on the two front sides. The measurements were performed in very dry conditions, and the polymer had been drying out for weeks at 3% humidity. The bridge-offset had over two weeks slowly drifted from 6 mV to stabilise around 12 mV, corresponding to a surface stress change of $\sim$ 24 N/m. Under these conditions also small increases in the humidity gave rise to a compressive resistor stress. The polymer layer on the sensor used in these measurements was quite thick more than 50μm, lending a significant moment to the effect of the stress in the dried out polymer. The neutral axis of the system could have shifted significantly due to this stress. If the neutral axis had shifted to the opposite side of the resistor, a swelling of the polymer layer would cause a compressive stress in the resistor (equation 2.1.5). Estimating the polymer layer to be 10 μm thick and using equation 2.1.4 and the tabulated structure of the AFM sensor (table 2.1) we found that the neutral axis would have shifted to the middle of the resistor at a polymer stiffness of 1.7 GPa. For comparison Young's modulus of the polymer SU8 is 4.4 GPa[7] which would place the neutral axis in the polymer itself.

3.4.1 Model

Several publications have appeared on cantilever based absorption measurements similar to the ones above [16, 55, 58]. However, no quantitative interpretation of the observed signals has been proposed. In an effort to understand the signals and get an estimate of the sensitivity of our sensor we developed a simple model. The model describes the alcohol concentration in the measurement chamber as a function of time due to evaporation of a small droplet and the through flow of carrier gas.

When a drop of liquid alcohol is injected into the chamber, the alcohol will evaporate and give rise to a time dependent concentration of alcohol vapour in the chamber, $n(t)$. The change in the molecular concentration of gaseous alcohol in the chamber is described by the rate of evaporation of the alcohol from the

[7] http://www.somisys.ch/properties.htm

drop minus the flow rate out of the chamber, due to the constant through-flow of the carrier gas

$$\frac{dn}{dt} = \frac{1}{V}\left(Q_{AM} - n\,Q_0\right) = \frac{Q_{AM}}{V} - \frac{n}{\tau_0}\,, \tag{3.4-0}$$

where Q_{AM} is the molecular flow of alcohol from the evaporating drop, V is the volume of the chamber, Q_0 is the volumetric flow of the carrier gas and $\tau_0 = V/Q_0$ is the residence time of the system. As the surface area of the droplet decreases the alcohol flow decreases. The model is shown schematically in figure 3.8.

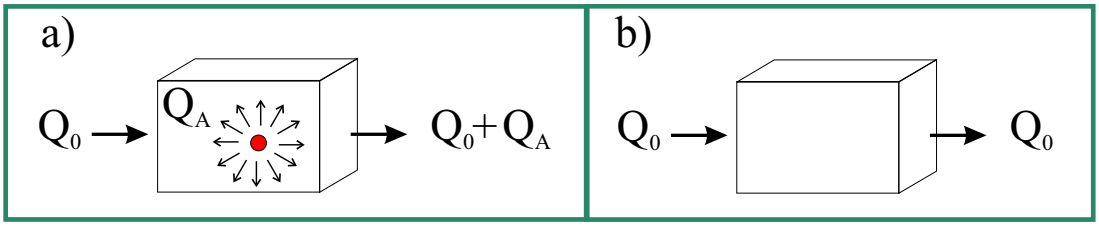

Figure 3.8: Sketch of the evaporation model. **a** shows the situation while the droplet is evaporating and there is a molecular flow of alcohol from the droplet surface. **b** is the case where the droplet has evaporated and the concentration decreases due to the through flow of gas, Q_0.

To solve equation 3.4.1 we first find the time dependence of the molecular flow of alcohol, Q_{AM}, from the mass balance of the drop as it shrinks

$$\frac{dm}{dt} = -Q_{AM}M, \tag{3.4-0}$$

where m is the mass of the drop and M is the molecular mass of the alcohol.

We assume that the injected liquid alcohol forms a spherical drop and that Q_{AM} is diffusion limited in a boundary layer around the drop. At low vapour concentrations the diffusion coefficient, D, can be assumed to be concentration independent, and when the diffusive layer extends to distances far larger than the radius of the drop the mass loss rate, dm/dt, can be approximated with an expression due to Langmuir [59]

$$\frac{dm}{dt} \approx -4\pi D n_{eq} R_s M\ . \tag{3.4-0}$$

R_s is the radius of the surface of the drop and n_{eq} is the molecular alcohol concentration of saturated alcohol vapour with equilibrium vapour pressure $P_{eq} = n_{eq}kT$, where k is Boltzmann's constant and T the absolute temperature. The diffusivity is calculated from $D = 1/3\lambda\bar{v}$, where $\bar{v}$ is the average molecular velocity in one direction and λ the mean free path in air at ambient conditions ($\sim 70nm$). From kinetic gas theory $\bar{v}$ is given by $\bar{v} = \sqrt{8kT/\pi M}$.

The mass of the drop is $m = 4/3\pi R_s^3 \rho$, where ρ is the density of liquid alcohol, hence

$$\frac{dm}{dt} = \frac{4}{3}\pi\rho\frac{dR_s^3}{dt} \ . \tag{3.4-0}$$

Combining equations 3.4.1 and 3.4.1 we obtain a differential equation in R_s which has the solution

$$R_s^2 = R_0^2 - (2Dn_{eq}M/\rho)t \ . \tag{3.4-0}$$

R_0 is the initial radius of the drop and at $t_0 = R_0^2\rho/2DMn_{eq}$ the drop has completely evaporated. Using equations 3.4.1 and 3.4.1 to express $Q_{AM} \approx 4\pi Dn_{eq}R_s$ and inserting the expression for R_s, given by equation 3.4.1, we obtain the time dependence of the molecular flow of alcohol

$$Q_{AM} = 4\pi R_0 Dn_{eq}\sqrt{1 - t/t_0} = Q_{AMax}\sqrt{1 - t/t_0} \ . \tag{3.4-0}$$

With this relation we may finally solve equation 3.4.1 and obtain an expression for the time dependence of the molecular concentration of alcohol vapour in the chamber.

While the drop is evaporating, $Q_{AM} > 0$ and $t \leq t_0$ (figure 3.8.a), and with $n(0) = 0$ we obtain

$$n(t) = \frac{Q_{AMax}}{Q_0}\ \exp(1 - t/\tau_0)\int_0^{1/\tau_0}\exp(u)\sqrt{1 - u\tau_0/t_0}\,du \ ; \qquad t \leq t_0 \ . \tag{3.4-0}$$

This integral can not be solved analytically, however it is easily evaluated numerically. For $t \geq t_0$ the drop has evaporated, $Q_{AM} = 0$ (figure 3.8.b), and with the initial condition $n = n(t_0)$ the solution to equation 3.4.1 is

$$n(t) = n(t_0)\ \exp(-(t - t_0)/\tau_0) \ ; \qquad t \geq t_0 \ . \tag{3.4-0}$$

Equations 3.4.1 and 3.4.1 describe the concentration of gaseous alcohol in the chamber as a function of time during and after the alcohol evaporation. Note that the model contains no fitting parameters.

3.4.2 Instantaneous absorption

In figure 3.9.a the measurements of the response to different amounts of ethanol (figure 3.7.a) have been plotted together with the alcohol evaporation model, equations 3.4.1 and 3.4.1, in terms of the partial pressure of alcohol in the chamber (the smooth lines and the right axis). The alcohol parameters used are listed in table 3.1. What must be fitted is the proportionality between the partial pressure and the voltage output from the sensor. In figure 3.9.a and b the proportionality factor is 70.

The agreement between experiment and model suggests that we are not detecting the diffusion of alcohol in the resist film. Rather, on the time scale of the

	Molecular weight (M) $1.66 \cdot 10^{-27}$ kg	Density (ρ) kg/m^3	Equilibrium pressure (p_{eq}) kPa
Methanol	32	791	19.7
Ethanol	46	785	9.0
2-propanol	60	785	7.8
1-propanol	60	804	4.2
Butanol	74	810	0.8

Table 3.1: Alcohol properties at standard ambient temperature and pressure

experiment, the resist seems to respond instantaneously to the alcohol concentration. The cantilever deflection can therefore be interpreted as a direct measure of the alcohol concentration in the chamber. Thus for 20 μl of liquid ethanol the maximum vapour pressure of alcohol is approximately 7 Pa. From figure 3.9 it is seen that a change in alcohol partial pressure of 1 Pa, corresponding to a sensitivity of 10 ppm, is resolvable. In the tail of the measurements there is a significant discrepancy between the model and the experiment. The measured response does not directly stabilise at zero but overshoots, corresponding to further contraction of the polymer. Full reversibility is reached after about an hour, when the signal returns to its initial value.

Figure 3.9.b shows the measurements of methanol, ethanol and 2-propanol, together with the evaporation model with the different alcohol masses and vapour pressures from table 3.1 inserted in the evaporation model (figure 3.9.b), smooth curves). The correspondence is still fair, but less convincing than for the different amounts of ethanol.

In the case of methanol part of the discrepancy can however be due to an increase of humidity connected to a methanol injection. The humidity levels recorded during the alcohol evaporations are shown in figure 3.10. The humidity scale on all the graphs is the same (0.1% top to bottom). An increase is seen in the methanol measurement which is absent in the measurements of ethanol and propanol.

It seems the resist-coated cantilever reacts in the same way to the different alcohols and simply monitors the concentration of alcohol vapour in the chamber. Different alcohols seem to be distinguished by this technique due to their different evaporation rates and not because of different diffusion behaviours or chemical reactions in the resist film [42]. The timescale for alcohol diffusion in a 10 μm resist film is expected to be in the sub-second range [60]. Hence, in order to study diffusion in the resist and not in the flow chamber, the response time of the measuring system should be considerably reduced. The response time can be tuned by changing the volume of the measuring chamber and the flow rate of the carrier gas, which determine the system residence time. The behaviour in the tail of the measurements might indeed be due to more complex chemical processes in the film. Measurements at fixed times in the tail of the response for

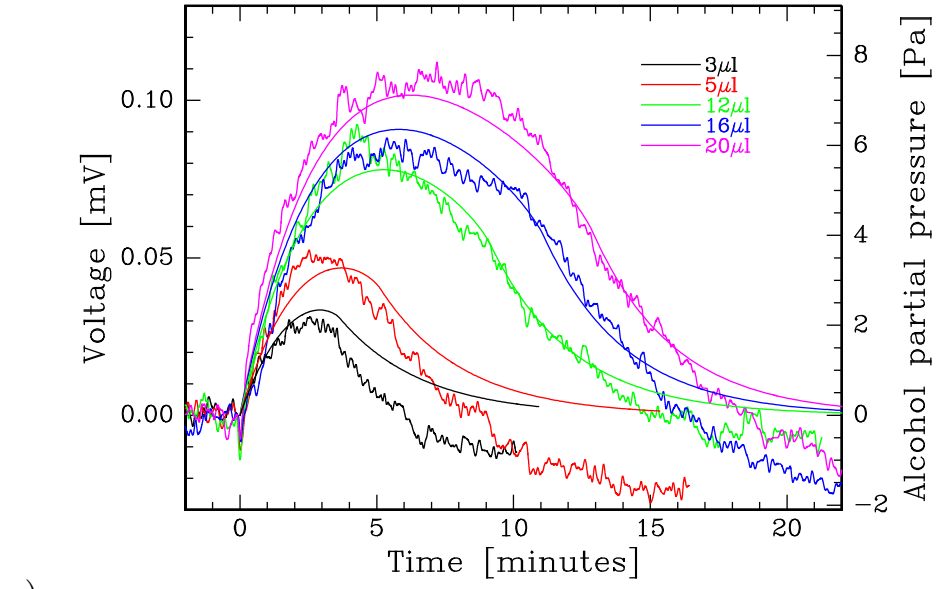

a)

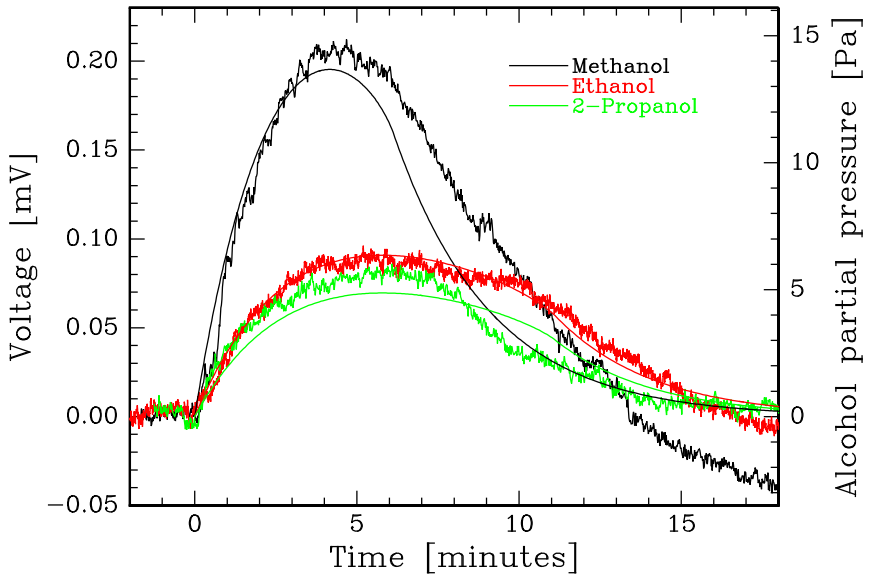

b)

Figure 3.9: The response of the sensor in figure 3.7 has been plotted with the alcohol evaporation model equations 3.4.1 and 3.4.1 (smooth curves). **a)** shows the measurements of different amounts of ethanol and **b)** the measurements on different alcohols.

different polymers and vapours have indeed been used by Baller et al. in an effort to achieve enhanced identification of the alcohols using a principal component analysis [55].

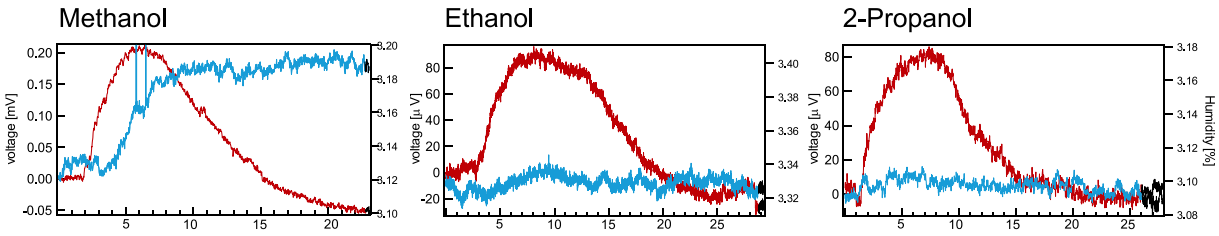

Figure 3.10: Humidity levels during alcohol measurements (Alcohol measurements in red, humidity blue line). The scales of the humidity are the same on all three graphs (full range 0.1%)

3.5 Further studies

The work on alcohol measurements was carried out in further detail by Louise Nygaard Christensen under my supervision [61]. We investigated the effectiveness of the reference cantilever now that the sensing lever was coated with a relatively thick polymer layer and the sensitivity dependence on the thickness of the polymer layer. The temperature dependence and long and short time reproducibility were verified to obtain information about possible 'memory' effects of the polymer, induced by plastic deformation.

The volume of the reaction chamber was reduced by three orders of magnitude to investigate the volume dependence of the signals. The new setup is shown in figure 3.11. The measurement chamber was a plastic tube with a volume of 0.40

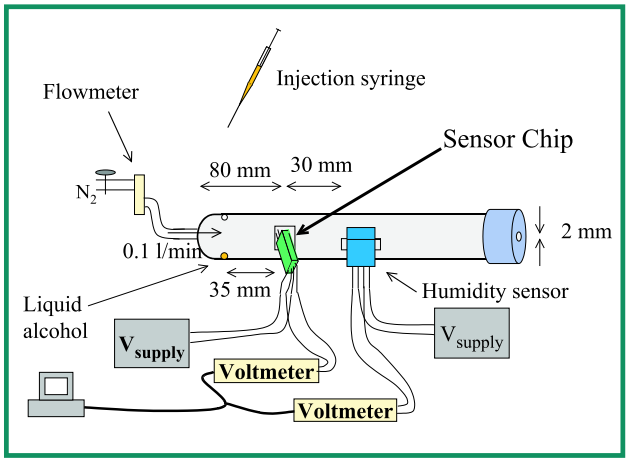

Figure 3.11: New Set-up for gas absorption measurements

l. Liquid alcohol was injected through a small hole in the top of the tube and the droplet deposited on the floor of the tube. A constant flow of nitrogen was flown through the tube to stabilise the conditions. In order to observe a signal it was however necessary to also decrease the nitrogen flow rate by two orders of magnitude compared to the previous measurements so with a nitrogen gas

flow of 0.1 l/min the Reynolds number was approximately conserved. There was no flow diffuser at the inlet and it turned out that the assumption of mixing in the chamber no longer applied. Also, the tubular shape of the chamber and the issuing parabolic flow profile gave rise to very long residence times of the injected alcohols. The humidity in these experiments was 10-15% and all experiments in this section were performed with the Poly5 type chips (table 2.1).

Series were made for different amounts of different alcohols and the influence of the flow rate was measured. The measurements were highly reproducible and for all alcohols a clear scaling was found with the injected amount of alcohol. However, the behaviour turned out to be poorly described by the simple evaporation model used above and the behaviour was not captured in a modified model.

The stress in the resistor was in these experiments found to be tensile, as expected from an expansion of the resist absorbing alcohol, but opposed to the compressive stress observed in the studies presented above (section 3.4). This can be due to a number of factors among which a thinner polymer layer and a higher humidity level, leading to a softer polymer, are probably the most significant. The combined effect would decrease the polymer induced shift of the neutral axis.

3.5.1 The on-chip filter

Earlier it has been shown that the on-chip Wheatstone bridge efficiently reduces the non-linearity of the response with respect to applied voltage [36] and temperature drift over hours [2]. It is not obvious that, with the polymer layer on the measuring cantilever, the uncoated reference cantilever would be an effective reference. The efficiency of the uncoated reference and the on-chip Wheatstone bridge was tested by measuring the voltage change over each of the two substrate resistors separately (figure 3.12.**a** and **b** and the accompanying sketch). A separate measurement was performed using the on-chip configuration (figure 3.12.**d**). Two μl of methanol was introduced at time zero. It is seen that only the resist-coated cantilever responded to the alcohol. The difference of the two data-sets **a** and **b** ($V_A - V_B$ figure 3.12.**c**) already reduces the noise level, which tells us that the polymer does not significantly change mechanical properties of the cantilever. Finally, the total noise reduction from measurement **a** to using the whole on-chip configuration **d** is a factor 25.

An ideal reference would be a cantilever coated with a polymer, of properties similar to the photoresist though not responding to alcohol vapour. However, these measurements show that the untreated reference cantilever already makes an important reduction of the noise level.

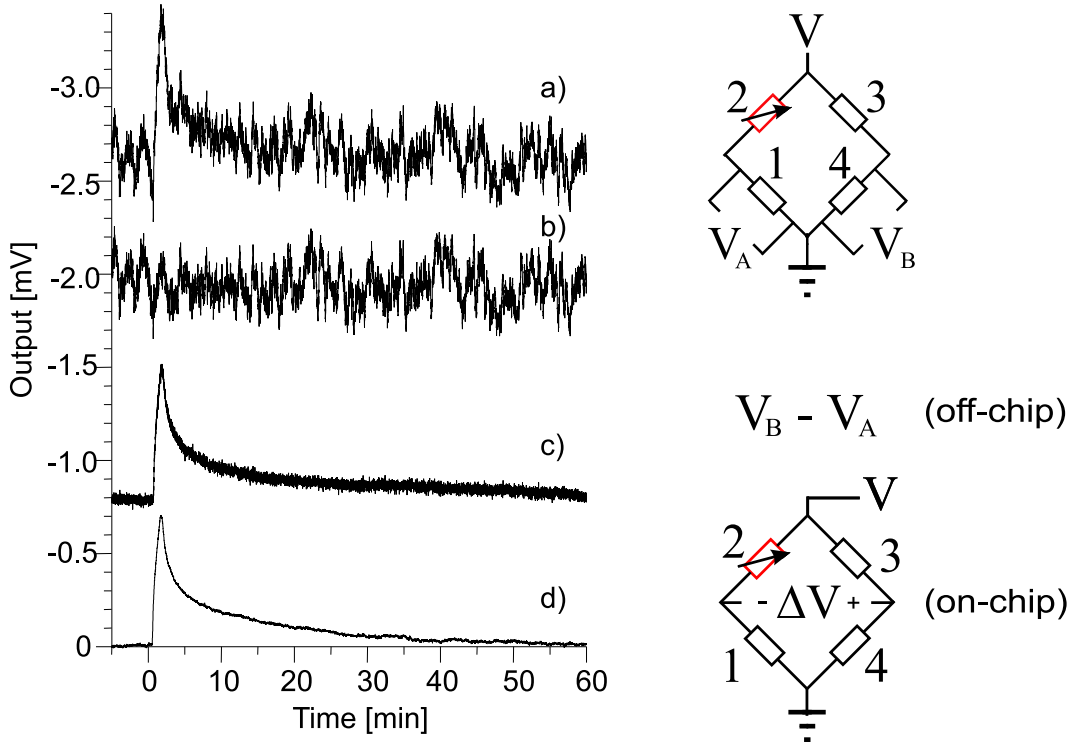

Figure 3.12: Signal to noise increase using the on-chip reference cantilever and Wheatstone bridge. Two μl methanol is introduced at time zero. **a**) the signal from the polymer-activated cantilever, V_A. **b**) is the simultaneous measurement on the reference cantilever, V_B, and **c**) is the difference between the data **a**) and **b**). **d**) is the signal obtained using the on-chip Wheatstone bridge configuration, ΔV. The curves are shifted vertically for convenience. The sketches show the set-ups for the measurement of curves **a**), **b**) and **d**).

3.5.2 Temperature

A temperature variation over a day and the corresponding sensor signal are shown in figure 3.13. The temperature changes were due to sun shining directly on the setup in the morning. A change in humidity was connected to the temperature change, but this was delayed by 4 hours in the chamber with respect to the temperature. We concluded that the sensor signal in figure 3.13 was mainly due to the temperature change. The sensitivity was 4K/mV, or 1 (N/m)/K, corresponding to an expansion and a compressive stress in the polymer. In conclusion, the reproducible detection of signals of the order of 0.05 mV, with this sensor, require a temperature stability of 0.2 K during the measurement. This is regularly obtained, thanks to the constant nitrogen flow.

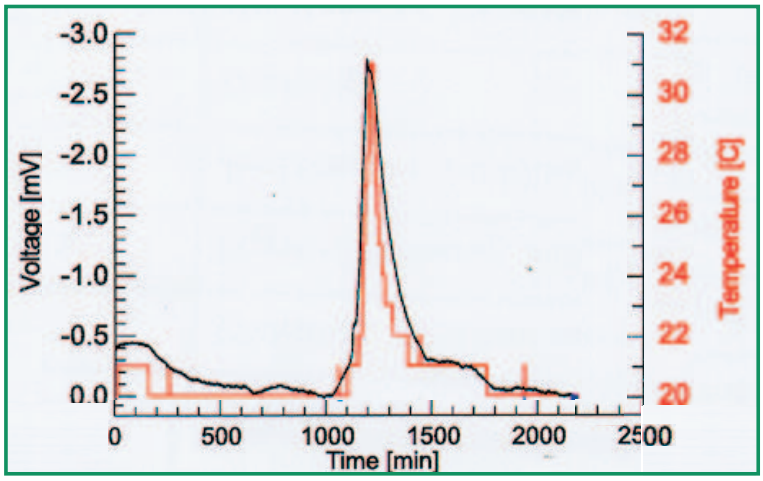

Figure 3.13: Temperature dependence of the resist. Here daily variations due to the sun heating the set-up in the morning.

3.5.3 Flow conditions

The sensitivity with respect to the injected amount of alcohol was, not surprisingly, increased at lower flow rates, confirming a dependence on absolute concentration. The simple evaporation model developed for the larger system (section 3.4.1) could not directly be applied. With the flow rates and the geometry in the small chamber the flow was closer to laminar and mainly diffusive mixing occurred. The signals obtained were highly dependent on wether the alcohol was introduced up stream or down stream from the sensor. Furthermore, the flow profile in the tube was expected to be parabolic. This gave rise to very long residence times, which were seen in the long tails of the signals (for example in figure 3.12). The evaporation profiles and the low degree of mixing in the second flow chamber made the time evolution of the alcohol concentration at the sensor quite complicated and a model that perhaps could have given a further understanding of the processes involved in the signal generation was not developed. No direct estimation of the sensitivity in terms of alcohol concentration was obtained.

3.5.4 Reproducibility

Reproducibility to within 5% was obtained for the magnitude and shapes of the signals from the introduction of alcohol also when repeated over periods of two months. Figure 3.14 shows four measurements of injections of 2 μl methanol, three within 10 days and the last one two and a half months later (28/2). Most of the uncertainty is expected to lie in the control of the amount of injected alcohol, which was performed manually. In the case of the last measurement it seems that also the time constants have changed a little. This could be caused by a slight shift in flow rate.

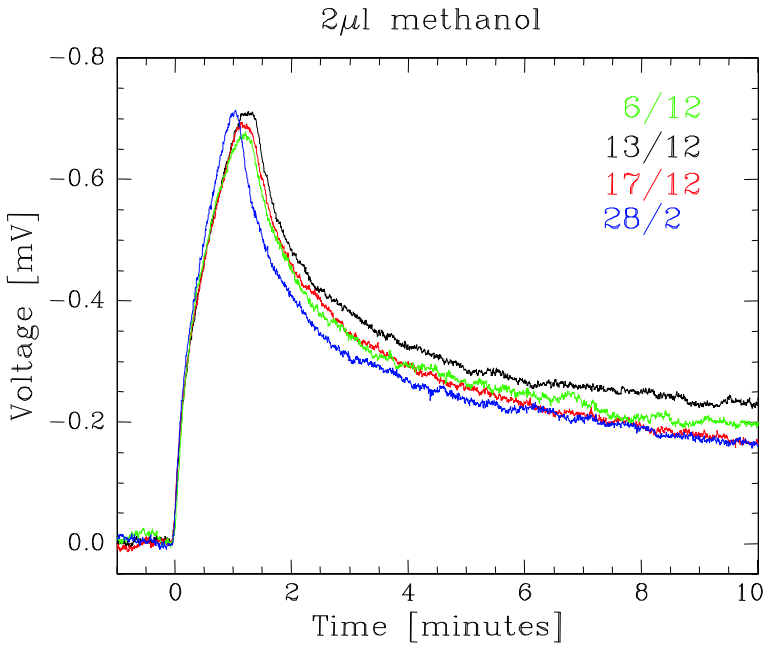

Figure 3.14: Four measurements for response to the injection of 2 μl methanol.

3.5.5 Different Amounts and Different Alcohols

Measurements of the reaction to five different alcohols were performed. In figure 3.15 the data from the injection of 3 μl of the alcohols methanol, ethanol, 1- and 2-propanol and butanol are shown. Compared to figure 3.7.b one can see that the behaviour has a different character, both quantitatively and qualitatively. Series of different concentrations of the different alcohols were made. As an example the series for ethanol, which also can be compared to figure 3.7.a, is shown in figure 3.16. A marked difference in the shape of the curve is noticed. All the alcohols showed scaling with volume in maximum peak height and time to reach the maximum. It was seen that the evaporation model from section 3.4.1 did not adequately describe the new system. Investigation of the alcohol properties in table 3.1 show that the sensor responses are not obviously explained from pure evaporation and diffusion characteristics of the alcohols. This is especially clear when comparing butanol and 2-propanol, which here have very similar initial response although according to equilibrium pressures and densities the response from butanol would be expected to be far weaker and slower.

3.5.6 Polymer thickness

The effects of different thicknesses of the polymer coating was investigated. Two different sensor chips prepared with polymer layers of different thicknesses were each subjected to 2 μl of methanol (figure 3.17). It was found that an approximately 4 μm layer increased the sensitivity by a factor of 7 compared to a very

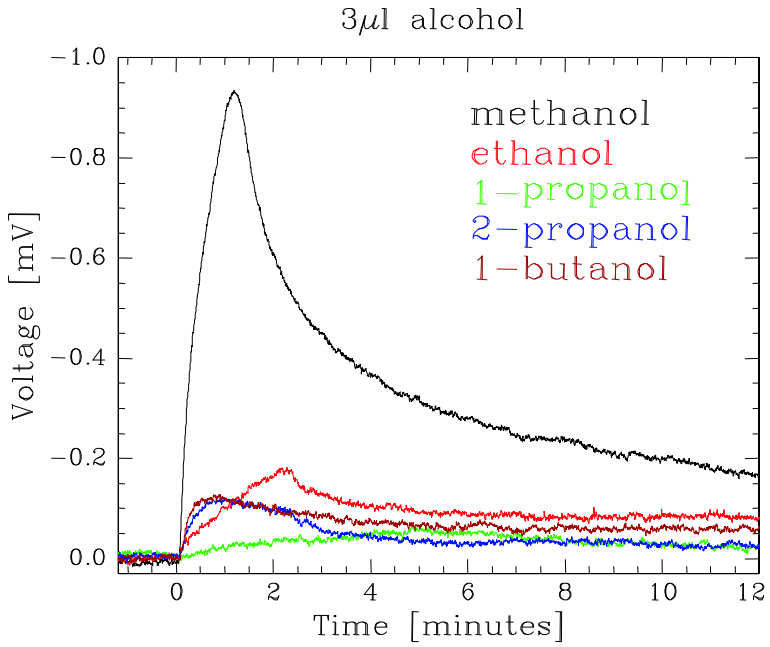

Figure 3.15: 3 μl of five different alcohols have been injected.

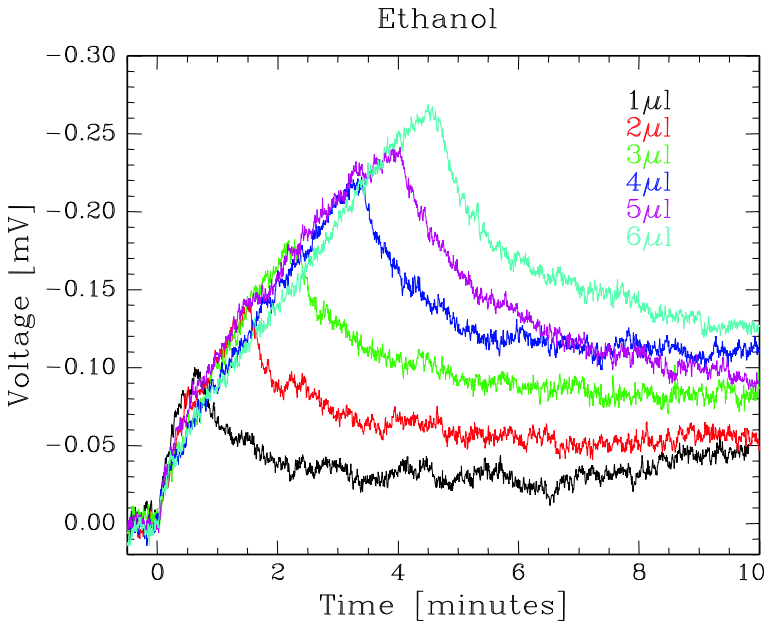

Figure 3.16: Different volumes of ethanol injected

thick layer (around 50 μm). The noise level and the reproducibility remained the same. Apart from the difference in peak height (maximum surface stress) it is also seen that the thinly coated sensor reacts faster than the one with thicker coating. The signals are in both cases highly reproducible, subtracting a slowly varying offset, and the noise levels are the same. Larger sensitivity towards vapours for

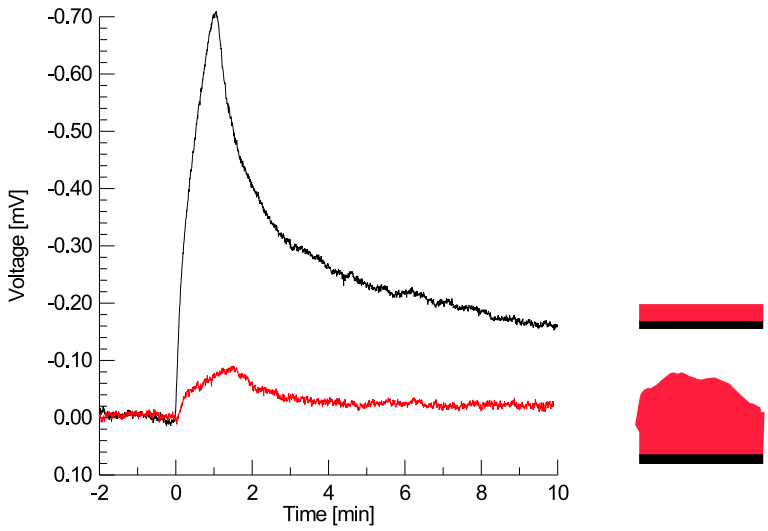

Figure 3.17: The graph shows the signal from two different sensors following the injection of 2 μl of methanol. The black curve, with the high peak, is the signal from the same sensor as in the figures 3.12, 3.14 and 3.15. The coating of the cantilever that gave rise to the red, small curve was similar to the thick coating one used in the measurements in the figure 3.7.

thinner polymer films has also been reported by Thomas Betts et al. [62]. They used polymers applied as stationary phases in polymeric chromatographic and investigated layer thicknesses 10-100 times thinner than the ones used above.

Two questions that arise are: First, the surface stress σ_s is related to the stress in the polymer film σ_F by $\sigma_s = \sigma_F \times t_F$ so if the stress in the film would be the same for a given alcohol concentration, then the thicker film should give rise to the largest signal. On the other hand, in a thicker film the contact area between the cantilever surface and the film is relatively smaller than in the case of a thinner film so less of the stress in the film is transferred to the cantilever. This could be a reason that a smaller surface stress signal is observed. Second, the thicker layer shows a significantly longer reaction time. This could be an indication that the dynamics we are seeing are connected to processes in the polymer film. As mentioned earlier (section 3.4.2) diffusion times are expected to be under a second. Perhaps the slow processes observed could be due to some gradual redistribution of stress in the film.

3.6 Discussion

3.6.1 Recent developments

One can renounce the attempt at a detailed understanding of the processes on the cantilever and use a neural network to recognise patterns associated with each

of the vapours of interest. Exploiting the possibilities of multiple sensitivities of a multi-cantilever array, functionalising the cantilevers with different polymers and multiplexed detection scheme, Marco Baller and colleagues trained a neural network to discriminate between complex odours such as natural flavours [55].

Battiston and co-workers developed simultaneous dynamic and static measurements [58]: in a dynamic measurement the AC component, containing the information on shift in resonance frequency, was separated from the DC, deflection sensitive part. This means the changes in mass and stress could be compared. This could shed light on what kind of processes are actually involved in the generation of the surface stress change. Also, one could separate reactions in the polymer from vapour concentration changes by a simultaneous, independent monitoring of the alcohol concentration with a conventional sensor.

The group of Prof. Baltes has been working on a highly integrated, multitasking, cantilever based gas sensor chip with a CMOS amplifier, on-cantilever Wheatstone bridge and several cantilevers for simultaneous detection of capacitance, mass and heat changes [18].

A paddle array of cantilevers developed for the detection of mass changes in samples placed on platforms at the end of long thin cantilevers, has been presented by B. H. Kim and collegues [63].

Inverting the problem, T. L. Porter et al have made direct swelling investigations by placing the tip of a (piezoresistive) AFM cantilever on top of a microscopic sample of polymer [64].

We have seen that many possibilities for the increased sensitivity and further refinement of this absorption based gas sensor development exist. However, we did not pursue this study of the Biosensor further as we were eager to test the sensor in the liquid environment. Due to considerations of for example changes in refractive index we expected the advantages of an integrated electrical, compared to an external, optical readout to be significant in such applications. Furthermore, the potential applications are plentiful and exciting.

3.7 Conclusions

The Biosensor chip has a good design for cantilever-based sensor applications. The sensor was used to investigate the response of a resist-coated cantilever to water and alcohol vapours.

We saw that the reference cantilever and the Wheatstone bridge arrangement reduced the noise level by a factor 25.

The mechanisms giving rise to the surface stress changes were in case of a thick, dry polymer directly described by the concentration of alcohol vapour, independent of the type of alcohol. A simple evaporation model described well the response observed in the alcohol measurements in a chamber with good mixing, and we conclude that the sensor monitored the instantaneous alcohol con-

centration in the measuring chamber. Based on this we deduced that alcohol concentrations of 10 ppm can be detected.

The response discriminated between different alcohols in this case not because of alcohol specific differences in the response of the polymer film, but rather due to differences in the evaporation rates of the alcohols. This turned out perhaps to be a special case: the response displayed highly characteristic profiles for the different alcohols in the case of a thinner, more sensitive polymer layer. These features were not captured in a simple alcohol concentration model.

Detailed studies under different conditions showed that while the measurements were very reproducible under given conditions, over long times, they depended highly on the thickness and condition of the polymer layer, the flow and mixing conditions of the chamber and the temperature.

The cantilever sensor is thus highly sensitive to the exact conditions of preparation and operation. Very controlled environments and procedures for coating the cantilevers should be developed if one wants to be able to predict and model the response. Alternatively, a neural network trained for each specific case is a possibility.

In a system where the vapour concentrations are well characterised the sensor is a highly sensitive tool for testing the response of the coating towards different environments.

It can not be ruled out that the response is associated with diffusion in the film, but given that the expected diffusion times are in the sub second range and the large qualitative differences in behaviour for thin and thick films, it seems more likely that the surface stress response is linked to subsequent stress redistributions in the polymer film.

Chapter 4

The Tongue – Introducing the liquid compatible sensor

In order to convert the gas sensing 'nose' into a 'tongue' operational in liquid sensing the exposed gold wires of the Biosensor and the aluminum bonding wires connecting the chip to the ceramic substrate (figure 3.1) must be protected from the liquid and a liquid cell with a flow system must be designed. Several coatings of the bonding wires and the chip were tested and the flow system was based on a homemade liquid cell and commercial syringe pumps, tubes and valves.

4.1 Protecting the electrical leads

The protection of the gold leads and bonding wires must be stable towards the chemicals we expect to use in the experiments, notably aqua regia, piranha, water and physiological buffers and also temperature stability up to the maximum cleaning efficiency of piranha, $\sim 60^{o}$C. We are grateful to Espen Friis for recommending to us the vacuum sealing wax Apiezon W[1], which he had previously used for the coating of STM tips [65].

The areas of the ceramic substrate where no wax was desired, that is the back side and where further connections would be made, were protected with heat resistant tape, prior to mounting the sensor chip. The chip was mounted and bonded and the assembly attached to a vertical micromanipulator, the cantilevers pointing upwards (figure 4.1). The micromanipulator was on a table with a heating plate. Wax was heated on the plate till $\sim 90^{o}$C, nearly boiling, and the chip assembly was slowly lowered into the wax under view of a microscope. The hot wax was pulled up the chip by surface tension and the chip was pulled out of the wax as soon as the wax reached the top of the chip, but before it spread

[1] Apiezon Wax W, Ax-Lab A/S, Strandboulevarden 64, DK-2100, Copenhagen Œ, Denmark.

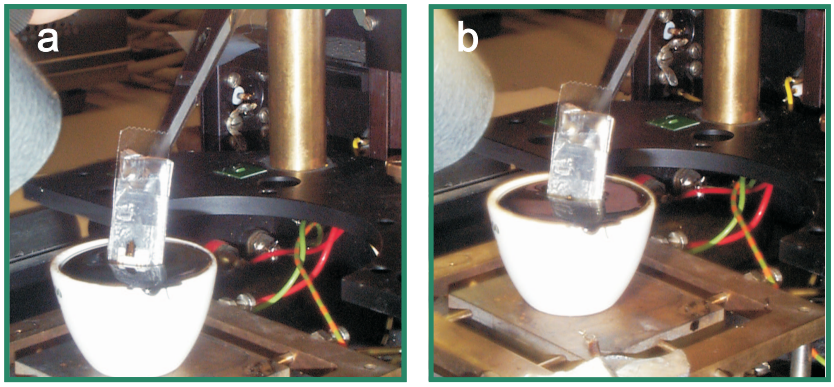

Figure 4.1: The chip, mounted on a ceramic substrate and bonded, is dipped into molten vacuum sealing wax using a micro manipulator. The process is followed through a microscope so the coating can be stopped before the wax flows onto the cantilevers.

out on to the cantilevers. The process was often repeated several times to get a good coating layer and to ensure the protection of the bonding wires.

The resistors on the cantilevers were protected in fabrication by a SiN layer on top (figures 2.2 and 2.9). A layer of insulating SiO directly under the resistors is a poor diffusion barrier for especially NaCl, but is followed by a thin, but effective Si barrier. On some chips, however, the protective Si layer had been partially etched away and this might be one of the reasons that some chips turned out to be very unstable in liquid.

This protection strategy worked very well in water but in buffers with detergent, as used in DNA hybridisation (section 5.2), bubbles were generated at the edge of the chip, typically near the attachments of the cantilevers to the substrate.

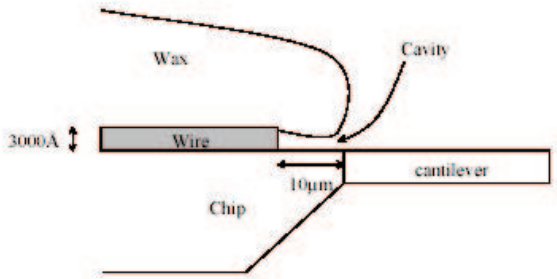

Figure 4.2: A breakdown of the resistors on the chip is preceded by generation of bubbles at the edges of the wax on the front of the chip. This could be due to a cavity as indicated in this sketch [44].

After trying several different adhesion enhancing cleaning steps (piranha and

HMDS[2]) with little effect and several different coating materials (epoxy glue, paraffin wax, beeswax and nail polish) without success, it was concluded that adhesion was not the problem. The reason was probably in the structure of the chip at the very top edge: the 300 nm thick gold leads run at a distance of 10 μm from the edge of the chip and are made by a lift off process which creates a steep step (figure 4.2).

When the voltage over the bridge is high and the gas production therefore large it is seen that the jet of bubbles comes out close to the cantilevers and in plane with the chip. The reason proposed was that the surface tension of the wax made it very difficult to seal the outer edge of the lead. As long as the chip was operated in DI water the surface tension and the low conductivity of the water made the protection sufficient, but once the surface tension was broken with detergent the water could brake into the cavity and electrochemical etching of the gold wires would proceed fast.

Several more sophisticated coating possibilities were investigated by other members of the bioprobe group, notably electrodepositable photo resist (EAGLE 2100 [44]) and batch processes such as tantalum oxide and silicon nitride [37]. This is an ongoing effort, as chips fabricated with protected leads would make preparations much simpler and greatly increase the yield, but the short term solution turned out to be a redesign of the chip lengthening the SiN protected poly Si leads of the resistors so that all the contacts and the gold leads could be pulled back from the edge of the chip. These are the so called FagPakke chips (figure 2.8, table 2.1).

It was possible to wax-coat these sensors so that they were operational in buffer solutions both for DNA and protein experiments.

4.2 First Liquid Applications

4.2.1 Ethanol in water

The very first measurements using a piezo resistive cantilever in liquid were performed in water and, using a polymer coated resist, the response towards ethanol was tested. A sensor already coated with photoresist (section 3.2) was wax-coated as described above. Electrical connections were made to the gold patterned leads on the ceramic substrate and the coated sensor was mounted the other way round on the micromanipulator used for the coating. A plastic box (1.4 ml) was filled with deionised water (DI) and the sensor was lowered into the water. At contact with the water the polymer swelled and stabilised after about one minute. The sensor showed excellent stability over many hours of immersion in water with a bridge supply voltage of 4 V.

[2]hexamethyl-disilazane: $(CH_3)_3SiNSi(CH_3)_3$.

To test the sensing capabilities of the sensor in its new environment ethanol was injected in the water with a syringe close to the sensor. In figure 4.3 one sees the response of the sensor over time. Different amounts of alcohol were injected, 60,

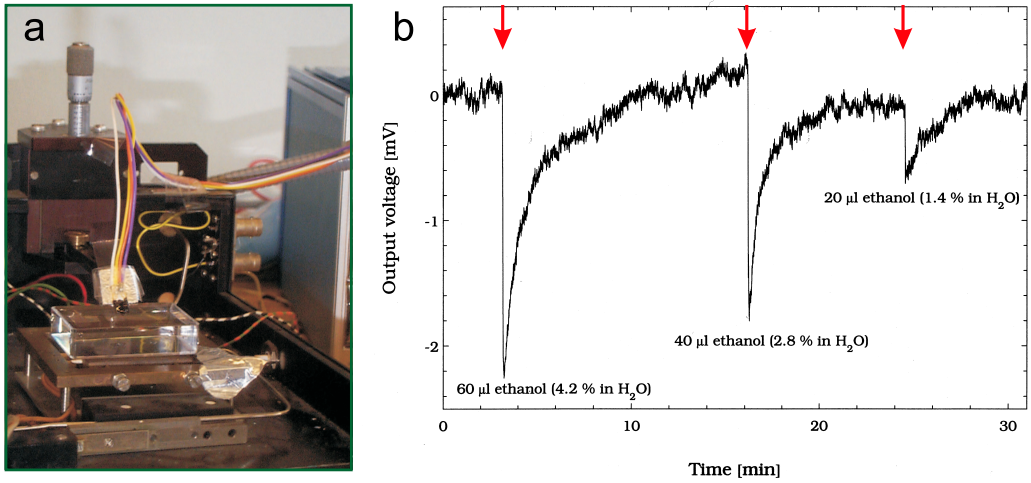

Figure 4.3: The response to ethanol injected into deionised water of a sensor functionalised with resist. The ethanol is injected with a syringe at the points indicated by the arrows – 60, 40 and 20 μl respectively. One can see that both the magnitude and the duration of the response depend on the injected amount [50].

40 and 20 μl, corresponding to respectively 4.2, 2.8 and 1.4 % v/v. The times of injection are marked with arrows. An immediate response of up to 2 mV , in the case of an injection of 60 μl ethanol, is seen corresponding to a contraction, a tensile stress, in the film. After approximately 8 minutes the signal has returned to its initial value. The sensor reacts to the alcohol injection in water as though the resist film is contracting. The alcohol could penetrate the resist and expel some of the water. Ethanol is a larger molecule than water so the response could be due to the difference in surface tension. The surface tension of ethanol is less than a third of that of water. The water could also be sucked out of the resist by a change in osmotic pressure due to change in concentration of ethanol in the water. After injection, it looks like the concentration of alcohol in the water decreases. It is not clear that this would be caused by evaporation of alcohol from the liquid surface[3]. In any event, it seems that the polymer also in water reacts instantaneously to the change alcohol concentration.

This is the first demonstration of a piezoresistive chemical cantilever sensor operating in liquid.

[3]I thank R. Berger for pointing out that this could make beer drinking quite stressful.

4.2.2 Temperature Sensitivity with a Gold Layer

An other, and more reproducible, way to sensitise a cantilever sensor is by coating it with gold. In chapter 5 we will exploit the strong binding between sulphur and gold to create biochemically functional surfaces. Here we will first test the temperature sensitivity of the Biosensor in water when one of the cantilevers is coated with gold and the other is not. When the environment of the chip changes temperature the gold coated cantilever will have an added bimetallic effect compared to the reference cantilever, given by the difference in thermal expansion between the cantilever materials and the gold.

Gold evaporation

Gold coating was performed in an E-beam evaporator[4]. Exploiting the vacuum compatibility of the wax, the gold coating was performed after the waxing, so the front side of the cantilever could be gold coated without short circuiting the gold leads on the body of the chip. To coat only one of the cantilevers with gold, while protecting the other, an integrated shadow mask/holder was made.

First, 100 Å chromium, for adhesion in liquid, was evaporated at a rate of 3 Å/s, then 600 Å gold at a rate of 15 Å/s. The deposition rates were monitored by a quartz crystal gauge.

After evaporation the substrates were stored in DI water until use. This was found to limit contamination of the surface.

This procedure was common to all the different gold substrates prepared also throughout chapter 5.

Temperature Measurement

The temperature measurements were conducted in a 10 ml glass beaker sitting on a hot plate. In the beaker was also placed a K-type thermoelement and a glass thermometer - the latter for calibration of the thermoelement. The temperature at the beginning and the end of the measurements was recorded from the glass thermometer and the behaviour of the thermoelement was considered linear in the measurement range (283-328K).

The wax-coated sensor, with one gold-coated cantilever, was placed in the beaker with thermometer and thermoelement and all was heated to 50°C. The heater was turned off and the setup left to cool. The Biosensor output vs temperature is plotted in figure 4.4. For the lowest 15 degrees there is a linear relation between the temperature and the readout from the Biosensor. The slope of the line is 0.062 mV/°C corresponding to 0.17 (N/m)/K (FagPakke2, table 2.1).

At temperatures above 35°C there are large fluctuations in the measurements. The reason is not clear, but certainly the motions in the water are larger at

[4]Alcatel, E-beam evaporator.

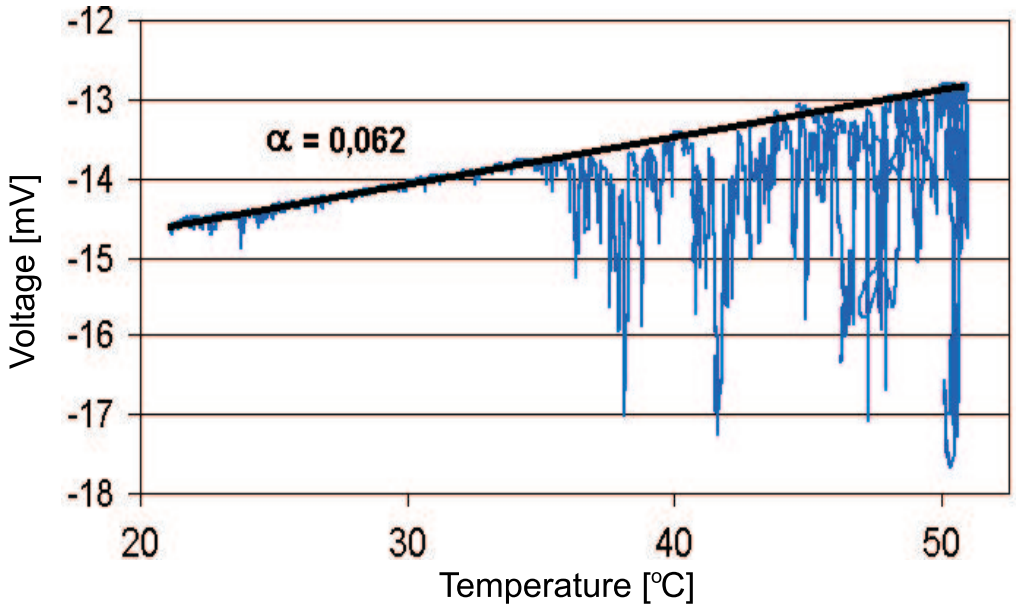

Figure 4.4: A measurement of the response of a sensor with one gold-coated cantilever in cooling water. The slope is 0.062 mV/°C [51].

higher temperature. The cooling from 50 to 35°C took far shorter than the last 15 degrees cooling, which also means less homogenous temperatures. Bubble formation on surfaces were also common at the higher temperatures. However, the fluctuation only go one way with respect to the decreasing temperature.

As we are measuring the difference in stress change on the gold coated cantilever compared to the uncoated reference, the signal is due to the stress generated in the thin gold/chromium film because of the difference in thermal expansion between the cantilever materials and the film. The stress in the metal film can be expressed as

$$\sigma_{Film} = \sigma_{sFilm}/t_{Film} = (\alpha_{Film} - \alpha_{Cant})E_{Film}\Delta T, \qquad (4.2\text{-}0)$$

where σ_{sFilm} is the surface stress of the metal film and $t_{Film} = 700$ Å it's thickness. We estimate the properties of the film by averaging Young's modulus, E_{Film}, and the thermal expansion, α_{Film}, over the thickness of the film[5]. The thermal expansion of the cantilever α_{Cant} is, by weighted average of the layers, estimated to approximately $1 \cdot 10^{-6}$ K^{-1} and using the values from table 4.1, we find $\sigma_{sFilm} =$ 0.09 (N/m)/K. This is approximately half the measured value of 0.17 (N/m)/K, a fair agreement[6].

In measurements performed while heating the water, the linearity was not as good. One factor is that the cooling was slower than the heating so the liquid

[5] $E_{Film} = (E_{Au}t_{Au} + E_{Cr}t_{Cr})/t_{Film}$ and $\alpha_{Film} = (\alpha_{Au}t_{Au} + \alpha_{Cr}t_{Cr})/t_{Film}$

[6] Taking only the gold film into account the estimated temperature sensitivity is $\sigma_{sAu}/\Delta T =$ 0.06 (N/m)/K, a factor 2.6 less than the measured value.

		Au	Cr
Young's modulus (E)	[GPa]	79	279
Thermal expansion (α)	[K^{-1}]	14.2 $\cdot 10^{-6}$	4.9 $\cdot 10^{-6}$

Table 4.1: Young's modulus and thermal expansion of gold and chromium.

temperature was more homogenous and the thermoelement and the cantilevers more likely to be at the same temperature. Another, related, factor is that the cooling happened from all sides whereas the heating was mainly from the bottom enhancing convection. To change this and be able to check the reversibility of the reaction one could use a 'bain-marie' and a better controlled heater.

In conclusion, the sensor with one gold-coated cantilever is temperature sensitive and great care should be taken to have stable temperature conditions when working with such a sensor. The temperature during an experiment should be stable to better than 0.2 K to stay below the typical noise of the cantilever measurements of 10μm (0.03 K to stay below the intrinsic noise of the sensor, $\sigma_s min$, table 2.1).

4.3 Liquid cell and flow system

In order to perform biochemical experiments we wanted to reduce the total volume of the system, limiting reagent costs and reducing reaction times. Small dimensions in the flow system also reduces disturbance due to turbulence by making the flow laminar. We also wanted to be able to change the fluid in the liquid cell while measuring so a flow system was developed. The liquid cell it-

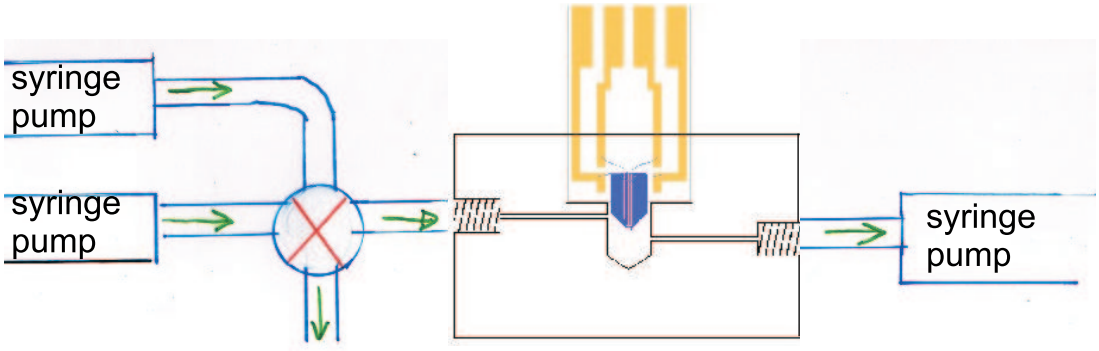

Figure 4.5: The liquid flow cell.

self (figure 4.5) was designed open at the top in order to minimise problems with trapped bubbles in the system. Also, this eliminated the need for electrical feedthrough. The top of the cell was shaped so that it supported the ceramic substrate on which the chip was mounted and could function as a holder. The volume of the reaction chamber was approximately 20 μl. Liquid cells fabricated

in both Teflon and polyetheretherketone (PEEK) were used and worked well, although the larger mechanical stability of PEEK was an advantage for example for cutting treads for nuts, used to connect to tubing and the syringe pumps.

Connectors to the gold leads of the ceramic, amplifiers and digital connections and Labview programs for data collection were developed together with the 'Nanohand' group at MIC.

The open design meant that the flow through the cell had to be maintained by two pumps: one pumping liquid into the cell and another sucking it out again. The pumps chosen, mainly for the reason of low noise pumping and stable flow, were syringepumps[7]. Syringes were bought from MERCKEurolab[8] and 1/16" teflon tubing, μ-fluidic connectors, nuts and flanges etc were acquired from Microlab[9]. With a manually switchable valve[10] the inflow could be switched from the cell to waste. This was used in particular to get rid of bubbles, created when syringes with different solutions were exchanged, and allowed for precise timing of the arrival of the new solution to the cell.

During experiments the chip and cantilevers could be checked visually with a microscope. This was useful also to check the level of liquid in the cell as the pumping was not always perfectly symmetric. Air in the pumping system should be avoided as it caused uneven flow.

The setup was tested for dependence on flow rate and it was seen that the output was very little affected by the stopping and starting of the pumps at relatively low flow rates, $\sim 10\mu$l/min (figure 4.6). At flows of $\sim 100\mu$l/min there was a short stabilisation period of typically 10-20 seconds.

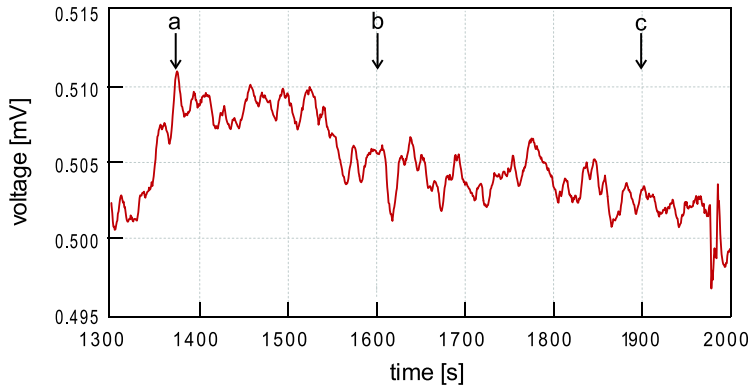

Figure 4.6: The output from the Wheatstone bridge measured at changing flow rates. At a) the pumps are stopped, at b) started at a flow rate of 10μl/min and at c) the flow is stopped again.

On the other hand, mechanical/acoustic shielding reduced the noise level as also,

[7]Harvard apparatus, PHD2000.
[8]Hamilton series 1000 and 1700, type C
[9]MIKROLAB AARHUS A/S, Axel Kiers Vej 34, 8270 Hœjbjerg Århus, Denmark
[10]Also MIKROLAB.

but to a lesser extent, did electrical shielding of the cell and connecting leads. A constant concern was a slow background drift of the signal. In the case of sensors with one gold coated cantilever this drift could easily be caused by small temperature variations (section 4.2.2). However, drift was observed even for some symmetrically prepared sensors. Measurements were started after a stabilisation period, which could vary between 10 minutes and hours depending on the individual chip used and the measurements to be performed. Measurements were started when the drift was less than the expected signal.

4.4 Conclusion

A functional protective coating of the electrical leads of the sensor was developed, which makes it operational the sensor liquid with low concentration of salt and detergent.

The function of the sensor in liquid has been demonstrated by ethanol sensing and by measurement of the temperature sensitivity of a gold coated cantilever. This sensitivity was found to be 0.17 (N/m)/K.

A flow system has been designed, which works as a system for testing the function of the Biosensor chip and makes it possible to change solutions continuously during measurements, without disturbing the sensor.

Chapter 5

The Biosensor

In this chapter we will investigate the use of the Biosensor chip as ... a biosensor. As the cantilevers respond directly to molecular binding on the surface, there is no need for the chemical, radioacctive or fluorescent labels used in common assays. Moreover, the process on the surface can be followed in real time.

Label-free detection of the kinetics of the molecular layers formed on gold can also be studied by various other techniques such as surface plasmon resonance (SPR) and the quartz crystal resonator (QCR). With X-ray photoelectron spectroscopy (XPS), one can study the details of the binding for the molecules to the surface, for example if it really is bound via a gold sulphur bridge, but will not yield further information on the kind of macromolecule is attached. AFM and STM can be used to investigate the spatial structuring of the layers and their stability.

We will look at the kinetics of immobilisation of short DNA probes and the development of an immunosensor for the detection of the bacterium Escherichia coli (E.coli). The biochemical systems and challenges that must be addressed in order to apply the cantilever sensor to microbiological systems will be introduced. The functionality of the systems on different substrates is verified with a DNA-array-like method using fluorescent labels.

We obtained nice Biosensor results from the immobilisation of DNA probes, and we might have detected a signal from the E. coli sensor.

5.0.1 The challenges

In order to detect the molecules of interest, the analyte, one side of the cantilever beam must be functionalised with a detector layer of molecules of specific sensitivity, the receptors. Several factors must be balanced when creating a receptor layer on the cantilever surface that will give rise to a surface stress change when it reacts with its analyte. It is crucial that energy generated by the binding of reacting molecules on the detector is transferred to the underlying surface as effectively as possible. The receptor molecules should therefor be in as rigid contact

as possible with the surface in question while retaining their activity.

Immobilisation

Immobilisation is the attachment of the detector molecule to the solid substrate, here the surface of the cantilever. The binding should be strong to provide stability of the layer and so that release of stress due to reorganisation of the molecules on the surface is minimised. If the bond to the surface, under some conditions, is stronger than the bond with the analyte, this furthermore opens for the possibility of regeneration of the sensor.

We are also concerned to keep the distance between the surface of the cantilever and the point of the interaction of interest as small as possible, to avoid long and floppy molecules and soft layers where there could be possibilities for stress release.

Localisation

Localisation is concerned with the issue that we want at most one of the cantilevers on the sensor to be coated with active molecules, and preferably the active layer should be confined to the upper side of the measurement cantilever.

'In situ' localisation can be obtained by self assembly if one has strong and specific reactions between the cantilever surface and detector molecules. Here we for example investigate the immobilisation of thiolated DNA on a gold surface. With this kind of 'functional' localisation it is possible to follow all steps in the preparation of and detection by the sensor in real time.

Proteins are generally quite sticky so, in this case, the simpler solution is a mechanical localisation where the molecules are printed or sprayed onto the particular area of interest. More and more automated systems become available for this kind of confinement.

Finally, various methods can be used to direct the immobilisation, for example electrochemically [66] or focused light can be used to immobilised a molecule in a specific place [67, 68].

Blocking

Blocking is to prevent non-specific binding of the analyte or other compounds to the non-functionalised surfaces, which would give rise to false signals. Different systems often require different blocking strategies, also because we are interested in making the reference cantilever as similar as possible to the detecting cantilever, while being nonreactive.

While both single and double stranded DNA can adsorb to surfaces by hydrogen bonds, these are normally so weak that they can be washed away by a rinse in deionised water (DI) and perhaps a bit of added detergent.

Proteins adsorb readily and strongly to most surfaces. It is therefore important that all surfaces where one does not want attachment, are blocked from interacting molecules. Normally, this is done by first adsorbing other proteins to the surface. Often the small globular protein albumin, from bovine serum, (BSA) is used but also a solution of skimmed milk powder is effective.

Functionality

The functionality of a layer of immobilised molecules is the ability to specifically bind the analyte. The activity of the molecules after immobilisation must be tested. Factors such as the density of molecules on the surface and immobilisation strategies, influence the ability of the molecules to function. Proteins with advanced recognition sites can be very sensitive towards conformational changes in close interaction with a surface. We used a fluorescence based verification to test the activity of our molecules under different conditions.

Signal generation (stress)

Finally we depend on the generation of a stress signal when the detector layer binds the analyte. We gather inspiration from early work on microcantilevers, especially the first measurements on adsorption of alkane thiols. One must also keep in mind, that a maximum stress signal not necessarily is the same as a large fluorescence signal.

5.0.2 Surface stress and biomolecular surface layers

Stress generation due to the adsorption of macro molecules on a surface is a highly complex matter.

Recently, Guanghua Wu et al. [26] and Lavrik et al. [27] discussed stress generating mechanisms during the formation of the molecular layers on the cantilever surface.

First, the change in the surface free energy is given by [25]:

$$dU = \sum \mu_i dn_i + TdS + \varphi dQ + \gamma^S d\Omega. \tag{5.0-0}$$

The first factor is, the free energy generated due to the binding itself. Stress releasing surface restructuring may take place after the binding, as is seen for example in silicon surface reconstructions. This is contained in the last term. The second term is from the entropy change due to immobilisation and the third the electrostatic energy due to added charges.

Macromolecules have in addition possibilities of conformational changes. They can for example spread out on the surface and proteins can unfold upon contact with a hydrophobic surface. Contraction, relative to the conformation free in solution is also possible [24].

Cross binding between macromolecules on the surface, for example through van der Waals attractions and hydrogen bonding between the molecules, will contribute both with free energy and with stiffening of the layer.

Monolayers of flexible molecules can have important entropic interactions, which can be a very important term if the molecule density is high. This is the case for example in polymer brushes and for some of the thiolated molecules we will be looking at here. A dense monolayer can be formed for example if the affinity to the surface is high for parts of the molecule whereafter the flexible parts must stretch thereby reducing their entropy.

Uniformly charged molecules generate a repulsion in the layer. The electrostatic contribution to the generated stress can be tuned by the ionic strength of the buffer, as ionic screening reduces the decay length of the interaction.

A change in the interaction between the solvent and the surface, a change in hydrophobicity in an aqueous solution for example, will also change the surface energy.

It is not simple to predict what the sum of all this will be in a given situation, and this is a place where a direct, time resolved measure of the surface stress development could be useful.

5.0.3 Langmuir adsorption

The simple Langmuir adsorption model is a very general theory of molecular adsorption on surfaces [14, 69]. It is basically a statistical model based on an assumption of a number of equivalent binding sites, a constant concentration of binding molecules that impinge on the surface with a temperature related rate and stick to the surface with an adsorption probability. The particles adsorbed on the surface have a probability of desorption and at a given temperature and concentration, there will be an equilibrium where the number of molecules that adsorb and desorb are equal. This corresponds to the equilibrium coverage of the surface. The time dependence of the molecular coverage of the surface at constant temperature, $\theta(t)$, is described by the Langmuir isotherm:

$$\theta(t) = A\,(1 - \exp(-kt))\,; \tag{5.0-0}$$

where t is time, $k = k_{ads} \cdot c + k_{des}$ is the observed rate constant at a concentration c of molecules at the surface. k_{ads} and k_{des} are the rate constants of adsorption and desorption respectively. $A = k_{ads} \cdot c/(k_{ads} \cdot c + k_{des})$ is the equilibrium coverage. This relation was first experimentally tested by measurements of mass increase due to submonolayer adsorption on large surface areas [69].

5.0.4 The biochemical systems

The first biochemical system we chose to investigate with the Biosensor was the specific detection of DNA. DNA sequences specific to many different diseases and

micro-organisms have been identified and forms the basis of a hastily growing and ambitious industry based on the so-called DNA chips. The principle is that under specific conditions one can recognise and detect these sequences. Also DNA is one of the sturdiest biomolecules thus making it relatively easy to work with.

We took the step from genomics to proteonomics developing localisation and immobilisation with the a biotin avidin system. We used biotin attached to bovine serum albumin (BSA) in order to lift the small biotin molecule from the surface for interaction. The system showed good functionality in fluorescence tests, but we did not obtain results from the cantilever measurements.

Bacteria detection using the Biosensor was tried using an immunoassay: E. coli antibodies were non-specifically bound to gold and E. coli was specifically recognised by the antibodies.

In general proteins are more delicate and complicated to work with than the DNA. Especially the immunodetection system of E. coli proved to be difficult to master.

5.0.5 General considerations

The gold/sulphur solution

Immobilisation by a gold sulphur bond is a quite common method in biotechnology, which makes for example single strands of DNA modified with a -SH group commercially available. The stability of a monolayer of molecules anchored with Au/S bond is expected to be be good, as the bond strength is $\sim$ 170-210 kJ/mol[1] and the enthalpy of the reaction is -21 kJ/mol [71].

In the case of the Biosensor, the immobilisation via the gold-sulphur bridge is attractive because it is relatively simple to prepare the measuring cantilever with a gold layer, the sulphur gold bond is strong, so stress releasing movements on the surface are reduced, the molecules are expected to form a monolayer on the surface, and finally this method in the case of ssDNA involves only one short spacer molecule. This is expected to be of importance in the stress generation.

Clean Au

An important issue when relying on the formation of monolayers on gold is the cleanliness of the gold surface. A whole range of cleaning procedures exist including fresh evaporation, UV ozone, oxygen plasma treatment, treating the surface in a clean flame, cleaning in piranha or finally etching away the top layer of the surface with aqua regia [49].

With the Biosensor the cleaning step has been studied also for the adsorption of alkane thiols from air [49] and it was found that the adsorption rate was highly

[1]The free energy of a covalent bond is $\sim$ 150-850 kJ/mol, depending on the type of bond [70]

dependent not only on the cleaning, but also on the exposure to air after cleaning. Even short exposures to air were seen to deteriorate the reactivity of the gold. In order to avoid exposing the gold surface to air at all, methods of cleaning and immobilisation were investigated that could be performed 'in situ'. That is, all the steps, cleaning, immobilisation, washing and hybridisation could be performed in the same flow system.

For this, aqua regia etching of the Au surface was most compatible as this is a room temperature process. Further, AFM studies showed that etching roughens the surface [72]. This increases the effective surface area accessible to the surface active molecules and a correlation in stress signal size with the roughness of the gold layer was seen. The signal for adsorption of alkanethiols was enhanced as the layer got rougher and decreased again as the etching started to remove the gold entirely [49].

On the downside, the etching is difficult to control. Because of the uniqueness of every sensor chip it would also be very attractive to be able to repeat the same experiments with the same chip. However, because of the changing roughness, cleaning the same probe several times by aqua regia etch does not give reproducible measurements

5.1 Verification by Fluorescence

It is important, for the evaluation of signals obtained from the Biosensor, to have an independent method for determining what processes have been going on. We used a fluorescence based equipment to evaluate our biochemical systems. The method will be exemplified using a biotin avidin system. A localisation technique suitable for proteins, and evaluation by fluorescence microscopy will be described. Finally, a Biosensor experiment is shown.

The fluorescence studies give us the possibility to test the localisation, blocking and functionality of our biochemical system.

5.1.1 DNA chips

The DNA is made of two strands of nucleic acids each carrying a sequence of bases: adenine (A), cytosine (C), guanine (G) and thymine (T). The bases can pair up so that A pairs with T and C with G so that strings with complementary sequences can join and form the characteristic double helix structure [73]. This pairing is called hybridisation. Under the right temperature and buffer conditions one can obtain a situation where only strands that match perfectly will join. This means that in a sample, prepared such that the DNA strings are separated in single stranded DNA (ss-DNA), it is possible to identify a given sequence using a ss-DNA string made of the complementary base sequence - the so-called probe DNA.

Several different strategies can be used to detect the hybridisation. For example tagging a strand of interest with a fluorescent label is currently often used. At the basis of the DNA chip technology is that the hybridisation can take place also when the probes are immobilised on a surface.

In the sample to be investigated the interesting sequences can be amplified, that is copied in large amounts, and each copy can be tagged with for example a fluorescent label. The surface, with the immobilised DNA probes, is exposed to the sample and then washed well, so that only sample molecules which attached to the DNA probes on the surface will remain. On a standard microscope slide one can have many thousands of spots with different probes. The labeled molecules which have attached to the probes on the slide can then be detected in a fluorescence scanner.

Immobilising antibodies or antigens to the surface instead of DNA probes, the method can be used also for analysis based on immune reactions and more generally immoblisation of functional proteins is making the transition from genomics to proteomics possible [74].

5.1.2 The Fluorescence scanner

A fluorescence scanner illuminates a sample with light of a given wavelength and with high resolution and sensitivity detect the emitted light a different, specified wavelength.

The laser scanner at the Microelectronics Center, Packard Imager[2], excites the sample at either 552 nm or 651 nm and detects the emission at 568 nm and 674 nm. This corresponds to the absorption and emission wave lengths of the fluorescent markers Cy3 and Cy5 respectively. We have used Cy3 dyes in avidin/biotin experiments and the Cy5 dye in DNA and bacteria experiments.

The highest spatial resolution of the scanner is 10×10 μm. In any given scan one can choose to use the Cy3 or Cy5 channel and the result is a colour coded image of the detected intensity.

Both the intensity of the exiting laser and the detecting photomultiplier tube (PMT) can be adjusted to ensure maximum sensitivity in the desired range of signals, while avoiding saturation and minimising the background. These intensities are normally optimised for every scanned sample and quoted in % of maximum as xx;yy, where xx is the intensity of the laser and yy is the intensity of the PMT, both in % .

The laser intensity can vary between scans which makes it difficult to extract absolute results. For precise, absolute measures of the amount of fluorescent molecules on a given surface, it is necessary to include calibration points on each sample. This could be a drop of a known concentration of the fluorescent molecule, used in the test performed, put onto the slide and left to dry just before

[2]Packard Instruments Co.

scanning.

The instrument is very sensitive to the focusing of the laser on the surface, which makes complicates work with samples that are not standard microscope slides. After the different materials of the surfaces of the cantilever chip had been investigated, using diced pieces of wafer (for example figure 5.11), and we had chosen to work on gold, the rest of the experiments were performed on standard microscope slides coated with a cromium/gold layer.

A progam[3] is available for quantification of the measurements. With this templates can be created to measure the detected fluorescence in a given area (in digital light units, DLU), and background areas can be chosen for substraction.

We were not aiming at a thorough fluorescence study of the systems, but mainly investigating the necessary conditions for a given biochemical reaction on the cantilevers of the Biosensor.

5.1.3 Biotin Avidin

As an example of a protein system for the fluorescence studies, we looked at a well known biotin avidin system, which has been used for example in AFM studies of ligand binding forces [75].

Biotin, also called vitamin H, is a small molecule (244.3 Da) often used as a label for detections performed with fluorescent marked avidin. One avidin molecule (66kDa) can bind up to four biotin. The biotin avidin bond is strong, close to the strength of a covalent bond, and therefore expected to be able to produce a large surface stress. Another reason for the popularity of biotin/avidin systems is that the molecules are quite sturdy and relatively easy to work with.

We used biotin attached to the protein bovine serum albumin (BSA) on the surface. This lifts the biotin of the surface so it can interact with the avidin. Also, BSA is a much used blocking agent, which should make the blocked and functional surfaces very similar.

Immobilisation, blocking, functionality and localisation were studied by fluorescence. Unfortunately, we did not obtain any signals from cantilever measurements.

Materials

Bovine serum albumin (BSA) was purchased with biotin labels[4] and without for blocking and control[5]. Avidin was bought with Cy3 labels.

Dilutions were made in phosphate buffered saline (PBS) (0.01 M)[6] and the washing/blocking solution was 0.7 mg/ml BSA in PBS with 0.01 % Tween20, a

[3]BioChip Imager, version 3.10, Packard Instrument Company.
[4]Sigma A-8549
[5]Sigma A-2153
[6]10mM sodium phosphate, 0.9% NaCl, pH 7.4.

non-ionic detergent.

AvidinCy3 calibration

Titrations of avidin Cy3 in concentrations of 1 mg/ml to 10^{-11} mg/ml were prepared and pipetted onto a gold coated glass slide, in 0.5 μl droplets, and left to dry before scanning. The slides had been kept in DI water after evaporation but had not otherwise been cleaned. Out of concern for possible quenching of the fluorescence signal by the gold, the experiment was also performed on a surface blocked with BSA before the droplets were deposited. The result was the same if the slide was not blocked. Except for the highest concentration (nominal, 1 mg/ml, as supplied), two droplets, each from an independent dilution series, were put on the slide.

Figure 5.1 shows a scan of the BSA blocked slide (intensities 95;85). Rings have been drawn around pairs of droplets of equal concentration. At the bottom right one spot of 1 mg/ml (nominal concentration as supplied) above it two spots of 0.1 mg/ml, then 0.01 mg/ml etc. The right and middle row are filled with spots of diluted avidinCy3 down to a concentration of 10^{-11} mg/ml. At the top

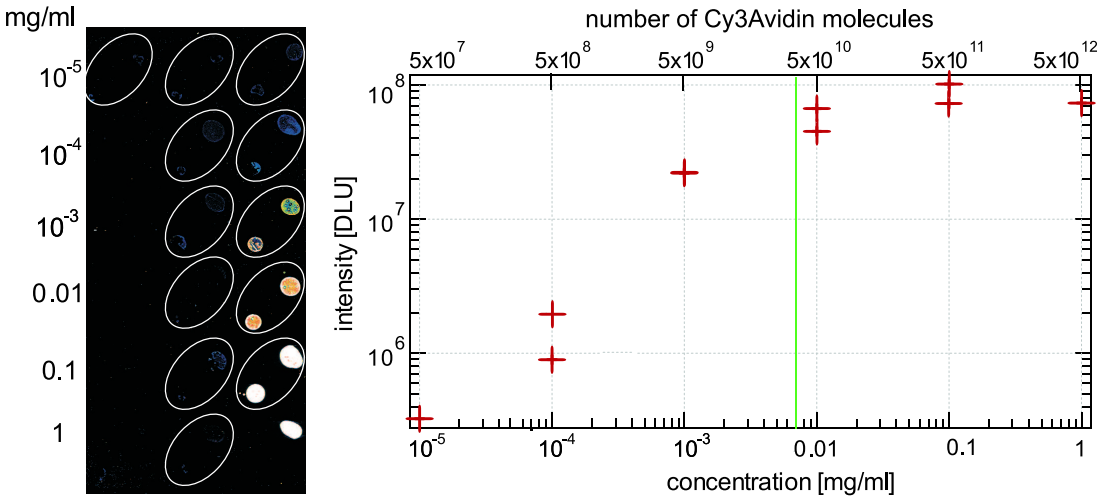

Figure 5.1: Fluorescence of avidin Cy3 on gold

left pure PBS has been put down.

Next to the scanned slide a plot of the measured fluorescence intensities is shown.

Only the dilutions in the right row can be detected. For the lower concentrations in the middle of the slide very light spots can been seen, equivalent to the ones for pure PBS. Both on the scanned image and the graph it is seen that at the scanning intensities shown the signals from the highest concentrations (1 and 0.1 mg/ml) saturate.

Avidin is a 66kDa molecule, from which the number of molecules in a 0.5 μl droplet indicated at the top of the graph follows. To find the degree of coverage, we assume that avidin is a globular protein with a diameter of 8nm. At dense monolayer coverage this gives $3.5 \cdot 10^{10}$ molecules/spot of $\sim$ 1.8 mm diameter. This is marked with a line in the graph and there should be molecules enough for a monolayer coverage in a 0.5 μl spot of a concentration of 10 μg/ml. The background level is close to the signal from 10^{-5} mg/ml which sets the detection limit just under a coverage of 1% .

Immobilisation, blocking and functionality

The binding of avidin to biotinylated BSA (BBSA) adsorbed to a gold surface was investigated by fluorescence.

Method: BBSA was titrated in tenfold dilution series from 10 mg/ml to 0.1 μg/ml with PBS buffer. Four droplets, of 0.5 μl, from two independent titration series, were put onto a gold evaporated glass slide. BSA was put down in the same way. The drops were allowed to dry and the slide washed in blocking solution for 15 minutes under vigorous stirring. After drying avidinCy3 was pipetted in a dilution series (1 mg/ml to 0.01 μg/ml) and allowed to dry, before incubation with avidinCy3 (10 μg/ml) in a 3.6 ml reaction chamber for 1 hour on a shaker. The slide was again washed in blocking solution as above, then with PBS and 0.01% Tween20 and finally swiftly rinsed in DI water. The slide was then dried and scanned.

Results: An example of a resulting slide, scanned at (95;85), is seen in figure 5.2, far left. The BBSA series is to the left, four spots in a square for each dilution, the avidinCy3 in the middle and the BSA without biotin in the left row. First, we can note that the BSA blocking is effective, the background is 500 times less than the maximum signal and it is seen that the BSA, left row, does not give a signal. For avidinCy3 left to dry directly on the surface there is a signal of $5.5 \cdot 10^6$ DLU, so it is possible to stick avidinCy3 to a blocked surface.

The measured intensities of the BBSA row (to the right), averaged over the four spots, are plotted as a function of concentration, to the right figure 5.2. The signal is constant for the first three dilutions and then drops nearly to about twice the background level. A dirty spot contributes to the higher signal for 10^{-3} mg/ml. In general, it can be noted that the washing and drying procedures could be refined.

The magnitude of the signal, for all three of the highest concentrations, is $4{\cdot}10^7$ DLU, the same as was measured for a monolayer coverage of pure, dried avidinCy3 (figure 5.1). BBSA is of roughly the same size and mass as avidin so at a concentration of 10^{-2} mg/ml we can expect that roughly a monolayer of BBSA was deposited. A coverage of a monolayer of BBSA is just detectable. The fluorescence signal is not saturated at any point so we may conclude, from the constant signal at higher concentrations, that either the excess BBSA has been

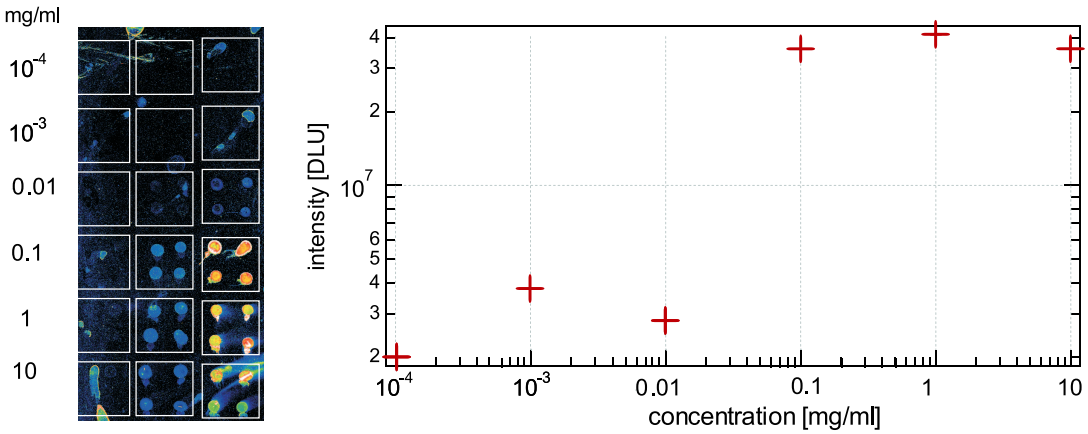

Figure 5.2: Fluorescence of BBSA (right row) and avidin Cy3 (middel row) on gold, four spots of the same concentration in each square. Left row: control with BSA.

washed off or the avidin in any case can not access more than the top layer.

We can conclude from the fluorescence measurements that we have a system that works both with regard to blocking, immobilisation and functionality for BBSA concentrations of 10 to 0.1 mg/ml.

Localisation

Proteins are very sticky so for localisation of the proteins to one side of the measurement cantilever we used an upgraded version of the technique used for polymer coating in chapter 3.2. The proteins are mechanically confined, as they are put on on the surface where they are wanted, whereafter the remaining surfaces are blocked.

Equipment: A Cell tram oil pump, electronic micromanipulator and glass capillary holder, originally developed for micro insemination, was purchased from Leica. Needles, with an inner diameter of 10-15 μm, were prepared from glass capillaries[7], on equipment[8] put at our disposal, with kind instructions to its use, by Mads Sabra and colleagues, at MEMPHYS, Department of Chemistry, DTU.

Spots of biotinylated BSA (BBSA) were put on gold evaporated in squares on a glass microscope slide, in concentrations of 1 mg/ml, 0.1 mg/ml, 10 μg/ml and 1 μg/ml, 30 of each. The slide was then blocked, incubated with AvidinCy3 and washed as described for the larger spots (section 5.1.3).

Results: With this equipment we made spots with a diameter of approximately 200 μm, figure 5.3. A detectable signal is seen for BBSA concentrations down to 0.1 mg/ml, which is a concentration 10 times higher than the limiting concentration for the 0.5 μl spots (figure 5.2). In order to get a quantitative

[7]World Precision Instruments, 1B100-3.

[8]Pipette puller: Flaming/Brown Micropipette puller, model P-87, Sutter Instrument Co. Tip shortener: Mikro Forge, MF-900, Narishige.

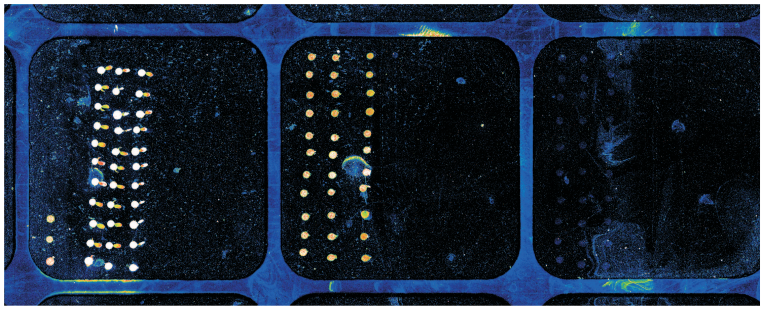

Figure 5.3: MicroSpots, diameter $\sim$ 200μm (scanning 95,85). Concentrations of BBSA in the applied droplets in each square, left to right: 1 mg/ml, 0.1 mg/ml, 10 μg/ml

comparison between the two spot sizes an accurate determination of the average fluorescence from a spot, is needed. Here this is a bit involved, as the shapes of the spots are very irregular.

An interesting feature are the light rims around the gold squares, these are not seen in figure 5.1, which has the same patterning but has not been washed or incubated. After incubation the background signal is much lower on the gold than on the glass surface, either because the blocking is less effective on glass or it is not as easy to wash it. The background is a classic problem in this type of scanning arrays.

The drying times, reaction times and concentrations of molecules on the surface are different from the situation of the spots of ten times larger diameter in figure 5.2. If we assume that the spot area to drop volume scales, then the 200 μm diameter spots correspond to a volume of $\sim$ 5 nl and a concentration of BBSA of approximately 0.05 mg/ml is needed to obtain a monolayer coverage.

We see that surface concentration is still the important parameter in the immobilisation of BBSA and that one should expect to use ten times higher concentrations on the cantilevers than found from studies of 0.5 μl drops.

Microscope verification

It is not possible to image a wax coated sensor in the scanner so we used a fluorescence microscope[9] to inspect a Biosensor where BBSA had be put down on one cantilever using micro-pipettes. It was then rinsed and incubated with avidinCy3. At the top of figure 5.4 is a false colour image of the sensor viewed in fluorescence.

The avidinCy3 signal is strong and well localised on the front side of one of the cantilevers. Only a small spec of fluorescence is visible from the back side. At the bottom are white light images taken during the positioning of the sensor. Mechanical localisation such as this can also be done on an industrial scale, with

[9]We thank Ivan R. Perch-Nielsen for lending us his equipment.

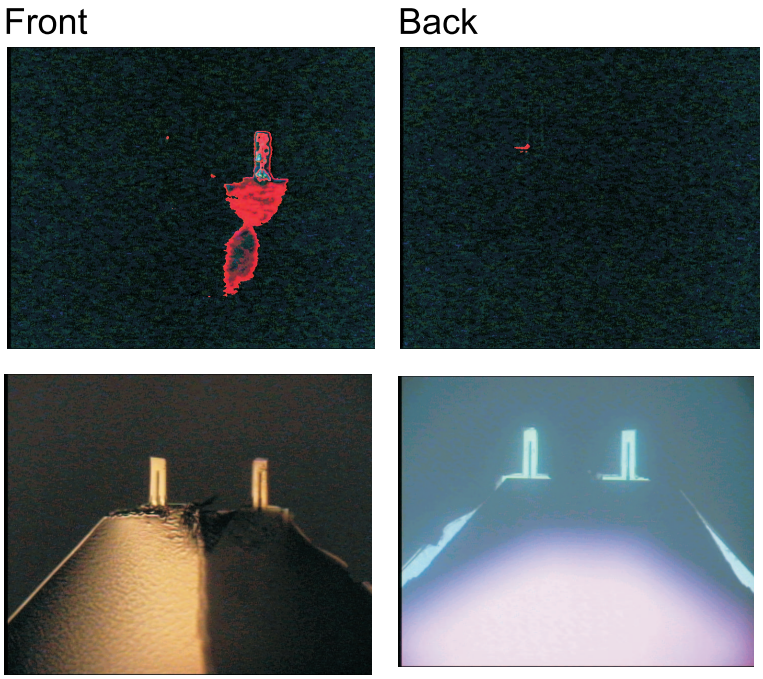

Figure 5.4: Fluorescence investigation of localisation. At the top false colour images of the fluorescence from the chip after incubation with avidin-Cy3. Below, the corresponding white light images. The fluorescence signal is strong and well localised.

the necessary precision using for example ink-jet printing [76, 77]. This is also a non-contact technique and thus suitable for the fragile cantilevers.

Checking a cantilever measurement

We performed measurements on a Biosensor chip with two gold coated cantilevers prepared following the same immobilisation procedure as for the microspots (1 mg/ml BBSA). After immobilisation the sensor was mounted in the flow cell and allowed to equilibrate in blocking solution. The measurement is shown in figure 5.5. The avidin incubation solution was injected in the period between the two arrows at a flow rate of 10 μl/min. Before and after there is no flow. There is a downwards trend in the output of 15 μV ($\sim$ 42 mN/m), which stops after 12 minutes. We did not reproduce this and do not think it is a signal due to the binding of avidin. This is also not simply due to the shift in the flow, which is the same as in figure 4.6. The signal would indicate a formation of tensile stress, that is the surface layer contracts upon the binding of avidin. While this is not impossible it is unexpected, as it requires some attractive interactions or a release of a compressive stress in the BBSA layer. With the fluorescent microscope we could check the immobilisation, figure 5.6, which showed a low signal and poor localisation, compare figure 5.4.

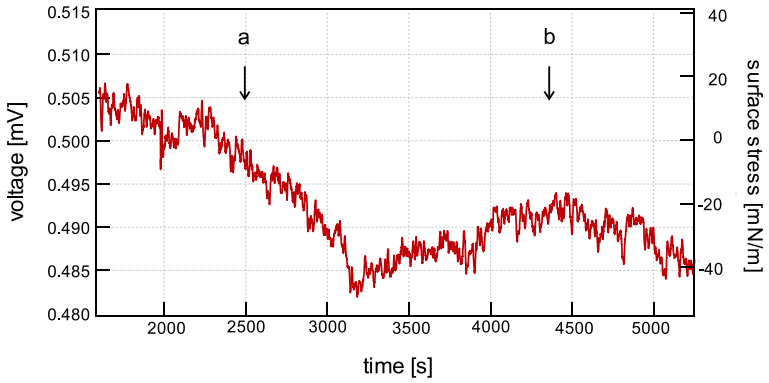

Figure 5.5: A time series of a sensor functionalised with BBSA on one cantilever subjected to a flow of avidinCy3 incubation solution between the points a and b. Before and after, there is no flow. The other surfaces are blocked with BSA.

The biggest difference in the two situations is that the in figure 5.4 the sensor had been incubated with avidinCy3 in a magnetic stirrer.

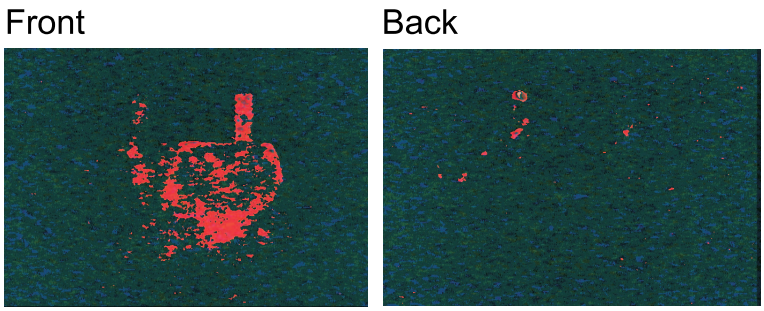

Figure 5.6: False colour images of the fluorescence from the sensor used in figure 5.5. The fluorescence is weak and the localisation not very well confined.

5.1.4 Conclusion

AvidinCy3 showed binding to a monolayer of BBSA, non-specifically adsorbed to gold, in fluorescence measurements. Blocking with BSA was good, especially on gold, which should ensure a good reference probe. The layer was stable for days and the BBSA/AvidinCy3 system was easy to work with. A localisation technique was developed, and it was seen that although it worked, it was good to be able to cross check after an experiment.

5.2 Immobilisation of thiolated DNA oligos

Preliminary work on the detection of adsorption of a monolayer of single stranded DNA (ss-DNA) on a gold coated cantilever, was conducted together with Rodolphe

Marie [44, 52]. The immobilisation and the functionality of the ss-DNA probes on different surfaces was tested by fluorescence. We measured the kinetics of the self assembly of thiolated ss-DNA probes on a gold coated surface with a Biosensor.

5.2.1 Introduction

Instead of using the fluorescence labeling and subsequent detection in an advanced, but bulky and expensive, scanner we want to use the Biosensor for the detection of the hybridisation of specific DNA sequences.

We needed to find a way to immobilise the DNA probes on one of the cantilever surfaces, test the hybridisation, and design a suitable experiment.

The localisation and immobilisation method was semi automatic based on the self assembly of thiolated molecules onto a gold surface. This immobilisation could be performed in situ and followed in real time if the nonspecific binding of the DNA probes to the other surfaces of the sensor was low. The selectivity was investigated using the fluorescence method.

5.2.2 Materials

The probe DNA was a 25'mer ss-DNA. Short strands like this are often called oligos. The oligos were purchased ready modified as illustrated in figure 5.7. Two hydrocarbon spacer molecules, connected by a disulphur bridge, are attached to the 5' end of the oligo. A group acting as a protective cap (dimethyl-1,3-trityl, DMT), prevents the sulphur bridge from reducing spontaneously. The probe

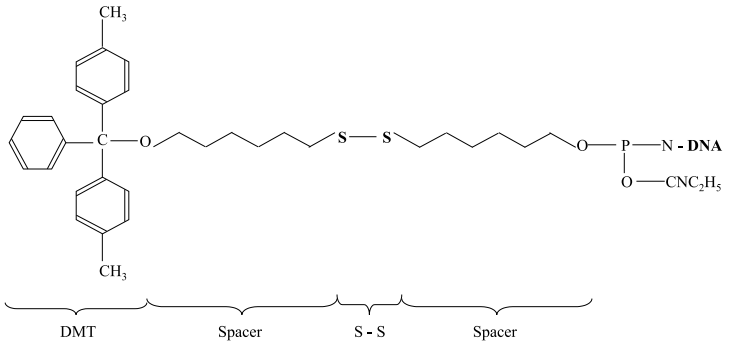

Figure 5.7: Fluorescence results on surface selectivity of DNA hybridisation. From [44].

oligo, modified as described above, and the complementary oligo, the target[10],

[10]The sequence of the ss-DNA probe was 5' AT TAA TGC TAT GCA GAA AAT CTT AG 3' and the complementary target then 3' TA ATT ACG ATA CGT CTT TTA GAA TC 5'. For details see http://www.glenres.com

labeled with the fluorescent marker Cy 5', were acquired from DNA technology ApS[11].

The buffers for the immobilisation and hybridisation were made on the basis off 20×SSC[12], a solution of sodium (3M) and sodium citrate (0.3M). For immobilisation 1×SSC (1:19 dilution) was used. A detectable signal would most likely be generated by fast immobilisation kinetics and a concentration of 10 μM ss-DNA probes was chosen for the immoblisation solution.

The hybridisation solution was made on the basis of 5×SSC. The amount of target DNA in the hybridising solution was calculated according to the amount of immobilised probes so there would be at least ten times the amount of target DNA necessary for 100% hybridisation.

The substrates used in the fluorescence tests were diced silicon wafers, approximately 1×2 cm pieces, with Si (native oxide), SiO (thermal oxide), SiN and gold surfaces, the latter prepared as in section 4.2.2.

The surfaces were cleaned using a 33% dilution of aqua regia and an etch time of 2 minutes were chosen, for the fluorescence studies on the basis of measurements of the etch rates [44]. The lead-protecting wax was resistent to the etch.

5.2.3 Surface selectivity

Fluorescence experiments, to determine the selectivity of the immobilisation and the efficiency of the hybridisation, were performed for the four different surfaces, Au, Si, SiO (thermal) and SiN. The experiment is described in detail in [44].

The hybridisation efficiency showed large preference towards the gold surface. The selectivity with respect to Si (native oxide) and SiN was close to 100, and 10 for SiO.

From X-ray photoelectron spectroscopy, it was further found that the protected oligos (figure 5.7) adsorbed to the surface, either by full oxidation of the sulphur bridge upon contact with the gold surface or in an intermediate state, where the sulphur bridge was in contact with the gold but still seemed to be intact [44].

We could conclude that it would be possible to functionalise a gold coated cantilever sensor in situ, relying on the specificity of the gold sulphur bond. We saw that the biochemical system was functional so it should be possible to observe kinetics of the immobilisation on cantilevers. Hybridisation was expected to be possible on cantilevers prepared this way.

[11] DNA technology ApS, Århus, Denmark.
[12] Promega,

5.2.4 Cantilever measurements

The experiment with the Biosensor was conceived so the whole sequence of cleaning the gold surface, immobilisation of the thiolated probes and hybridisation could be performed in one uninterrupted measurement.
The immobilisation part of the experiment was designed as follows:

- The sensor chip was mounted on ceramic substrate, coated with wax and chromium/gold was evaporated onto the measurement cantilever. The prepared sensor was stored in DI water until use.
- The sensor was assembled with the flow system, 4 V applied to the Wheatstone bridge and DI water was pumped through at 25 μl/min, this is roughly one chamber volume per minute. The system was allowed to stabilise until the drift had settled to less than 0.5 mV/100 s.
- Aqua regia, 33 % was pumped through, at 25 μl/min, for four minutes after which the flow was switched back to DI water at a flow rate of 100 μl/min. The rinsing in DI water was continued for at least 10 minutes.
- The immobilisation solution (10 μM protected DNA probes in 1×SSC) was pumped through, at 25 μl/min, for 10 minutes.
- The system was then rinsed with DI water, at 50 μl/min, till the signal stabilised.

All reagents for use in the experiment were allowed to equilibrate at room temperature before the experiment.

Results

The development of the surface stress measured during the first 200 seconds of the introduction of the immobilisation solution is shown in figure 5.8. The solution arrives in the reaction chamber at time zero. Note that the arrival of the solution into the reaction chamber is not marked by any disturbance. A decrease in the stress is seen during the first 10 seconds, followed by a global increase which stabilises after approximately 100 seconds, at a surface stress of 12 N/m. This corresponds to a compressive surface stress in the adsorbing layer of molecules and that the cantilever is bending away from the gold surface.

Hybridisation

After the stabilisation period following the immobilisation the flow was changed to the hybridisation buffer (without target molecules) at a flow rate of 25 μl/min.

At the introduction of the hybridisation buffer the signal quickly became unstable and the output diverged.

As mentioned in section 4.1 it turned out that the wax coating was not compatible with the hybridisation buffer, and the leads of the sensor were etched

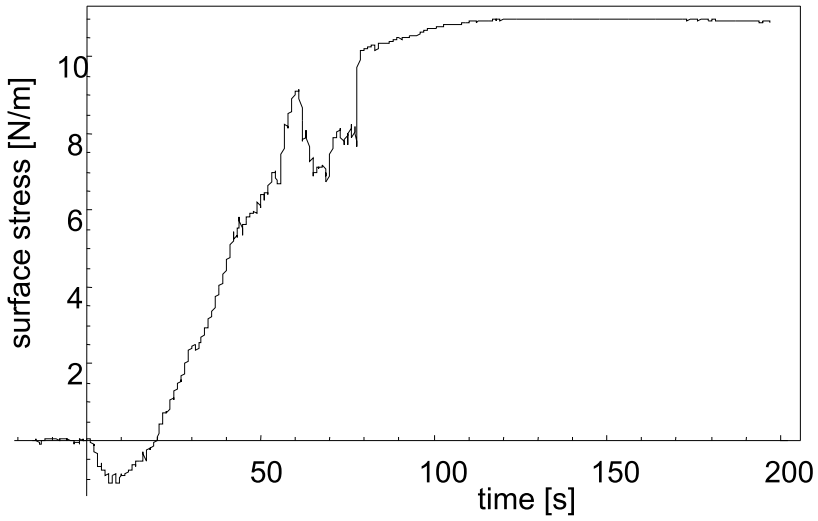

Figure 5.8: Immobilisation of thiol oligos on a gold coated cantilever [44].

away. This lead to extensive investigations on adhesion and alternative coating possibilities [44].

Langmuir adsorption

Following the work reported by Rüdiger Berger et al. on the adsorption of alkane thiols from air [14] and work using on thiolated double stranded DNA (ds-DNA) [78], the adsorption was assumed to follow Langmuir isoterms and the surface stress assumed directly proportional to the number of adsorbed molecules. A subset of the immobilisation data (figure 5.8) was fitted with a superposition of two Langmuir isotherms [44]:

$$f(t) = A_1 \left(1 - \exp(-k_1 t)\right) + A_2 \left(1 - \exp(-k_2 t)\right). \qquad (5.2\text{-}0)$$

k_1 and k_2 are the two observed rate constants, were k_2 is believed to reflect the adsorption of the DNA oligos and k_1 is interpreted as reflecting the desorption of some contaminants pushed of the surface by the high affinity of the gold sulphur binding. From the fit in figure 5.9 k_2 was found to be $4.6{\cdot}10^{-2}\mathrm{s}^{-1}$. As the enthalpy for the gold thiol reaction is very negative (-21 kJ/mol [71]) the desorption rate constant is expected to be very small and $k_2 = k_{ads} \cdot c + k_{des} \sim k_{ads} \cdot c$.

In order to determine the value of the equilibrium binding constant, $K = k_{ads}/k_{des}$, from which the free energy of the adsorption could be calculated, $\Delta G = -RT \ln(K)$, Rodolphe Marie conducted further experiments, with different concentrations of immobilising probe oligos and determined the observed time constants. It was found that the free energy associated with the adsorption of the thiolated DNA oligos from solution was -32.4 kJ/mol [52].

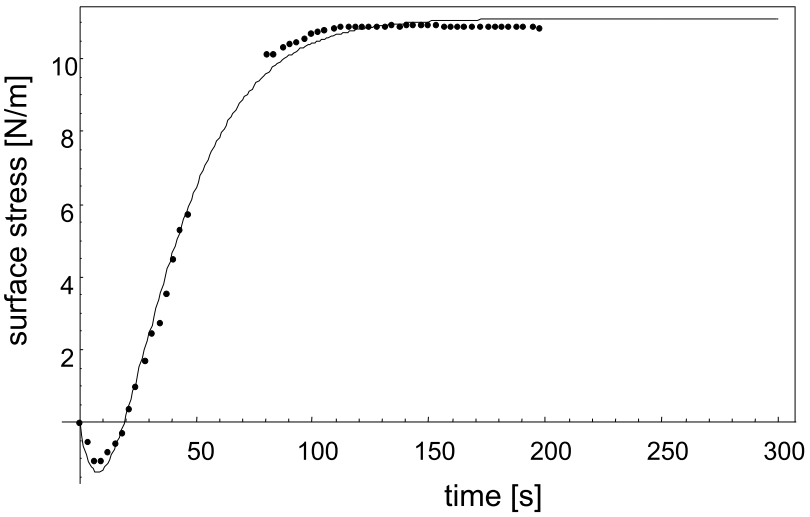

Figure 5.9: The immobilisation mesurements fitted with two Langmuir isoterms [44].

Discussion

The observed stress signal for the immobilisation of the thiolated 25'mer ss-DNA is $\sim 5-10$ times larger than the stress developed upon adsorption to gold surfaces that had not been aqua regia etched [52]. This is consistent with the observations by Allan Hansen et al. who, also using the Biosensors, observed a signal increase of a factor 4-5 for the adsorption of hexane thiols (after 500 seconds: 0.1 N/m un-etched and 0.8 N/m etched 1 minute) [49]. The non-etched signal further compares very well with the alkane thiol measurements by Berger and coworkers who also measure a saturation stress for a hexane thiol of 0.1 N/m [14, 79].

A stress of 1 N/m for adsorption of the ss-DNA is however still large compared to the stress observed by Wu and colleagues for the adsorption of a similar system: for a 25'mer in ~ 0.2 M phosphate buffer they measure approximately 10 mN/m [26]. Even though there are many uncertainties, for example in the value of Youngs modulus for SiN, it is not easy to point to a reason for this difference of two orders of magnitude. The main difference between the two experiments seems to be the buffer: Wu et al used a phosphate buffer while in the present work 1×SSC has been used.

The free energy of -32 kJ/mol compares well to the free energy derived from the rate constant in a QCR study of the adsorption of thiolated ds-DNA : -35 kJ/mol [78].

This is actually a bit surprising as we, following Wu [26], would have expected the entropy contribution from the ss-DNA to be more important than from the ds-DNA. This could be balanced by a higher density of molecules combined with the larger electrical charge.

Several reports of the observation of hybridisation on microcantilevers were recently reported [26, 21, 22]. The largest hybridisation signals are up to 10 mN/m. Especially Hansen et al. [22] studied the effect of several different mismatch configurations and Wu et al. [26] used differences in ionic strength at immobilisation and hybridisation to illustrate the role of entropy in the signal generation.

5.2.5 Conclusion

We saw that the preference of hybridisation to thiolated ss-DNA adsorbed to gold was high compared to SiN, Si and SiO. We showed that the immobilisation of thiolated ss-DNA onto a gold coated cantilever could be measured with the cantilever sensor.

The possibility of performing online sensitive monitoring was shown.

The electrical protection of the leads on the sensor chip must be improved to be able to detect hybridisation at high ionic strength.

5.3 Towards bacteria detection

Together with Lars Helt Veje, we took the fist steps towards the application of the Biosensor as a bacteria detector. We investigated the direct adsorption of anti-E. coli antibodies on Au and studied the E. coli binding activity of the immobilised antibody using a fluorescence based immunoassay. The successful procedure was used to prepare the Biosensor for detection of E. coli in a liquid sample.

5.3.1 Introduction

Fast sensitive and cheap bacteria detection is naturally of large interest for example in the food industry. Escherichia coli (E. coli) is a concrete example, where one needs to test against malignant, distress causing strands.

A classical and widely used detection method is the Enzyme-Linked Immunosorbent Assay (ELISA). The possible E. coli in a sample must be grown until the sample would be saturated with E. coli, if any bacteria were present (1-2 of days of growth if the food is good). Several chemical steps follow before the final, typically fluorescent, detection. Even if the sensitivity would not permit growth step to be entirely skipped, direct detection with a cantilever would greatly simplify such a test and cut the reagent costs.

The first microcantilever-based bacteria detection was performed precisely with E. coli. The measurement was a detection of the mass change due to the adsorption of whole bacteria and performed in air [80]. Sensitivities down to a single cell were predicted in vacuum.

For us, the E. coli detection is also interesting because it would be an example of an immuno-based detection, that is a detection gaining its high specificity from the recognition properties of antibodies.

Antibodies

Antibodies, or immunoglobulin (Ig), are proteins of the immunesystem, which are able to recognise virtually any molecule. Any one antibody recognises a specific structure - the antigen of the antibody. The subclass IgG are produced in great numbers against foreign intruders in the body of a mammal and they constitute the recognising part of the adaptive immunsystem, which gives rise to immunity. IgG consists of two heavy and two light chains connected by di-sulphur bridges (figure 5.10). One end of the chains is constant and the other is highly variable.

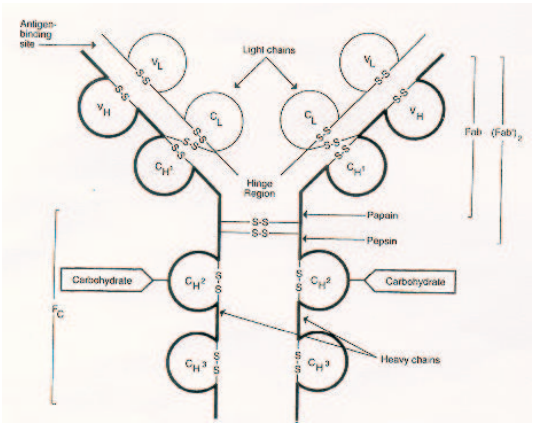

Figure 5.10: A schematic drawing of an IgG molecule.

The variable regions of a heavy and a light chain together form a very precise pocket for recognition of the antigen. The constant part of the heavy chains form the 'tail' of the IgG, or the Fc region. In any one antibody the recognition sites will be the same.

In order to exploit the specificity of the antibodies as the sensing element on a surface they must be immobilised in such a way that the recognition sites are preserved, functional and accessible for the antigens.

Immobilisation strategies

Many different strategies exist for the immobilisation of active antibodies. They range from simple adsorption of antibodies onto a clean surface (typically polystyrene, glass or metal) to multilayer structures that provide both specific orientation and distance from the surface and even larger matrix structures, which allow for a higher concentration of immobilised antibody per surface area. In the present case, where the signal generation depends on the stress transferred from the

binding sites to the solid support, it seems important to eliminate soft spacer layers and bring the binding event as close to the surface as possible.

Our experience from the DNA oligo immobilisation (section 5.2) and the work on the Biosensors with alkane thiols by Allan Hansen [49] inspired us to use gold as the substrate for immobilisation. Gold surfaces are easily prepared on the cantilevers and the relative inertness of the metal make the surfaces relatively well characterised. There are indication that in spontaneous adsorption the Fc is less structurally stable and adsorbs more readily than the Fab portions [81]. Furthermore, the di-sulphur bridges in the IgG might dissociate on the gold and contribute to a strong binding.

5.3.2 System design

We decided to adsorb the E. coli antibodies directly on to a gold surface and tested the system using the fluorescence scanner (section 5.1).

Materials

Polyclonal rabbit-anti E. coli IgG from Biogenisis[13] and Cy5 labeled goat anti-rabbit IgG from Amersham[14] (2Ab*) were used in the first tests of immobilisation and blocking. With these antibodies we did not achieve good E. coli recognition, so for the functionality tests we switched to a different system.

Affinity purified antibody (1Ab), isolated from a serum pool from goats immunised with whole cells of E. coli O157:H7, and heat killed E. coli positive controls (approximately $7 \cdot 10^9$ cells/ml) were purchased from Kirkegaard & Perry Laboratories[15]. For studies of the immobilisation and functionality, a part of the antibodies was fluorescent labeled with FluoLink Cy5 monofunctional dye[16] using a micro P-30 Tris chromatography spin column from BioRad[17]. The labeled 1Ab (1Ab*) was tested on polymer slides[18] for recognition of E. coli, both as supplied and after disruption by lysis.

Lysis was achieved by boiling the bacteria with an anionic detergent (10% sodium dodecyl sulphate, SDS) for 15 minutes. PBS with 0.1% Tween20 was used for washing solution and blocking was achieved either with BSA (10 mg/ml) or with 0.1-1% skimmed milk powder (SMP)[19] in washing solution.

The 1Ab was titrated in tenfold dilution series from 1 mg/ml to 10^{-4} mg/ml with PBS buffer.

[13] Biogenisis Ltd, Poole, England, Cat no. 4329-4906
[14] Amersham Pharmacia biotech, Uppsala Sweden; PA 45004
[15] Kirkegaard & Perry Laboratories, Gaithersburg, MD
[16] Amersham Pharmacia biotech
[17] BioRad, Rockville Center, NY
[18] FAST, Schleicher & Schuell, Dassel, Germany
[19] Matas A/S, Allerød, Denmark

Fluorescence

In figure 5.11 we see a qualitative test of the binding of E.coli antibody (1Ab) to the surfaces of four different materials (Au, SiO (thermal), SiN and Si (with native oxide)), with different pretreatment and the blocking efficiency of the BSA procedure has been tested. The prescence of 1Ab on the surfacee was detected using an antibody against 1Ab: 2Ab*, where the star indicates the fluorescent group. The general sequence of the experiments is sketched in figure 5.11.E. The detailed treatment of the samples has been summarised in table 5.1. The spots of primary antibody are placed as indicated in the sketches in figure 5.11.A with the highest concentration in spot '1'.

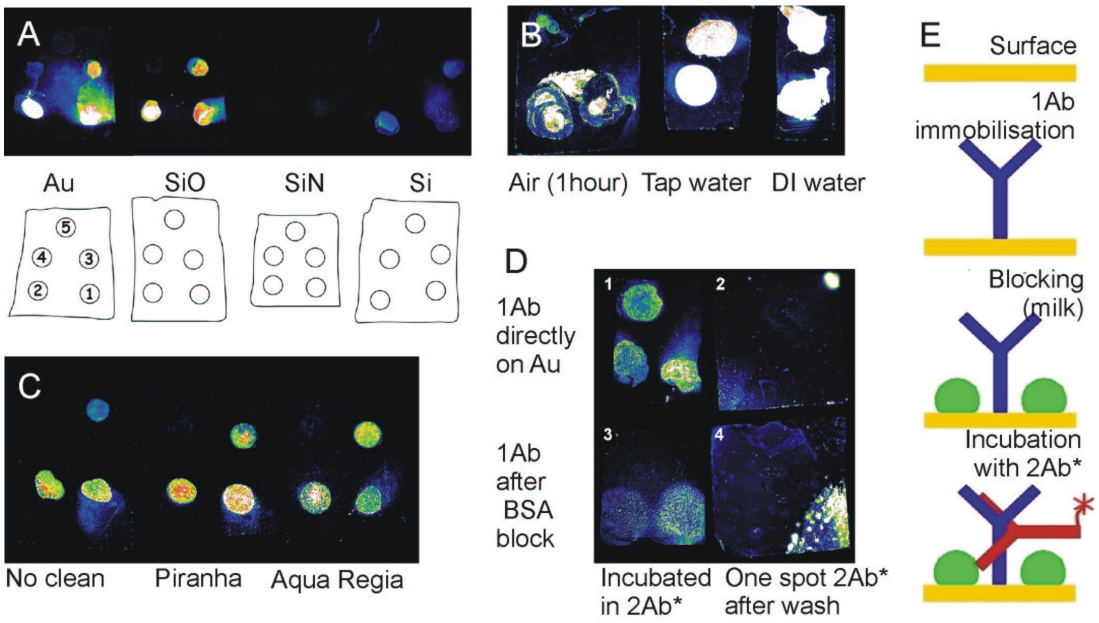

Figure 5.11: Adsorption of 1Ab: Surfaces of different materials (A). Different treatments of gold surfaces: (B) storage after evaporation, (C) cleaning procedures and (D) BSA blocking. (E) sketch of experimental sequence. Spots are titrations of 1Ab (0.15 μl) as indicated in (A) and table 5.1.

It was found that the efficiency of the binding of 1Ab on gold surfaces was higher than on Si, SiO_2 and Si_3N_4 surfaces (figure 5.11.A). Especially the selectivity towards SiN was pronounced[20]. However, we decided against relying on this selectivity for the immobilisation of antibodies.

The Au surfaces remained active for 1Ab immobilisation for weeks after the evaporation when stored in DI water, while one hour exposure to air decreased the binding markedly (figure 5.11.B). Further cleaning with piranha or aqua regia did not seem to affect the binding (figure 5.11.C). Finally, the BSA blocking

[20]This is a bit remarkable as SiN was the surface used as substrate for immobilisation of antibodies in a successful bacteria weighing experiment [80].

Samples	BSA block	1Ab mg/ml	PBS wash	BSA block	2Ab*	PBS wash	Scanning % Laser ; PMT
A	–	$1-10^{-4}$	–	1 h	20μg/ml 1/2 h	1/2 h	75;70
B	–	1	3 min	1/2 h	1μg/ml 1 h	1/2 h	75;70
C	–	$1-10^{-3}$	–	1/2 h	1μg/ml 1/2 h	1/2 h	60;60
D1	–	$1-10^{-2}$	–	1/4 h	1μg/ml 1/4 h	1/4 h	75;70
D2	–	$1-10^{-2}$	–	–	–	1/4 h	100;100
D3	1 h	$1-10^{-2}$	15 min	–	1μg/ml 1/4 h	1/4 h	75;70
D4	1 h	$1-10^{-2}$	–	–	–	–	95;85

Table 5.1: Treatment of the samples figure 5.11

worked well as seen by the low background in all images and even blocked against antibody left to dry on the blocked surface (figure 5.11.D). Later it was found that blocking with SMP was even better than BSA and at a fraction of the cost. Blocking efficiency is further enhanced by adding detergent (0.1% Tween 20). The detergent is also important in the washing step to rinse of proteins that are not specifically bound.

The functionality of the antibodies on gold surfaces was tested on microscope slides with an evaporated gold layer, figure 5.12. The evaporation was as described in section 4.2.2. Substrates for an experiment were taken from the DI water container and dried. Drops of 0.2 μl of the primary 1Ab dilutions were applied to the surface and allowed to dry. The slides were then washed in PBS with 0.1 % Tween20 in order to detach weakly adsorbed antibodies. The free parts of the surface were blocked against E. coli and further antibody adsorption with SMP. It was then exposed to E. coli for an hour under gentle stirring. The surface was then washed again, before they were allowed to react with 1Ab* (0.5 μg/ml) overnight. After another wash the surfaces were dried and imaged in the laser scanner. Figure 5.13 shows fluorescence measurements from a microscope slide where five different, ten-fold dilutions of anti-E. coli 1Ab (1mg/ml to 10^{-4} mg/ml) were pipetted onto the surface, one drop of each dilution on each of 12 gold square. The left row has been exposed to whole and the right to lysed E. coli. The efficiency of the SMP as a blocker against both E. coli and 1Ab* is high: the background is $< 5\%$ of the strongest signal. Separate tests without E. coli showed no cross-reactions between 1Ab and 1Ab*, so we may conclude that the recognition between E. coli and both 1Ab and 1Ab* is good. From the graph it is seen that the lanes exposed to both whole and lysed bacteria have equal intensities after 1 hour of exposure. The dashed line is from the reaction with lysed bacteria. The S-shape of the curve is expected for this kind of system. The higher intensities at 0.1 mg/ml could indicate that higher densities of 1Ab on the surface hinders binding. $3 \cdot 10^6$ DLU corresponds to a maximum of 0.2 ng 1Ab* (about 1/10 of a monolayer of antibodies of 150kD and 12×12 nm), but there were problems with the callibration so it could be 100 times less.

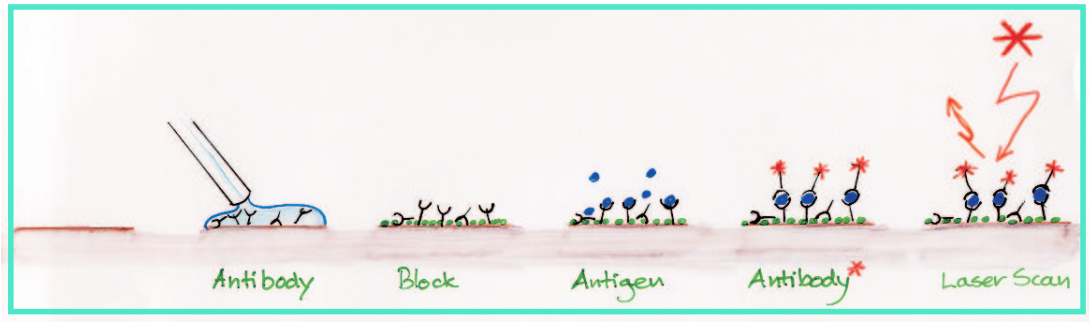

Figure 5.12: Sketch showing the steps in the testing of functionality of antibodies non-specifically adsorbed to a surface. Droplets of primary antibody, in different concentrations, are applied to the surface and the surface blocked. The surface is incubated first with antigen, then with fluorescent labeled antibodies then finally scanned in the laser scanner. Between all steps the slide is thoroughly rinsed.

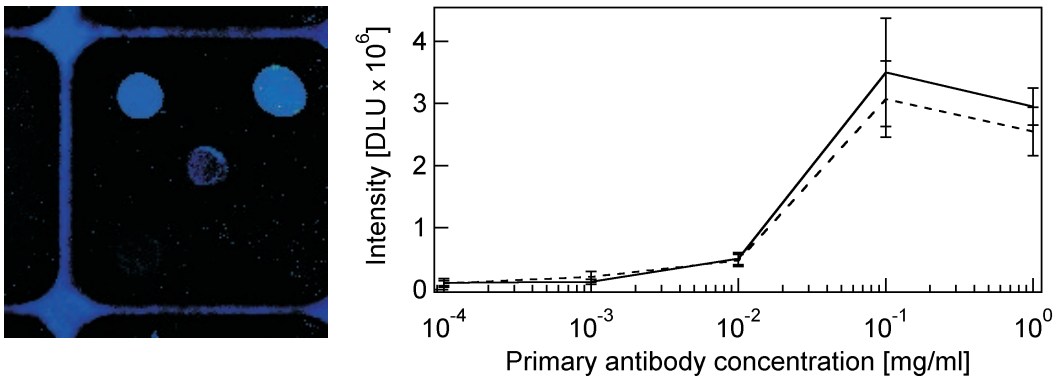

Figure 5.13: Functionality test on gold. The activity of adsorbed antibodies was tested against lysed and non-lysed E.coli. On the left an scanning image of a test square is shown. The black surface is gold evaporated onto a glass slide (blue outline). On the square shown, five ten fold dilutions of antibody have been applied (1mg/ml to 10^{-4} mg/ml). The points in the plot are the fluorescence averaged from six such squares in DLU. The solid line is from squares exposed to whole E.coli and the dashed line is from squares exposed to lysed E.coli.

Experiments were performed to determine the time for saturation of the reaction with E. coli. The results were ambiguous, but suggested that it could take a day to reach saturation. The specificity of the binding with regard to other bacteria was not investigated.

In conclusion, it turned out to be difficult to reproduce the measurements quantitatively, but overall there was recognition binding activity from the gold adsorbed anti-E.coli antibody, when incubating with E.coli for an hour. In any case, the experiments were not designed with sensitive quantification in mind.

We had hoped to achieve larger binding activity by lysis, but this did not seem to be the case. However, for the same number of bacteria a lysed sample could

make more surface antigens accessible to the immobilised antibodies, and the number of binding events on the cantilever surface is expected to be larger with a lysed sample, thus perhaps generating a larger stress. Also, the sensitivity might be larger towards lysed bacteria because for each bacteria more surface antigens would be able to get to the surface. Thus, it takes about 5000 whole bacteria to cover the cantilever (projected area), whereas, given that the antibodies are against surface antigens, 700 bacteria could do the job if broken up in pieces.

5.3.3 Cantilever measurements

Anti-E. coli (0.1 mg/ml) was deposited on the Au coated cantilever surface (the detector cantilever) as described in section 5.1.3. All remaining surfaces were blocked using SMP.

The prepared chip was mounted in the flow cell (figure 4.5) and allowed to equilibrate for at least one hour in washing solution, under a constant flow of 5 μl/min. The voltage output from the Wheatstone bridge was measured over time and recorded.

Figure 5.14 shows timeseries from E. coli detection experiments. The left axis shows the voltage output and the right axis the corresponding change in surface stress. Figure 5.14.a shows the entire time series of a sensor, including the equilibration in a flow of wash solution. Figure 5.14.b is a close up of the region where E. coli is injected: In section A pure buffer solution is flowed through the system and in section B the flow is shifted to buffer with E. coli ($7 \cdot 10^9$ lysed bacteria/ml) at the same flow rate. In C the flow has been shifted back to pure buffer. Four experiments were performed with four different sensors. In two experiments nothing happened - the two others are shown together in figure 5.14.b (blue, dashed line).

It is possible to see a consistent signal in B, but especially for the solid curve it is very close to the resolution limit given by significant fluctuations. The maximum of the signals, reached approximately 15 minutes after the flow has been switched back to pure buffer, are 50 μV and 100 μV, corresponding to surface stresses of respectively 0.13 and 0.25 N/m. After the delay the signal relaxes, when E.coli is no longer flowed through the system.

The surface stress signal measured is positive, corresponding to an expansion of the detector layer, hence a compressive stress in the layer.

Discussion

The stress development we observed for the E. coli binding to 1Ab on the cantilever was comparable to the largest stress due to protein binding interactions observed till now with optical readout where Moulin et al. in [82] report a stress development of up to 0.2 N/m over a period of 12 hours for IgG adsorbing directly onto a gold surface. G. Wu et al observed signals of up to $\sim$ 60 mN/m

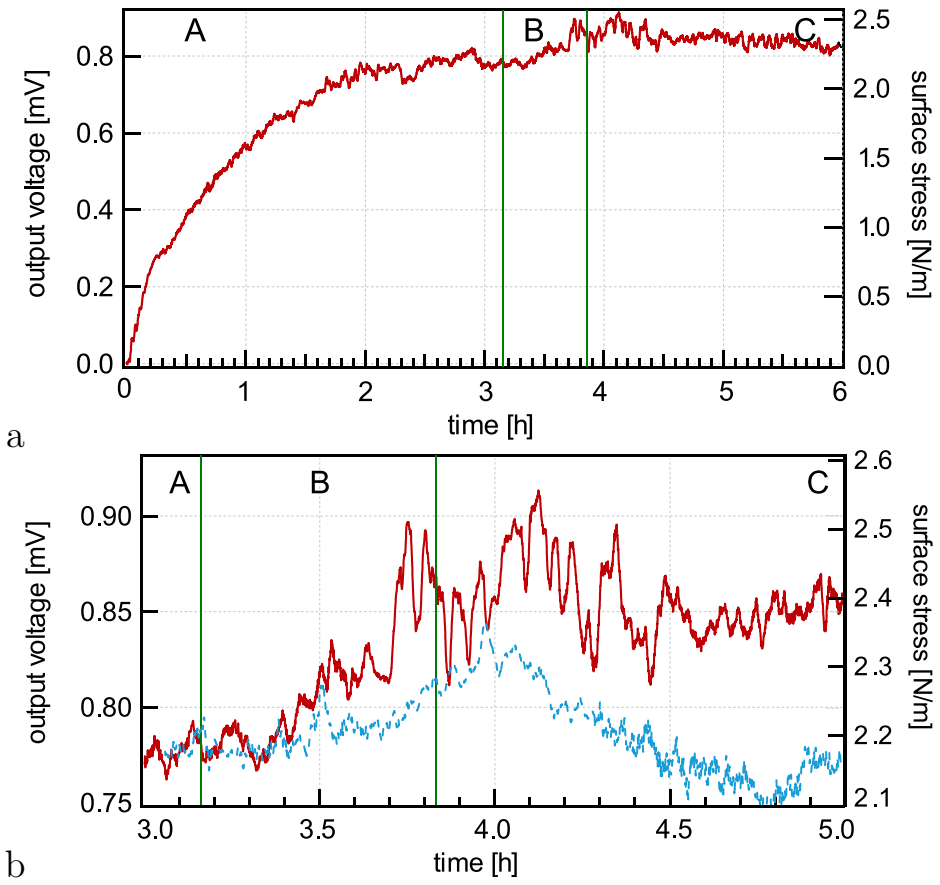

Figure 5.14: Time series of E. coli measurements with a Biosensor. **a** The whole sequence starting with the equilibration upon contact with buffer (section A). In section B the solution with lysed E. coli is pumped through and in section C again pure buffer. **b** is a zoom of **a**. Included, in blue dotted lines, is a second E. coli measurement performed with a different sensor.

(corresponding to $\approx 20\ \mu$V for our chip) at high antigen concentrations after 4 hours [23]. This was a diffusion limited experiment which could explain the long reaction time. Other studies of protein interactions on cantilevers report stress developments that are 10-100 times weaker [13, 21, 55, 83–85].

Still, the signal we observe is barely above the noise of the present experiment. The noise is also 3-4 times larger than in for example the biotin-avidin experiments (figure 5.5). This could be due to molecular movement on the cantilever but, more likely, it is a feature of the particular batch of sensor chips used and illustrates the large variation in stability of the current sensor chips. The experiments were performed with only one gold coated cantilever, but even then, the signals correspond to a temperature change of 1- 2 K. We have seen that a flow change alone does not give a signal in the sensor (figure 4.6). From the fluorescence experiments we know that E. coli does not absorb to gold surfaces blocked with skimmed milk. Nonspecific adsorption on the back side of the can-

tilevers are canceled out by the reference. A nice termination of the experiments would have been an overnight incubation with 1Ab* and subsequent inspection in the fluorescent microscope. The specificity of the system should be tested with non-E. coli bacteria.

5.3.4 E.coli protocol

Further bacteria detection and protein recognition experiments were discontinued, awaiting new generations of chips which promised to be of more stable performance.

For now a suggestion for a protocol for antibody based bacteria detection has been established.

- Two gold coated cantilevers should be used for optimal exploitation of the reference cantilever and reduced temperature sensitivity. The gold should be kept under water after evaporation. Ozone/UV cleaning could be a nice alternative.
- Mechanical localisation of E. coli antibody on the measuring cantilever and a non-sense antibody on the reference.
- Investigate also the effect of other immobilisation strategies (see below).
- SMP blocking.
- Equilibration of the prepared sensor in a flow of blocking solution. This could perhaps decrease desorption of antibody compared to pure PBS.
- Switching of flow to blocking solution with lysed E. coli. If the system is stable let it react for more than 40 minutes. Switch back to blocking and perhaps a rinse.
- Finally, incubate the sensor with Ab* overnight and check the localisation and binding in the fluorescence microscope.

Some suggested controls are: nonsense IgG on reference cantilever, test for specificity by subjecting the sensor to non E.coli and fluorescent check on cantilevers.

Further, one may consider using monoclonal Ab to acheive larger binding constants and presumably larger signal, although normally affinity purified polyclonal Ab are recommended to increase the probability of a signal.

Immobilisation

The immobilisation can be improved in several ways. Exploiting the inherent sulphur bridges in the IgG to achieve strong binding to a gold surface can be enhanced by dividing the IgG in different ways, exposing free sulphur while preserving the recognition sites [86, 87]. This carries the attraction that the antibody antigen binding event is brought closer to the surface.

Specific attachment to the gold can also be enhanced by engineering the IgG so that binding enhancing amino acid sequences are expressed in the tail region [88].

A well known method to control the orientation of the antibody, so as to ensure that the recognition sites do not face the surface, is to first immobilise protein A (or A/G) on the surface before the antibody. Protein A will tightly bind the tail of the antibody. This of course increases the molecular layer between the surface and the binding event we want to detect, but the gain in activity might be significant. Recently, good antibody recognition results were obtained on cantilevers by Wu and colleagues using immobilisation with a thiol linker [23].

Using a dealloying process to create a nanostructured surface Lavrik and coworkers obtain a 1.25 N/m tensile surface stress for the immobilisation of biotinylated avidin and about the half for subsequent avidin binding.

5.3.5 Conclusion

We established an immunoassay type system for the detection of whole and lysed E. coli bacteria, using a fluorescence based technique. The signals were not very strong, but significantly above the background.

The cantilever measurements were encouraging, although they did indicate that the sensitivity of the system at present is not high enough.

5.4 Discussion

Taking the challenges from the beginning of this chapter one by one we start with the immobilisation step which was solved satisfactory for the DNA oligo by a thiolation of the oligo. The attachement to the gold surface could be monitored in situ.

For the protein immobilisation we gambled on non-specific adhesion to gold, in the case of IgG, perhaps enhanced by spontaneous disruption of inherent disulphur bridges. This worked in fluorescence tests but it seems likely that the cantilever measurements could perform better if the immobilisation was optimised either by establishing tighter connections to the surface through crosslinking [85], added metal binding aminoacids to the antibodies [88, 89] or adding sulphur groups via amine coupling. The thickness of the detection layer can be further minimised, thus reducing the amount of energy that is lost in the spacer molecular layers, by using not whole antibodies but antigen-binding fragments of the Ab [86, 87].

The manual localisation was in principle ok though not very handy, especially on a large scale, but this is relatively easy to automate. In-situ localisation of the thiolated DNA to the gold surface was good.

Blocking was for DNA oligos solved with a detergent and for proteins cheap, skimmed milk powder was very effective.

We worked on assessing the functionality of the immobilised molecules using a fluorescence based assay. Even in situations where the fluorescence response was good the cantilever measurements were at best indicative. The functionality with regard to antigen binding could be better using monoclonal antibodies. In the case of the DNA experiments detection of hybridisation was not acheived due to the failure of the wax sealing in buffers with high salt and detergent.

The signal generation is increased by a strong, specific binding to the analyte and this could be critical. Also, the number of binding events is important, so not only many active probes but also small analyte molecules could be an advantage, for example the use of lysed vs whole bacteria.

The physical properties of the surface can also be optimised, for example roughening the surface so that the surface area accessible for interaction is increased for the same cantilever area. Roughening seems to enhance the stress signal: In the case of alkylthiol adsorption a light etch of the gold surface with aqua regia is seen to roughen the surface and enhance the amplitude of the signal with a factor of five [49]. However, these etches are not so easy to control, hence the reproducibility is not good. A quasi 3d surfaces obtained by coevaporation of silver and gold and a subsequent selective etch of the silver has been proposed by Lavrik et al. [27]. In this way they obtain an increase of surface area with a rigid matrix. They observe an increase of the signal to noise ratio of 1-2 orders of magnitude for the binding of IgG to surface immobilised protein A.

Finally, we should be able to reduce the noise on the Biosensor by at least a factor of 5-10; the limit of the intrinsic electrical noise of the poly silicon resistors is approximately 5mN/m. Especially in the DNA experiments where one gold coated cantilever is used, a sensitive temperature control would surely stabilise the signal. Recent reports [22, 26] have shown that single cantilever experiments with good temperature control and optical readout can perform at least as well as measurements using a reference cantilever system [21].

5.5 Conclusion and Perspectives

Immobilisation and localisation techniques were developed for detection of different biomolecular systems using the Biosensor chip.

The immobilisation of thiolated DNA oligo was observed and was described with a Langmuir isoterm.

Active E. coli antibodies were immobilised in a simple way on a gold surface. The activity of E. coli binding was tested by fluorescence measurements. In experiments using a cantilever-based device with integrated electrical readout we saw the development of a stress signal following the introduction of E. coli but it was not significantly above the noise level. The magnitude of the signal was larger, but in the same range, as earlier reported protein protein interactions.

We identified several possibilities for enhancing the signal to noise ratio.

Chapter 6

Summary Part I

We demonstrated the performance of the microelectromechanical chip as a sensor and the enhancement of the signal to noise ratio obtained by the combination of the integrated reference probe and the on-chip Wheatstone bridge.

It was found that the initial response of a polymer-coated cantilever could be described as proportional to the instantaneous vapour concentration in a large measurement chamber.

We established a laborious, manual and chip-by-chip procedure for protection of the electrical wires and bonds of the chip. Most importantly, combining the coating and a new chip design, the method proved effective in aqua regia and in buffers with high salt concentration and detergent.

In biosensing the best results were obtained for the in-situ immobilisation of thiolated DNA oligos on a lightly aqua regia etched gold surface.

A limit of resolution for the current chips and set-up was probably the main reason we did not obtain cantilever signals in protein recognition and bacteria detection measurements.

Pursuing the study of enhancement techniques both mechanical, through area enhancement, chemical, for example via buffer tuning, or perhaps magnetic [19] together with the optimisation of the sensor fabrication and a lock-in based detection I'm sure the necessary sensitivity will soon be reached.

Besides the application as a sensing tool, the question also remains about which phenomena we would like to understand better using this unique stress measuring device. For example G. Wu and colleagues [26] inspire a different direction of interrogation for obtaining new knowledge about collective molecular behaviour on surfaces, by playing with conditions where one or the other stress generating effect might dominate.

Part II

Nanotubes for Bio-Imaging

The ambition of the following research was to image biomolecules, on a solid substrate in buffer solutions, using the atomic force microscope with a carbon nanotube tip. The idea was to investigate especially how antibodies look, at the single molecule level, when they are immobilised on Au as used in the Biosensor. The atomic force microscope (AFM) is the tool of choice for such an investigation because of its high resolution and the ability to image individual molecules in buffer solutions. The resolution and the quality of the images obtained, depend very much on the properties of the tip used for the imaging. A carbon nanotube (CNT) is one or more sheets of graphite rolled up to form a tube [90]. Carbon nanotubes (CNTs) have many unique properties, some of which make them candidates for the ultimate AFM probe tip [91]. Developing AFM probes with CNT tips is expected to contribute significant improvements in the information obtained with the AFM [92].

This second part of the thesis begins with a short introduction to AFM and the importance of the properties of the imaging tip. An introduction to CNTs and their imaging properties precedes the presentation of the work on CNT probe assembly. The imaging of *purple membrane* and *IgG* follows. Finally, there is a short introduction to measurements on solvation layers investigated using quartz tuning forks with CNT probes.

The work was conducted in collaboration with Prof. Thomas Schmidt, Department of Biophysics, Huygens Laboratory and Dr. Ir. Tjerk Oosterkamp, Department of Interface Physics, Kamerlingh Onnes Laboratory, both at the Institute of physics (LION), University of Leiden, The Netherlands.

Chapter 7

Introduction

7.1 AFM

The AFM was invented in 1986 as a variation of the scanning tunneling microscope (STM) suited for the investigation of insulating surfaces [3]. In atomic force microscopy (AFM) a tiny tip, mounted on a flexible microcantilever, is scanned over a surface. By recording the movement of the cantilever one gets a picture of the interactions between the sharply pointed tip and the surface. The tip is normally fabricated together with the cantilever and sits as a miniature pyramid at the end of the cantilever. The AFM can operate in vacuum, ambient conditions and in liquids and especially this last possibility has inspired many efforts in the investigation of biological systems [93]. The range of the tip sample interactions that can be probed in AFM can be more than 100 nm compared to STM where the range is a few nm.

For the recording of the movement of the cantilever the first instrument used an STM. Several other readout methods have since been developed including the method using piezo resistors integrated in the cantilevers, as we have seen for the Biosensor, but by far the most common readout principle in use is the optical: A laser is shone onto the backside of the cantilever and the movement of the reflection is detected by a photo sensitive device [34], normally a quadrant photo diode.

The samples to be investigated are surfaces, which can be flat or structured, in principle with features as large as the traveling permitted by the piezo drive which controls the sample height. Soft biological samples must also be mounted on a surface and fixed well enough that they are not detached during the scan. The sensitivity of the AFM is usually limited by the thermal vibrations of the cantilever or in the case of optical readout, the shot noise of the photodetector.

In the early nineties the first applications of AFM to the imaging of DNA began to appear [31, 94, 95]. These measurements, performed in liquid illustrate the strength of the AFM, able to image soft biological molecules on an insulating

surface, under conditions approaching their natural state. This also opened for the possibility to study the dynamics of working enzymes [96] and observe the effects of their activity in real time.

The direction in imaging goes towards enhancement of the resolution and development of chemical specific imaging. This is to a large extent obtained by developments of the properties of the tip on the cantilever which is probing the surface. At the level of individual molecules information can be obtained about behaviour and mechanisms, which in a larger scale measurements are averaged out.

7.2 Modes of Operation

The AFM can be operated in very many different modes each specialised to cope with different imaging requirements. Here some of the most common are described .

Contact

In the basic mode of operation, *contact mode*, the tip is scanned over the surface. A chosen parameter is kept at a fixed value during the scan via a feedback loop which adjusts the separation between the tip and the sample. For example the deflection of the cantilever is kept at a fixed value, the set-point, corresponding to a fixed interaction force between the tip and the sample and during the scan the distance variations in order to maintain the set-point deflection are recorded. For deflections that are small compared to the length of the cantilever, the interaction force F is given by the deflection, Δz, and the spring constant of the lever, k: $F = k\Delta z$. In this way a map of constant interaction is obtained. With this method it is possible to obtain atomic resolution on hard surfaces [97] and, operating carefully in liquid, subnanometer resolution can be obtained also on soft structures such as proteins arranged in lattices in lipid membranes .

Tapping

Operating on soft samples in contact mode can be a risky business as the cantilever exerts a lateral pressure on the sample. The most obvious effect is that one can end up scraping the sample of the support so, zooming out, one sees a bare patch with dikes of soft material on each side. To avoid this one can use the *tapping mode*: The cantilever is excited close to its resonance frequency, for example mechanically, with an extra piezo drive, magnetically or acoustically, and the sample is kept at a distance and an amplitude so that the tip taps at the surface in each cycle. The amplitude of the oscillation can be kept constant so the tip interacts with a force given by the amplitude setpoint and factors such as the tip radius, the spring constant and the interacting materials.

Normally the cantilever is excited vertically, detecting interactions normal to the surface. This mode also has the advantage that the microscope is relatively insensitive to a slow drift in the equilibrium position of the cantilever caused by temperature fluctuations, because the feedback is not on the deflection of the cantilever but on its amplitude. The constant amplitude image is related to the topography although not necessarily in a simple way, as a shift in resonance frequency due to variations in the gradient of the force or mass change due to dirt picked up by the cantilever during the scan also will change the amplitude at the chosen frequency.

One can record the height variations necessary to maintain the chosen amplitude and at the same time follow the phase of the cantilever oscillation relative to the driving signal. The former gives the topographical image while the latter is related to the damping of the cantilever oscillation [98]. This damping can give additional information on specific interactions between the tip and the sample which are influenced by properties as the adhesion, the elasticity of the sample and so forth. Especially, the phase imaging can be used to map out chemical contrasts.

Non-contact

In the related family of modes, non-contact AFM, the tip is oscillated near resonance but with small amplitude. The tip is no longer oscillated at a fixed frequency but in such a way that the phase shift between the vibration of the cantilever and the driving signal is kept constant. The dynamics is then mainly dependent on the change in force gradient, which is felt in a change of the effective spring constant $k_{eff} = k - \partial F/\partial z$.

Both dynamic modes have their share of inconveniences among which damping of the cantilever oscillations when operating in liquid is a challenge especially in the promising area of bioimaging. When the motion of the cantilever is damped by surrounding liquid the Q-factor is reduced, meaning that the resonance peak broadens thus decreasing the sensitivity. This is one of the reasons that the highest resolution images of biological samples in liquid are still being obtained with carefully controlled contact mode imaging [99].

Force-distance curves

Force- or deflection-distance curves are obtained by changing the height of the sample and recording the corresponding deflection changes. The *force curves* thus obtained tell about the interaction forces at that particular point and can for example be used to study chemical interactions between tip and sample [100]. When the tip is in contact with a hard surface any further decrease in the distance between the cantilever and the surface will give a linear response of the photodetector. This can be used to calibrate the deflection sensitivity of the

detector. The force curves also give important information on the state of the tip by showing the adhesion between tip and sample in the retraction part of the curve.

The AFM probe can be functionalised by attaching molecules to the AFM tip. The forces needed to unfold and unbind can be measured and the functionality down to the single molecule level can be studied, even at intramolecular resolution. For example, the structural strength of single molecules were studied by the stretching and unfolding of IgG domains in titin fragments [101]. The first and still most common way to study chemical interactions is to use the adhesion force curves to measure the force needed for unbinding. In this way both the binding between avidin and biotin [75, 102, 103] and the recognition between complementary DNA strands [104] have been measured. It has been found that not only the force, but also the loading rates are critical [105, 106].

For measurements on the interaction between an antibody and its antigen a crucial element was a long spacer molecule [107]. The spacer provided distance between the bulk of the tip and site of the interaction and, adjusting the density of the spacers, made it possible to study the interactions of a single molecule. However, this limited the resolution because the spacer molecule was soft and flexible. Combined with a statistical analysis however, a spatial resolution of 1.5 nm was obtained. The approach was extended to continuous imaging in dynamic mode where the amplitude of the oscillations was reduced when the (half) antibody on the probe was close to surface immobilised antigen [108].

7.2.1 The AFMs at the Huygens Laboratory

Two Nanoscope IIIa, Multimode Scanning Probe Microscopes from Digital Instruments Inc., Santa Barbara, CA, USA were installed in the AFM lab in the summer of 2000. The Nanoscope Extender was used in connection with phase imaging and a Signal Access Module was used for any slightly alternative monitoring or modification of the signals. The instruments were mounted on vibration isolation tables[1]. The *Burleigh Box* which was installed on one of the AFMs, further significantly reduced the noise in the images. This is an isolation box which very effectively shields acoustic vibrations. It is no longer in production.

[1]One of them on a Halcyonics active vibration isolation table (`www.halcyonics.de`)

Chapter 8

Nanotubes as Nanoprobes[1]

We will look at carbon nanotubes (CNTs) as possible candidates for probe tips in AFM and discuss some different techniques for the assembly of such probes. Work will be presented on assembly using two different techniques and transmission electron microscopy will be used to verify the assembly.

8.1 The Probe Tip

At the heart of the AFM imaging lies the probe tip: it is the point of the tip that interacts with the surface and its properties directly influence what is seen with the instrument. The first requirement to obtain high resolution is that the tip is sharp on the scale of the interactions that are investigated. The radius of curvature should be small to be sensitive to small structures and the aspect ratio is important in order to minimise the interactions between the sample and the bulk of the tip. To obtain high reproducibility it is an advantage to be able to work with the same tip, so the durability is an issue. Another desired feature of a probe tip is the ability to modify the chemical properties. This opens for the possibility of chemically sensitive imaging.

AFM tips are mostly produced integrated with the cantilever by micro-machining of Si or SiN. The simple type is typically pyramidal in shape, defined by the crystal planes of the silicon. The radius of curvature and the aspect ratio can be enhanced by oxide sharpening and different etching procedures [1]. Currently commercial Si tips are available which have tip nominal tip radii down to 5 nm and cone angels of as little as 10 degrees[2]. These are very high quality tips, but they are very easily damaged and quickly worn if used on hard surfaces.

With regard to chemical modification many possibilities exist, for example inspired from surface functionalisation techniques (chapter 5.3.1), but all have a tendency of increasing the radius of curvature of the tip and reducing the

[1] This title is borrowed from the first paper on nanotube AFM probes by Hongjie Dai [91]

[2] For example the SuperSharpSiliconTips at www.nanosensors.com.

lateral resolution of the image. Also, in an effort to perform single molecule measurements and reduce non specific interactions, the probing molecules are attached to spacers. These are often long and quite soft polymers, which further reduce the resolution [107].

Ultra thin, long and very strong tubes of rolled up graphite, carbon nanotubes, have many properties which make them candidates for 'the ultimate probe tip' [91].

8.2 Carbon Nanotubes

Sumio Iijima hit the headlines with the discovery of the carbon nanotubes in 1991 [90], in the wake of the bucky ball excitement. A few earlier reports had gone all but unnoticed [109]. Since, there has been activities all over the world developing different techniques for the production and exploitation of this new material which is relatively simple to make and has fascinating properties. Carbon nan-

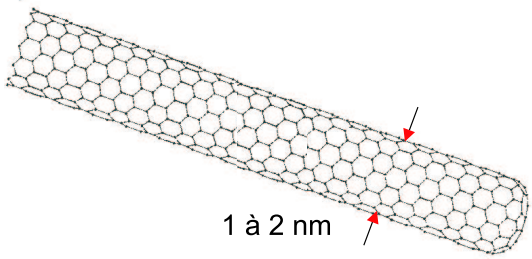

Figure 8.1: Sketch of a graphite sheet rolled up in to a single walled carbon nanotube.

otubes (CNTs) are rolled up sheets of graphite. The nanotubes come as single rolled up sheets, the single walled carbon nanotubes (SWCNTs) or in an onion structure where several sheets are rolled up one around the other, the multi walled carbon nanotubes (MWCNTs). Both the SWCNTs and MWCNTs often appear in bundles or ropes which makes it possible to view them also under the dark field of an optical microscope. Figure 8.1 shows a single walled nanotube. At one end it is capped by a bucky ball half sphere. They are very thin, some less than a nanometer, while they can be several micrometers long, and they are extraordinarily stiff with a Young's modulus of more than 1 TPa [110, SWCNTs] which is comparable to diamond, over ten times stiffer than silicon and five times stiffer than steel. Still they are so flexible that they can be bent double and spring back to their original confirmation with no apparent damage. However, perhaps their electrical properties were what really spurred the attention and imagination (see for example [111] and [112]). CNTs have metallic or semiconductor properties depending on the twist with which the graphite is rolled up – the chirality (the CNT in figure 8.1 has twist 0) – and they can sustain current densities up to one

billion Amperes per cm^2. Being able to use them as wires in micro electronics would mean a decrease in line width of nearly two orders of magnitude, compared to state of the art lithography. The small dimensions of the CNTs also make them fascinating because of the inherent quantum mechanical nature of the electronic properties. The creation of CNT transistors [113] and light emitting diodes [114] contribute to a bright picture of the nanotube future.

8.2.1 Making Carbon Nanotubes

Carbon nanotubes can be made using several different techniques. In the so called conventional arc discharge used by Iijima, the CNTs are generated when an electric field is applied between two graphite electrodes in an inert atmosphere, for example helium or argon. The carbon is dissociated by the electric field and in the soot created at the cathode one can find a zoo of carbon products among which bucky balls and CNTs. If a metal catalyst is used, for example iron or cobalt, single walled CNTs can be formed [115, 116]. The CNTs generated in this way are of high quality, with few defects, but a cleaning procedure is required to separate them from the other carbon products [117].

In the chemical vapour deposition (CVD) method the reactive carbon is created by heat dissociation of carbon containing gasses. The gas, typically CO or C_2H_4, is blown over a supported catalyst which is heated to between seven and nine hundred degrees C. In [118] Hafner and coworkers make high quality SWCNTs at a quite high yield. With CVD there seems to be good possibility of controlling the positions of growth of the CNTs and this has been exploited in the efforts to integrate CNTs with SPM probes by growing the tubes directly on the cantilever tips [119–120].

Also laser evaporation techniques have been used to create CNTs [ref 1 in haffner98] and, using liquid nitrogen as inert atmosphere and cooling agent CNTs can even be made by arc discharge in a table top setup [122].

The goal, which has not yet been reached, is to be able to control the properties of the CNTs grown, so the growth methods are still being explored. Especially the electrical properties, given by the chirality of the tube, but also the diameters, the lengths, the positions and directions of growth are parameters which it is desirable to master.

In the following I will concentrate on the mechanical and chemical properties of the CNTs which make them attractive as AFM probe tips.

8.3 Why are CNTs interesting as scanning probes

Earlier this year Jason Hafner and coworkers from the laboratory of Charles Lieber at Harvard published a review on the preparation and use of carbon nanotube tips in scanning force microscopy [92]. The interesting properties of the

CNTs in AFM are both mechanical and chemical.

8.3.1 Mechanical

First of all CNTs have very small diameters, the single walled CNTs can be less than one nm thick. This gives the possibility of very high resolution on for example isolated macromolecules. As they are straight tubes and can be micrometers long the aspect ratio is extremely high and bundles of tubes can be used to probe deep trenches with steep slopes. This also means that the sharp tip and the interaction with the sample are far away from the bulk of the silicon tip and non-specific interaction is minimised. In addition this geometry reduces the capillary forces between the tip and a sample imaged in ambient conditions [91], one of the factors which set a lower limit on the minimum forces with which one can image.

The large stiffness of the tubes, Young's modulus of 1 TPa, mean that they are very strong - they have a high durability. Metrology with sharp Si or SiN tips on hard surfaces suffers from serious degradation after a few scans, particularly if the tips are very sharp. Imaging with CNT tips show very little wear even after several hours of scanning [123]. The stiffness of the CNTs also means that all though they are very thin they can still be relatively long before thermal vibrations at room temperature seriously degrade the maximum resolution: The lateral spring constant, k, of a cylindrical rod of radius r and length l is given by $k = 3\pi Er^4/4l^3$, where E is the Young's modulus. If we approximate the thermal vibrational amplitude by assigning $1/2k_BT$ to the lateral vibrational mode, where k_B is Boltzmann's constant and T is the absolute temperature, we get for the vibrational amplitude $x = \sqrt{k_BT/k} = \sqrt{k_BT4l^3/3\pi Er^4}$ [124].

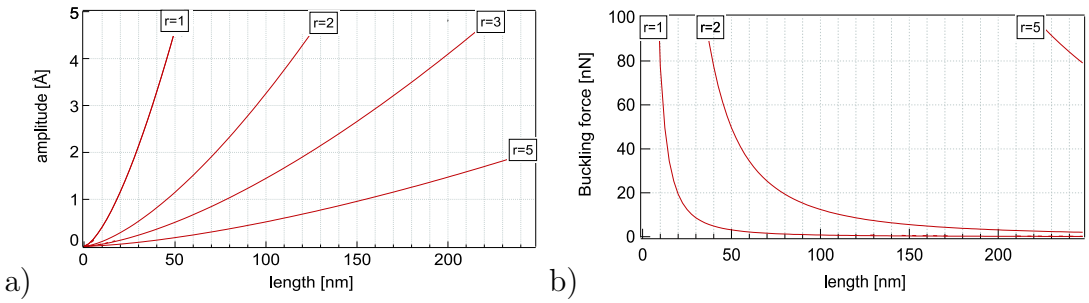

Figure 8.2: a) Thermal vibrational amplitudes at room temperature for CNTs of different radii, r, and lengths. The examples are for both CNTs (Young's modulus: $E = 1$ TPa). **b)** Euler buckling forces for the same parameters as in a).

In figure 8.2.a graphs of this amplitude are plotted as a function of length for four different CNT radii. Apart from limiting the thermal vibrations, some stiffness is desirable to avoid that the CNT bends sideways while imaging thus either sliding of the imaged molecule or sticking to the sides of crevices [125]. Thus a

vibrational amplitude of 5 Å corresponds to a spring constant $k = 16$ mN/m and it takes less than 200 pN to deflect for example a 100nm long and 4nm wide CNT by 10 nm.

Another factor of importance to the imaging capabilities of a CNT tip is the buckling force, that is the force above which the tube buckles elastically when it is pressed down on a surface. The Euler buckling force of an elastic column is $F_{\mathrm{E}} = \pi^3 E r^4 / 4l^2$ (figure 8.2.b) [91]. If this force is expected to be a maximum of 10 nN a CNT tip of 2 nm diameter should be no longer than 25 nm. On the other hand it might also be attractive to have a tip that will buckle above a certain force in order to protect the sample. Typical forces associated with such deformations are fractions of nN [99]. The tip however is also protected from damage by this behaviour because the buckling is fully reversible for the CNTs. This has been measured for example in [91].

8.3.2 Electrical etch

In order to obtain high resolution images from CNT tips it is critical to be able to control the length of the CNT within a few nm because of the thermal vibrations and the buckling force (figure 8.2). It is often necessary to be able to adjust the length of the CNT tip on an assembled probe. Since the very first assembly the method of choice has been the so called electrical etch [91, 124]: short pieces of the CNT can be etched away by applying a voltage, typically between 5 and 40 V, to the tube., for example between the assembled probe and a metal surface. Hafner and coworkers show clearly in reference [124] how the CNT length of an assembled probe can be regulated within a couple of nanometers when short pulses and moderate voltages are applied. Moreover, this etch in ambient air has been shown to produce CNTs terminated with carboxylic acid (paragraph 8.3.3) and it has been demonstrated that etching in the presence of different gasses the terminal groups of the CNTs can be modified (for example H_2, O_2 and N_2) [126].

Moreover, the electrical etch occasionally seems to sharpen a MWCNT resulting in higher resolution images [127]. If this can be sufficiently controlled such a probe seems the ideal for bioimaging as the aspect ratio still is very high and the tip very sharp and modifiable. The added thickness further up the CNT adds lateral stiffness so the distance to the bulk of the cantilever tip may be increased without loosing resolution due to the thermal vibrations.

8.3.3 Chemical

Perhaps the most interesting feature of the carbon nanotubes for biochemical use of the AFM is the well defined chemical properties of the tip. The end of the tip can be closed with a cap as in figure 8.1. However, it can also be opened by different oxidation procedures [128]. Especially, during an electrical etch in air bits of the tip are burnt of and primarily the end of the tip is oxidised. This

creates an active tip at the end of an otherwise unreactive tube. Stanislaus Wong and coworkers also demonstrated, that the form of oxidised carbon at the end of a nanotube etched in air is carboxylicacid (COOH) [126]. They demonstrate this by performing adhesion force titration experiments: The chemical composition of the end of the nanotube can be probed by measuring the adhesion to a surface of known composition at different pH values. A hydroxy presenting surface can be formed using thiol chemistry on a gold surface. At low pH values hydrogen bonds can form between the COOH of the tip and the OH on the surface. As the pH value is increased the COOH is deprotonated and becomes negatively charged. The pH of the transition of the adhesion force at approximately ph 4.5 is characteristic of COOH deprotonation (figure 8.3). There might be a few

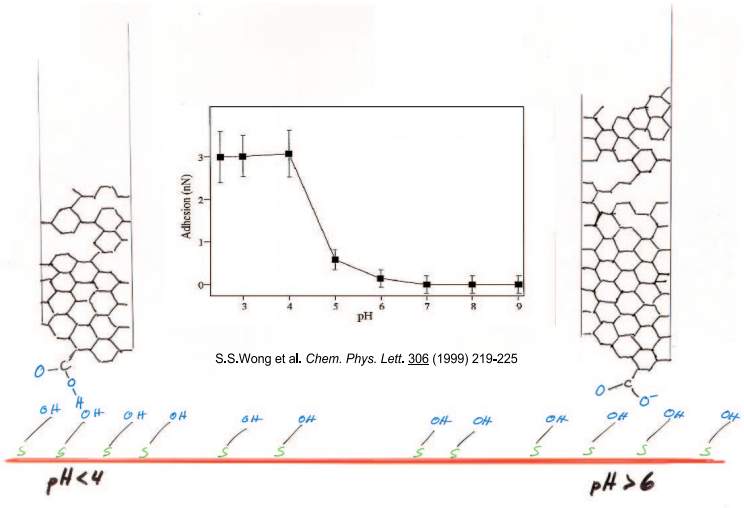

Figure 8.3: Adhesion measurements for a CNT, shortened in air, on an OH terminated surface. At the pH characteristic of COOH deprotonation the adhesion between the CNT and the surface decreases. [126].

COOH groups at the tip end but probably only a small number of them will be favourably placed for interaction with the surface.

One can also exploit the ability of the COOH group to form covalent bonds with an amine (NH_2) – the peptide bond which is the glue of the protein backbone. Using phase imaging and adhesion force titrations Wong et al. demonstrated chemically sensitive functionalisation with benzene amine and biotin [127]. Force curves were performed with a biotin functionalised tip on an avidin coated surface in which it was possible to distinguish single and double binding events. The unbinding force was found to be ~ 200 pN. This is slightly larger than the values found by Hermann Gaub and coworkers [75, 102] and G. U. Lee et al. [103] using SiN tips. With the CNT tip the major part of the measurements were single molecule events. This illustrates the role of the CNT as a spacer, providing

distance to the non-specific interactions of the bulk tip and the small, reactive, tip limiting multiple interactions of probe molecules.

In brief, once they have been assembled to a probe, the CNTs indeed seem to provide the ideal AFM tip, particularly for investigating specific molecular interactions.

8.4 Methods of CNT probe assembly

The first report of successful integration of CNTs and micromechanical probes was reported by Hongjie Dai and coworkers in 1996 [91]: The tip of a Si probe was coated with adhesive by touching it to an adhesive tape. Under the dark field illumination of an optical microscope the tip was approached to bundles of MWCNTs and some were picked up. In this first study both the strength and the flexibility of the CNTs were confirmed and the imaging capabilities of the CNT tips both in AFM and STM were shown. As we have seen (section 8.3.1), the length of the CNT is a critical parameter for the imaging properties of a CNT tip and the principle of the control of the length of the CNT tip by electrical etch was also demonstrated by Dai in this first publication. The principle of assembly is still in use, also for commercial CNT probes[3], and naturally other approaches have been explored. Three current developments in assembly strategy will be described briefly in the following.

8.4.1 Direct Manipulation

What is here called *direct manipulation* can bee seen as a refinement of the first assemblies, as it also is a process under direct view but now the view of a Field Emission Scanning Electron Microscope (FE-SEM) [129, 130]. The other essential element in this method is the CNT 'cartridge' where the CNTs are aligned on a sharp razor blade [131] (figure 8.4.a). The FE-SEM contains two independent high precision three dimensional piezo manipulators. The resolution limit of the FE-SEM is slightly better than 10 nm so the method uses MWCNTs or bundles of MWCNTs. The cantilever tips and the CNTs on the razor blade substrate are mounted on the manipulators and brought into contact (figure 8.4.b). The CNTs are fixed to the tip by carbon deposition arising from focusing the electron beam of the microscope [130] (figure 8.4.c) and finally the CNT can be shortened by applying a field between the tip and the cartridge, while making contact with the attached CNT (figure 8.4.d).

This method of attachment was the basis of one of the first commercially MWCNT probes made available from Seiko Instruments Inc.

[3]Piezomax Technologies, Inc.

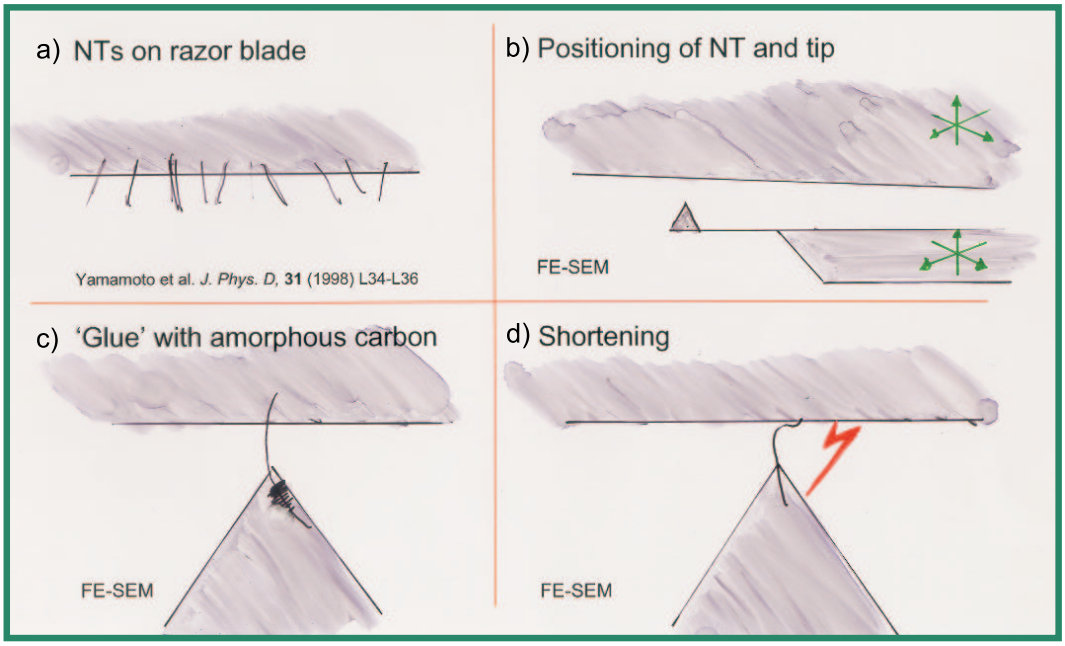

Figure 8.4: Principle of the direct manipulation.

8.4.2 Direct Growth

An attractive development for batch fabrication of CNT probes is the growth of CNTs directly on the probe tips. The first reports used a *pore growth* method [121, 119]. The AFM tip is first flattened against a hard surface and small holes are etched perpendicular to the flattened surface by an anisotropic reactive ion etch. Catalyst is deposited in the holes and the growth of the CNTs is guided by the direction of the holes. As the tip is flattened while mounted in a fashion similar to the one used while imaging, the flattened surface will be parallel to the imaged surface. If the density of holes and the catalyst are well controlled this should give CNT tips with the desired orientation. That is, with normal incidence during imaging. One of the problems is of course that this method does involve a bit of individual handling of the tips. Another is, that the CNTs are not very firmly attached.

The *surface growth* technique is completely batch compatible as no individual tip manipulations are involved: the CNTs are grown from catalyst deposited directly on the pyramidal Si/SiN tip [120]. As the CNTs get longer at some point they topple over and the growth continues along the surface. When they reach an edge of the pyramidal tip they tend to bend and continue growing along the edge. At some point a CNT will reach the tip of the pyramid and continue growing out from it. This behaviour can be partly explained from considerations of the adhesive energy vs the binding energy. By careful control of catalyst density and growth conditions a single SWCNT tip can be obtained. The yield

for individual SWCNTs is about 10% and for 75% for bundles of SWCNTs [132].

8.4.3 Pick-up

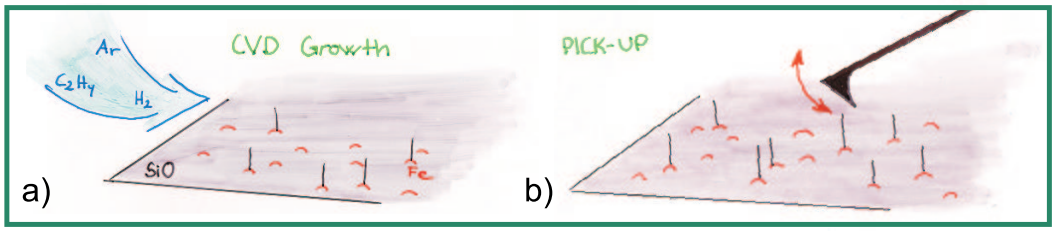

Figure 8.5: Principle of the pick-up technique. **a)** CNTs are CVD grown from a low concentration of catalyst on a Si surface. **b)** While scanning the sample in tapping mode a CNT can spontaneously attach to the tip of the cantilever, sticking by non-specific forces along the major part of the tube connected to the Si of the tip.

The 'Pick-up' technique, figure 8.5, is one of the most recent integration techniques developed in the laboratory of Charles M. Lieber [124]. In this approach SWCNTs are grown by CVD from a catalyst deposited on an oxidised silicon surface. This is the same principle as in 'direct growth'. Catalyst in a low concentration on the surface is annealed and reduced. The temperature and time of exposure to the carbon containing gas is controlled to assure SWCNT growth and to control the length of the CNTs. If the growth is stopped while the CNTs are still less than a critical length of about a micron, the CNTs will stand straight up from the surface. The CNTs on the sample are transferred to a cantilever tip by scanning the sample in AFM using tapping mode (fig. 8.4.3). While scanning, one can see the spontaneous pick-up of a CNT as a sudden increase in the apparent sample height. The larger part of the CNT will be adsorbed to the cantilever tip with non-specific forces, primarily van der Waals forces. Typically ten to a couple of hundred nm of the CNT will be protruding from the apex of the pyramidal tip of the cantilever. The adhesion of the CNT to the tip can be enhanced by coating the tip in UV glue prior to the pick up or by cleaning the tip in HF before the pick-up and baking the tips afterwards. Especially for use in liquid environments the non-specific interactions alone are not sufficient.

8.5 Probe Assembly using the Pick-up technique

We now proceed to describing the work we performed at the University of Leiden on assembly of single walled carbon nanotube tips.

The CNT samples used were grown by Tjerk Oosterkamp, following the recipe in [124]. After preparation the CNT substrates were stored and used in ambient conditions.

Figure 8.6 shows an AFM image of a substrate, on which CNTs have been grown. $2 \times 2\mu$m was scanned with an AFM in tapping mode in air. In a) you

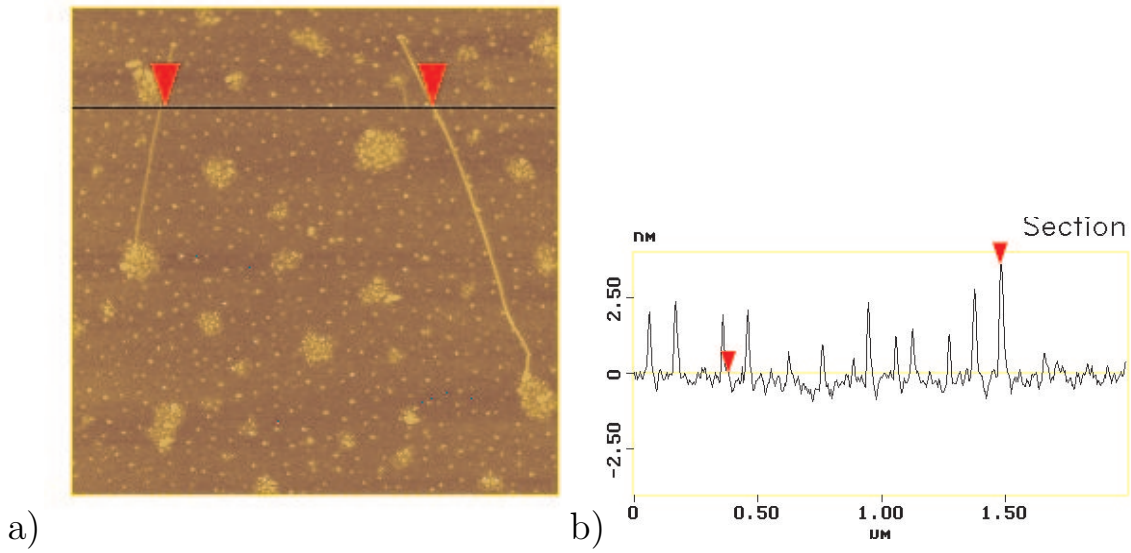

Figure 8.6: a AFM of SWCNTs lying on the SiO surface on which they were grown. Scan area: $2 \times 2\mu$m. **b** Profile across the line indicated in a). The triangles mark the SWCNTs.

can see the catalyst as small bumps on the surface and two $1 - 2\mu$m long CNTs are lying down. They could have toppled over because they had grown too long or they could have been knocked over by the AFM tip during a previous scan over the area. The line scan shows the height of the two CNTs to be about 2 and 3 nm respectively. Typically the heights measured in the scans are representative of the actual thickness of the CNTs and in this case the heights correspond to expected diameters of SWCNTs grown under the above conditions. The apparent width of the tubes is convoluted with the shape of the probe tip. Nevertheless, in principle it is still possible that the CNTs we see are in fact small bundles.

It is while making scans as the one above that pick-ups can occur. Figure 8.7 shows a 10×10 μm scan during which a pick-up event takes place towards the bottom of the image, scanning form the top. After the pickup event, giving rise to an apparent height increase of 369nm the tip was retracted manually. The spike before the plateau could be a near pick-up event where a tube fell of without properly attaching. No features can be distinguished in the image because it has not been plane fitted.

In figure 8.8 the image has been line by line first order plane fitted. A pick-up event takes place approximately at the middle of the scan. Note that the hight information in this image is corrupted by the plane fit. The slow scan direction is

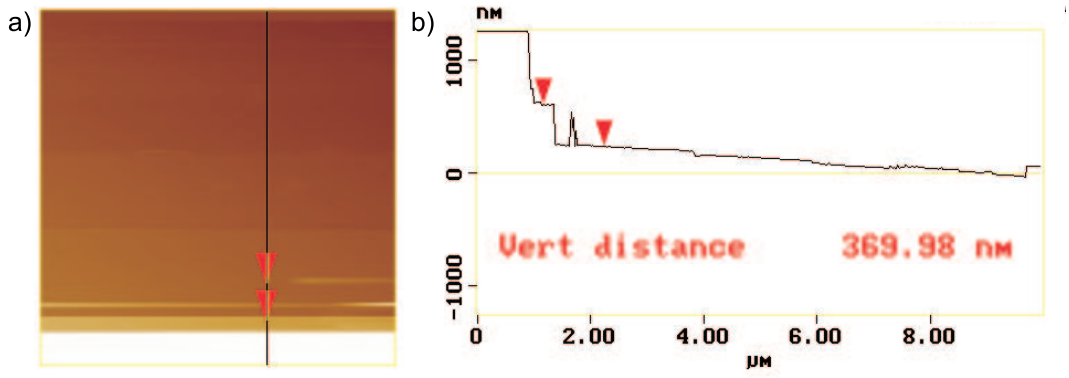

Figure 8.7: a) A scan with the pick-up of a CNT occurring towards the end of the scan (downwards). The scan area is $10 \times 10\mu$m. **b)** A line scan along the line indicated in a) showing a spike, which is probably a near pick-up event, a plateau at 369 nm form a pick-up and finally the manual retraction of the tip (far left).

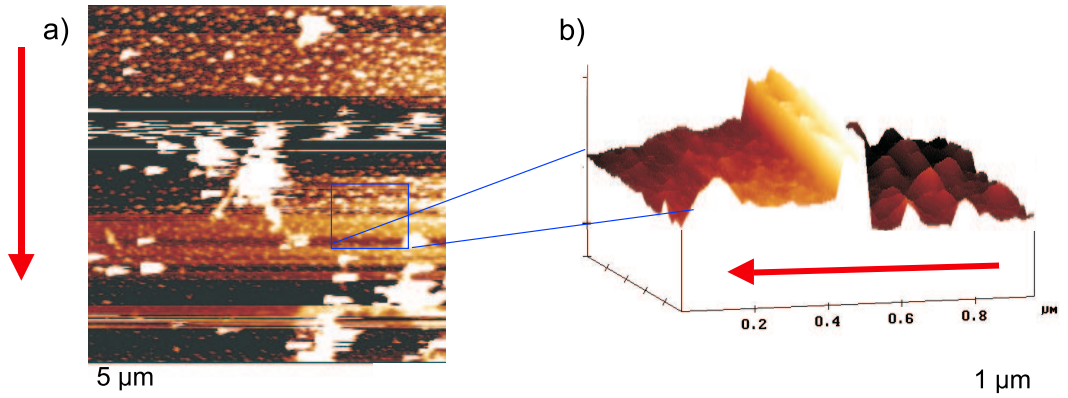

Figure 8.8: a) A plane fitted scan with the pick-up of a CNT occurring approximately in the middle of the scan. The arrow shows the slow scan direction. The scan area is $5 \times 5\mu$m. **b)** A $1 \times 1\mu$m profile view from the side of an area around where the pick-up is taking place.

from top to bottom. Preceding the event large variations, large contrasts, are seen in the image. This is because the scanning tip runs into the CNT a few hundred nanometers before the position where a pick-up can take place. This typical behaviour sometimes does and sometimes does not result in a CNT attached to the tip. One of the first indications that a successful pick-up has taken place is an increase of the apparent height, as seen above, of the sample due to the added length of the scanning tip. In the specific case of the pick up in figure 8.8, the enlarged profile image b) shows, from an angle from the left side in the scan direction, that the the resolution is enhanced after the pick-up. This is an indication that the protruding tip of the CNT is short enough that the thermal vibrations are not deteriorating the image. We later saw from the force curves of this tip, that the CNT was approximately 20 nm long, which indeed limits the

thermal vibration amplitude to less than 2 Å for a CNT with a diameter of 2 nm (figure 8.2).

A suspected pick-up event can immediately be investigated by making force distance curves. In tapping mode this means taking amplitude vs distance and

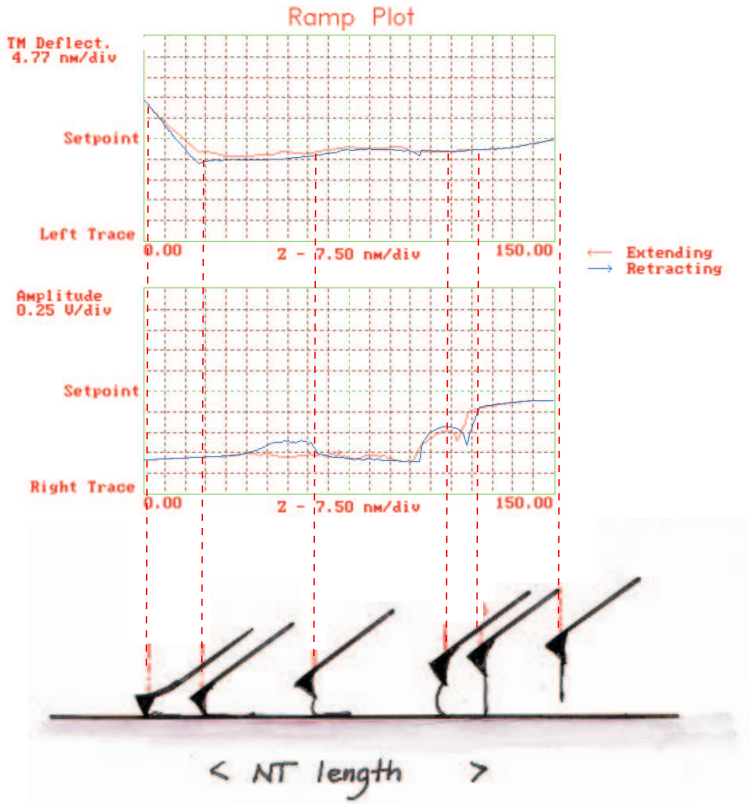

Figure 8.9: Deflection and amplitude vs distance curves for a CNT tip. At the bottom a sketch of the cantilever position corresponding to different points on the curve

deflection vs distance curves on a smooth part of the substrate, figure 8.9. The probe is approaching from the left: the cantilever is vibrating freely close to resonance, free amplitude ~ 0.75 V. The deflection is essentially zero only modulated with some interference. As the tip approaches, the CNT gets in contact with the surface and the amplitude decreases. The amplitude is however recovered a bit as the CNT buckles and is then reduced to essential zero, still with no change in the deflection of the cantilever. Approximately 130 nm after the first changes in the amplitude the cantilever begins to bend and we get a deflection. The distance from the first response in the amplitude to the beginning of the linear deflection is interpreted as the length of the CNT. The CNT is thus strong enough to hinder the vibration of the cantilever but not stiff enough to bend it. These curves can be repeated many times. The curves are not completely reproducible, the buckling does not always occur in precisely the same way. They are an excel-

lent illustration of the flexibility of the CNTs. This evidence for a CNT tip is, however, only indirect and the final confirmation is a direct view of the assembly (section 8.7).

8.5.1 Shortening

Shortening of the SWCNT assembly was done in an AFM modified for doing scanning tunnelling microscopy. The probe was scanned in tapping mode over a doped silicon substrate. The probe and the substrate were connected to a computer controlled power supply which could give 150 μs pulses of 1 to 40 Volts. In general we had trouble finding the midway between no reaction and the CNT being kicked right of the probe. This would perhaps be solved using the cleaning and baking procedure suggested for increased attachment (section 8.4.3).

8.6 Assembly using Direct Manipulation

Assembly of MWCNT probes, using the direct manipulation method, described in section 8.4.1, was carried out under the supervison of Suzi Jarvis at JRCAT, AIST in Tsukuba, Japan.

The CNT cartridge with CNTs aligned on a razor edge was prepared in Osaka. The CNTs are produced by conventional arc discharge [117], suspended in isopropanol and aligned on the razor blade using a high frequency AC field [133].

The razor blade substrate, was mounted on one of the manipulation stages in a field emission scanning electron microscope (FE-SEM) and the tip, on which the CNT should be attached, was mounted on the other manipulator using specialised holders. After focusing and approaching the substrate and tip a suitable (bundle of) CNT(s) was chosen (figure 8.10.a). Manipulating so the CNT lay against the surface of the tip, the FE-SEM was focused on the contact area for 10-20 seconds. The focusing caused contaminants in the SEM chamber to be deposited in the area and the CNT was thus glued to the surface. This gluing was repeated a few times for stability. By manipulating the razor edge the CNT could be held and fixed in a desired direction — typically the direction which would give a normal impact on the sample once the probe would be mounted for imaging (figure 8.10.b to c). Even during lower resolution viewing in the FE-SEM contaminants were deposited both on the CNT substrate and on the tip. Especially CNTs on a cartridge that had been in use for a while would be coated with a layer of (presumably) amorphous carbon. Once the CNT was attached to the tip the fixing and the CNT were stable enough that the layer of amorphous carbon could be literally scraped off! In figure 8.10.b you can see a small 'hat' on the tube: This is a sheath of amorphous carbon which was mechanically removed. This rough handling did not seem to affect the CNT. Finally, the CNT was shortened

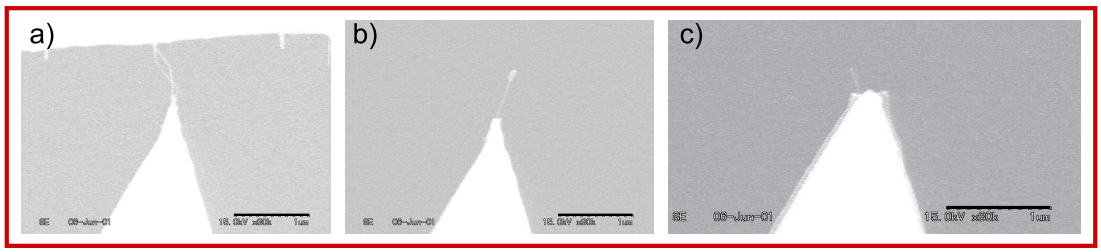

Figure 8.10: A MWCNT probe being assembled. a) The razor blade is at the top of the image, here pressing down a bit so we see that a couple of CNTs, or CNT bundles, are attached. In b) there is only one CNT left. There is a small cap of amorphous carbon at the end of the tube which is being mechanically removed. c) The CNT tip has been further shortened and the direction has been adjusted to give close to normal incidence when the cantilever chip is mounted for AFM imaging. The cantilever and the supporting chip are to the right of the image. The scale bars are 1 μm.

to a desired length by pressing the razor blade down on the CNT and applying a short pulse of 5-20 V between the blade and the tip (figure 8.10.b to c). The pulse was a capacitive discharge, time constant $\tau = RC$. C is set to 1 or 10 μF and the length of the pulse depended on the contact between the tube and the tip and between the tub and knife edge.

In addition to ordinary cantilever tips, we also mounted CNTs on etched gold tips mounted on quartz tuning forks, which were to be used for the detection of solvation layers (chapter 10).

8.7 TEM imaging

Some of the assembled CNT probes were imaged in a transmission electron microscope (TEM)by Frans D. Tichelaar[4]. Figure 8.11 is an image of an approximately 2.5 nm wide CNT mounted on a Si tip[5] — the direct confirmation that we indeed did manage to attach SWCNTs to the tips using the pick-up technique. The CNT is contaminated so the structure can not be resolved and so apart from the small diameter, it cannot be verified that it is a SWCNT.

The contamination was most likely a problem connected to the TEM imaging as it grew during the imaging. Approximately one minute after figure 8.11 was taken the thickness of the contamination layer had grown by nearly 9 nm (figure 8.12). To obtain information on the structure of the SWNT on the probes investigations could be made on SWCNTs collected from the substrate before the assembly.

In the case of one of the MWCNTs probes prepared in Japan we did not observe growth of the contamination during 20 minutes of imaging (figure 8.13).

[4]National Centre for High Resolution Electron Microscopy, Laboratorium voor Materiaalkunde, TUDelft, The Netherlands

[5]Nanosensors, FM-W cantilever, k 2.3-4.4 N/m, f_0 73-90 kHz.

Figure 8.11: TEM image of a tip assembly presumably with a SWCNT. The width of CNT is approximately 2.5 nm. Image by Frans D. Tichelaar, TUDelft

It is not as yet clear what caused this difference. The MWCNT tube had not had the amorphous carbon layer scraped of and we could not determine wether there was one or more nicely structured MWCNTs beneath the amorphous carbon layer or wether the MWCNT was disordered (figure 8.13).

8.8 Conclusion on CNT probe assembly

Two methods were used to assemble CNT probes. Using the Pick-up technique we assembled probes with SWCNTs. The length of the part of the tube extending from the silicon tip was determined using force curve measurements. From TEM

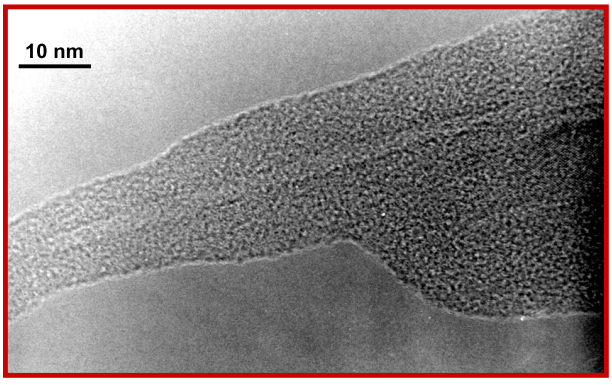

Figure 8.12: An image taken about one (!) minute later than figure 8.11. The thickness of the contaminant layer has increased by $\sim$ 9 nm. Image by Frans D. Tichelaar, TUDelft

Figure 8.13: TEM image of a tip with a MWCNT assembled using the direct manipulation technique. The amorphous layer is carbon and probably deposited during the assembly. The outer diameter is approximately 24 nm and the inner tube(s) is 6-7 nm wide. Image by Frans D. Tichelaar, TUDelft

images it was confirmed that we indeed had attached a CNT. Cantilevers and quartz tuning forks were successfully prepared with MWCNT tips using a method of direct assembly. The orientation and length of the tips were controlled.

Due to contamination problems during TEM imaging the structures of the CNTs on the probes could not be confirmed.

The direct manipulation method was more equipment demanding, but had the benefit of a high degree of control and also a known strong attachment between the CNT and the probe. This is an important factor especially for operation in liquid. The strength of the pick-up method is that it is possible in a simple way to assemble probes with CNTs of the smallest diameters on an AFM. As yet the direct manipulation seems to be the more mature, while the pick-up method still is very promising. Finally, direct surface growth still seems an appealing alternative to consider.

Chapter 9

Bioimaging with AFM

In this chapter we present work on imaging of biological systems with the atomic force microscope (AFM). First, in order to asses the performance of the instruments, a test system, purple membrane, is imaged. Then we turn to immunogolublin G, which we image with SiN tips and with a MWCNT tip, prepared in the previous chapter. With the CNT probe, the difference in phase contrast is especially interesting. Finally, we take a look at IgG on a gold surface.

9.1 Introduction

The aims of bio imaging with the AFM is to directly study the structure, dynamics and chemical functionality of larger bio-molecules and molecular complexes in buffer solutions. The AFM is the only tool with which one can obtain nm resolutions in close to native conditions, that is in a buffer solution, immobilised on a surface. With the AFM individual molecules are directly addressed, so for example stoichiometric difference in a population can be investigated [134].

The AFM can not give the three dimensional, atomic detailed information of X-ray crystallography, but there is no need to crystallise the molecules under investigation. For larger and floppy molecules it can be next to impossible to make the crystals, and if successful, the information connected precisely to the mobility of the molecule will be lost.

In pure imaging, the AFM has been seen as filling the gap between electron microscopy and optical imaging [93]. The resolution of the AFM will perhaps never quite rival the resolution of cryo-electron microscopy [135], but with the AFM one has the possibility to observe the real time dynamics of individual molecules in situ.

Dynamics of molecules and conformational changes connected to the functionality of the molecules can be studied in high detail for example with fluorescence resonant energy transfer (FRET). This is based on energy transfer between fluorophores over limited distances and requires already quite good guesses as to

where the sites of interest are, as the fluorophores must be attached at well defined positions in the molecules. The AFM can be a tool to provide such guesses.

AFM is a surface technique so the hydrodynamic conditions are those close to an interface. This can be compared to the conditions for the many processes taking place on the surface of a cell. The buffer solutions can be changed during imaging to vary the pH and the molecular response studied.

The first AFM images of single DNA, were published by H. G. Hansma and colleagues [95] and T. Thundat et al. [31] in 1992. Some of the best resolutions in bioimaging to date have been obtained in the imaging of proteins in lipid membranes, for example the studies of the purple membrane protein bacteriorodhopsin [136, 137]. These images, taken in buffer, have lateral resolutions around a nanometer. As the proteins in the native state are arranged in lattices, averaging of the image can bring the resolution to 5 Å.

It is comparatively simple to image biomolecules in air. However, besides being a more natural environment, imaging in liquid in general gives higher resolution. This is mainly because in ambient air there will always be a liquid layer on the surface which blurs the image. Further, the capillary forces must be overcome in order to image the molecules. This sets a lower limit for the scanning forces that can be used.

Carefully controlled tip sample interaction is an important factor, as often it does not require interactions of more than a fraction of a nN to deform a soft molecule [137]. The interactions due to electrostatic effects can be minimised by adjusting the salt concentration and the pH of the buffer [138].

Another reason proposed for the high resolutions obtained on protein crystals embedded in lipid bilayers is linked to the small hight differences and the close packing. The idea is that the full force of the interacting tip could be cushioned by the surrounding structure.

The immobilisation of the molecules is also an important parameter in bioimaging. It must be strong enough to hold the molecules in place during imaging, but the molecules should not be deformed. In the case of functional imaging, also the dynamic function and the binding activity of the molecules should not be impaired.

Phase imaging is an alternative to classical force spectroscopy which can provide information on chemical contrast [98, 139]. High lateral resolutions can be obtained on properties not directly linked to the topography such as the compliance of the sample or chemical affinity. The precise interpretation of the data is challenging, because the phase lag is influenced by many parameters.

Truly new information about structures and functions of biomolecules gained from AFM has up till now been limited despite the large potential.

A thorough review on chemical and biochemical analysis using the AFM was published by Takano and coauthors [100] and Czajkowski et al. have written about the progress in structural biology, especially the possibilities offered by cryo AFM [140]. Willemsen and colleagues have recently reviewed developments

in AFM studies of biomolecular interactions [105].

The CNT tips should be able to provide an enhanced performance of the AFM in these efforts in structural and dynamic studies. The first high resolution images with a CNT probes are by Stanislaus S. Wong and coworkers from 1998 using both MWCNT [141] and SWCNTs [142]. Jun Li et al. looked at DNA in buffer solution with a MWNT [143]. As mentioned above the progress obtained using CNT tips in AFM, both in imaging and in specific interaction studies has been reviewed by Hafner and coworkers [92].

9.2 Purple membrane

The bioimaging capabilities of the newly installed AFM microscopes in Leiden were tested by imaging native purple membrane from the cell membrane of Halobacterium Halobium. The sample of isolated purple membrane [144] was kindly provided by Daniel Müller. Daniel Müller and colleagues studied the imaging of this system, obtaining some of the highest resolutions in biomolecular AFM imaging to date [136].

Purple membranes are the patches of the cell membrane in which the protein Bacteriorhodopsin (BR) is embedded. BR is a light activated proton pump and contains seven transmembrane α-helices which form a channel through the membrane. The proteins arrange themselves in trimers and the trimers organise in a hexagonal lattice.

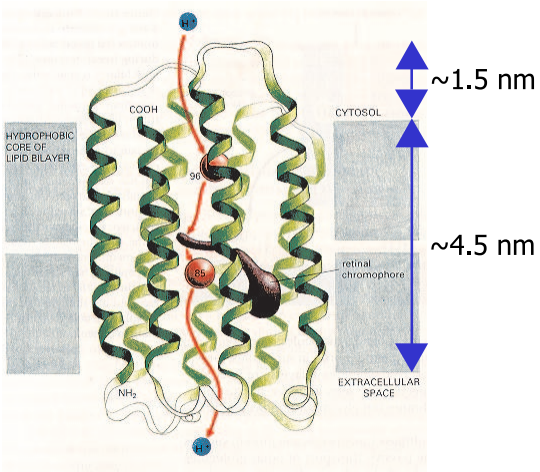

Figure 9.1: Sketch of the bacterial proton pump Bacteriorhodopsin (BR) in a lipid bilayer. BR consists of seven transmembrane α-helices connected by flexible loops. A proton is sketched on its path through the pump. The BR arranges in trimers and the trimers organise in hexagonal lattices. The membrane with BR is called *purple membrane*. From [145].

9.2.1 Sample preparation

Special substrates were prepared for the imaging. Mica disks, one cm in diameter, were glued on commercial AFM pucks within a previously prepared silicone rim. The hydrophobic rim allowed the sample to be manipulated in the AFM, in a half open configuration, with a drop of imaging buffer on the mica surface without the buffer spilling into the piezo elements of the scanner (figure 9.2). The membrane

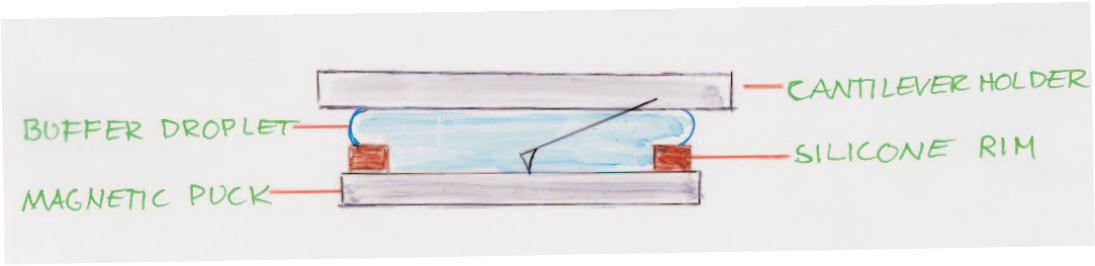

Figure 9.2: A sketch of the setup with puck, buffer droplet and cantilever holder. The half open configuration minimises problems with air bubbles.

fragments were thawed from -80^{o}C and diluted to a concentration of 20 μg/ml in buffer[1] and a 75 μl drop of the dilution was put on a freshly cleaved mica surface. After incubation at 4^{o}C for 20 min the surface is rinsed in buffer[2], fresh buffer was deposited and the sample was ready for imaging. The pH and ion concentration of the buffer have been carefully adjusted to balance the interactions between the tip and the sample [138]. Using the above procedure the fragments were immobilised with the inside, the cytoplasmic surface, facing away from the mica.

9.2.2 Images of purple membrane

The images were obtained in contact mode with a soft SiN cantilever[3]. Figure 9.3.a shows cell membrane fragments adsorbed onto the mica substrate imaged in buffer. Figure 9.3.b shows a close up on one of the fragments consisting of two patches of purple membrane separated by the lipid bilayer. The line scan shows height variations corresponding to the three different surfaces, purple membrane, lipid bilayer and mica, as expected. The bright dots could be multilayers of membrane, which have not been rinsed off. If the solution of membrane is left a little longer on the surface before rinsing one will see many more such dots.

In figure 9.4 the hexagonal lattice of BR is clearly resolved. Note that the lattice has slightly different orientations in the two patches. However, it was not

[1] 300 mM KCl, 10 mM TrisHCl. pH 7.6

[2] Most of the buffer was carefully sucked up, fresh buffer was added to the surface and resuspended. This was repeated about 10 times.

[3] Oxide-sharpened SiN (NP-S) tips from Digital Instruments. Nominal radius of curvature 5-40 nm. Spring constant $k = 0.06$N/m. V-shaped cantilever and Au coating.

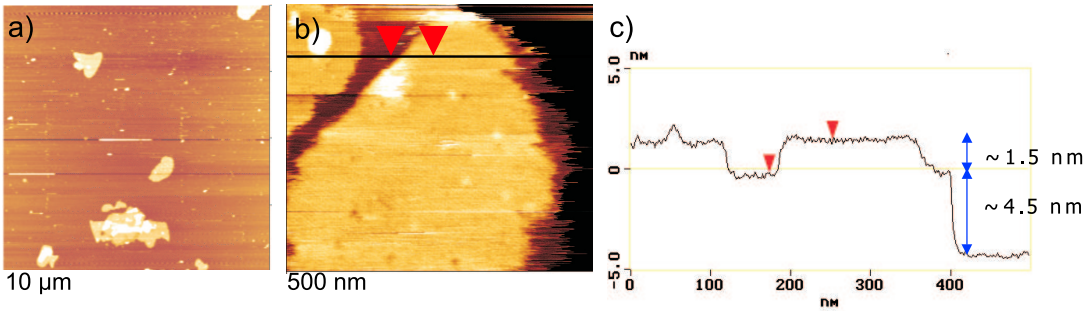

Figure 9.3: **a** Fragments of native cell membrane, adsorbed on mica and imaged in buffer. **b** Close up of a fragment with two patches of membrane with BR lattices which are separated by lipid bilayer without proteins. On the right hand side one sees the mica surface. **c** A line scan of the height variation along the line indicated in **b**. The height variations correspond closely to what is expected for the system (figure 9.1).

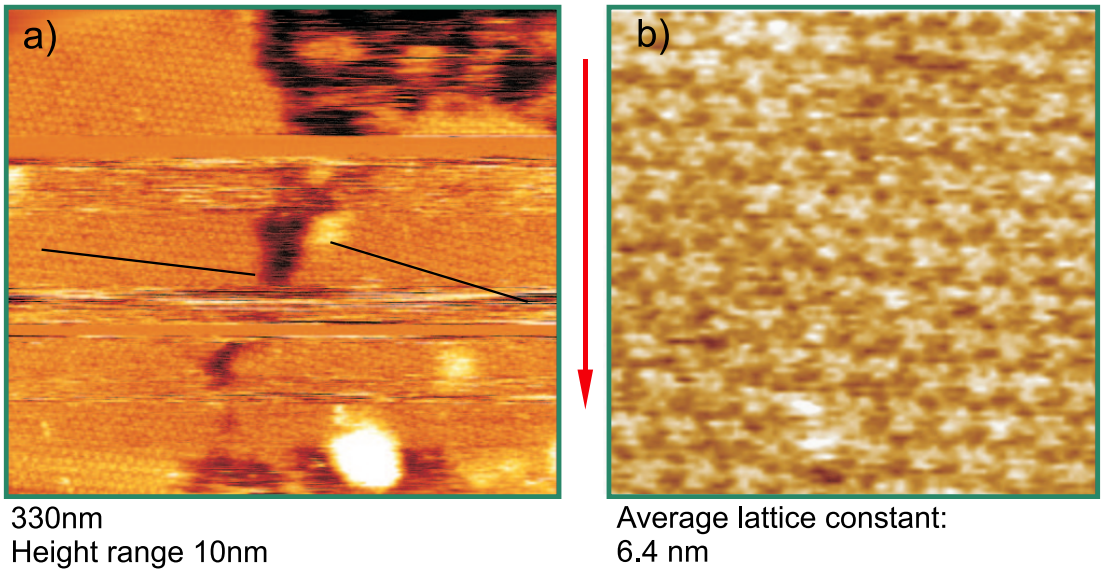

Figure 9.4: **a** AFM image (330×300 nm) of a native purple membrane taken in contact mode in buffer. The thin black lines indicate the orientation of the lattice in the two patches. **b** Enlargement (64×64 nm) of **a** where the hexagonal lattice is clearly resolved. In this image also the BR trimers are visible. The arrow indicates the slow scan direction

routinely obtained, primarily because the drift in the AFM caused the interaction force between sample and probe to change during a scan - without constantly surveying and changing the deflection set-point the contact would either be lost or the interaction would be so strong that no structure was resolved. This is seen as very smooth and very rough lines respectively in the large scale image figure 9.4.a. These problems can probably be overcome by better thermal control of the system and using a cantilever coated with Au on both sides to minimise the

thermal bilayer effect[4]. Alternatively one could image in tapping mode which is much less sensitive to drift, but is slower [139].

The reproduction of high resolution images of the purple membrane, the lattice and the BR trimes show that the microscopes perform well as bioimaging tools.

9.3 Immunoglobulin G

Besides wanting to know more about how the IgG behaves on the gold surface of the cantilever, in the context of the Biosensor work, it is a good molecule for testing the ability to image isolated biological molecules on a surface by AFM. The IgG has a well defined and recognisable structure and it is generally available in high purity.

Figure 9.5 shows the structure of the antibody immunoglobulin G (IgG) as determined from X-ray diffraction studies [146, Protein Data Bank ID:1IGT]. The dimension of the IgG is approximately 17×14 nm, each of the Fab being $8 \times 5 \times 4$ nm and the Fc $7 \times 5 \times 4$ nm [147]. The hinge region is highly flexible

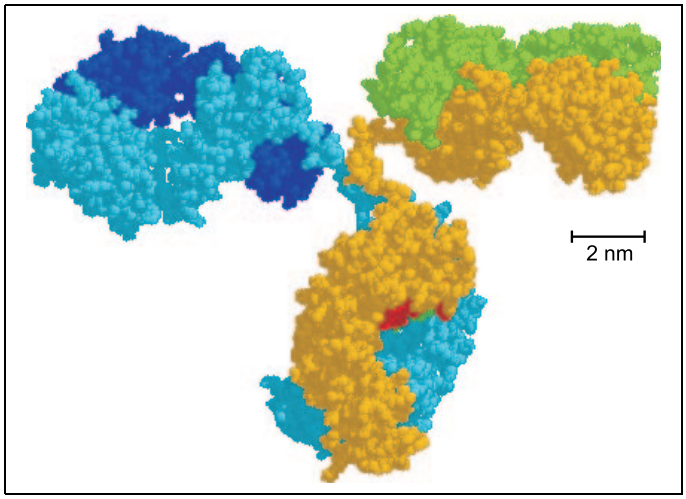

Figure 9.5: Crystal structure of an IgG antibody as determined by x-ray crystallography [146, Protein Data Bank ID:1IGT]. The IgG consists of four aminoacid chains, two heavy chains (light blue and yellow) and two light chains (dark blue and green). The red which can been seen between the tails of the two heavy chains are carbohydrates. [6]

so one would expect to see a range of different orientations of the subunits with respect to one another.

[4]One would want to blank the tip when coating with Au to avoid increasing the tip radius.

9.3.1 Previous imaging

Resolving the substructure of the IgG in AFM has not been obvious [148, 149] With cryo AFM however, the characteristic Y-shape and three lobed structure could be seen [150]. This could be due to the limited thermal vibrations but most likely the hardness of the frozen sample makes stronger interactions possible. With CNT tips the three lobed structure was clear as were conformational variations due to the flexible hinge regions [121]. The images showed very little tip induced broadening with IgG sizes of approximately 20 nm. Also IgM has been imaged to high resolution with CNT probes, showing flexibility of domains that had not been seen before [119].

An image of a crystal of IgG obtained by electron microscopy and optical averaging can be found in [147, page 210]. The picture is not sharp but after further averaging of this image, three separate regions of the molecule can be made out.

9.3.2 IgG sample preparation

1 mg lyophilised bovine IgG[7] was reconstituted in 1 ml PBS buffer[8]. The resulting protein concentration was measured by absorbance at 280 nm[9]. 20 μl of 10 μg/ml IgG solution was dropped on freshly cleaved mica and left to react for 8-10 minutes at room temperature before rinsing with DI water and drying with nitrogen.

9.3.3 Imaging IgG on mica in air

The IgG samples were imaged in tapping mode with force modulation Si cantilever probes[10]. Figure 9.6 is a 500×500 nm scan of the mica surface on which IgG has been deposited. The right image (the 'trace') is a height scan with a band of phase imaging in the middle for comparison with the 'retrace' on the right: although the scales are different the images are consistent. The line below the middle of the image could be a step in the mica, but most probably is an imaging artifact. A few aggregates are visible on the surface but mostly the field is dominated by single particles. A suspected single IgG molecule is measured to be 40 nm wide and 7 Å high in the line scan in figure 9.7. The expected width of an IgG molecule is about 20 nm. A simple estimation shows that a broadening of the image by ∼20 nm on a feature 1 nm high could be caused by a tip with a

[7]Sigma, I5506, lot: 109H9005.

[8]130 mM NaCl, 2.7 mM KCl, pH 7.6

[9]Nominally 100 μg/ml the concentration found from the absorbance measurement was 85 μg/ml, using [concentrationinmg/ml] = 10·Abs/$E^{1\%}_{280}$, ["UV-160A" UV-Visible Recording Spectrometer from Shimadzu].

[10]Nanosensors Force modulation (FM) Pointprobes. Divingboard type, spring constant k = 2.8 N/m, tip radius < 10 nm, resonance frequency 60-90 kHz.

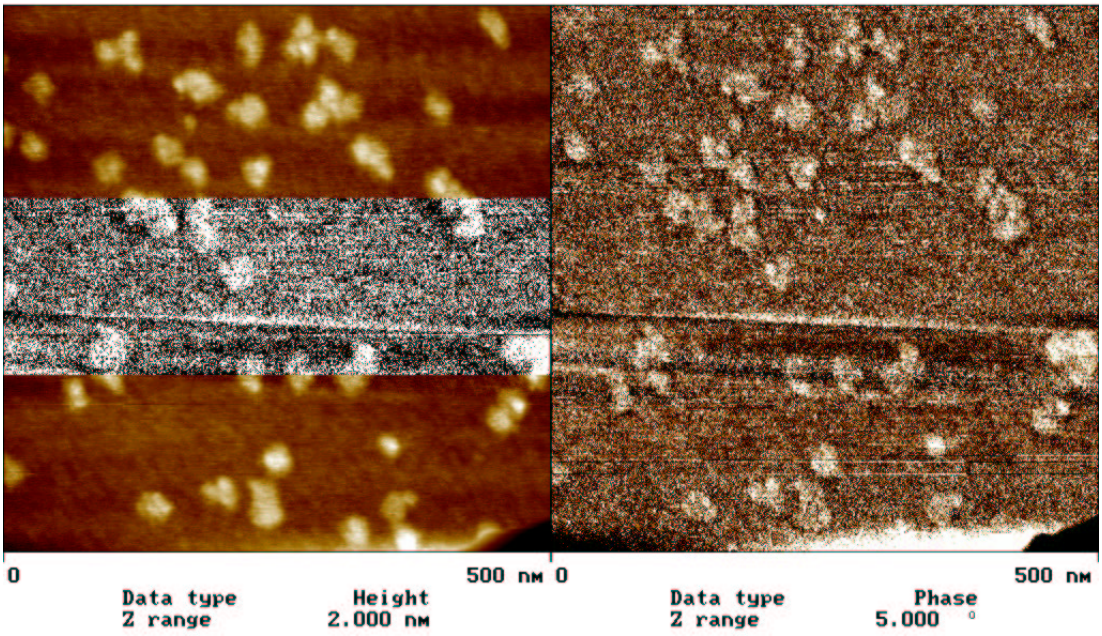

Figure 9.6: IgG on mica in air. Tapping mode, height and phase image

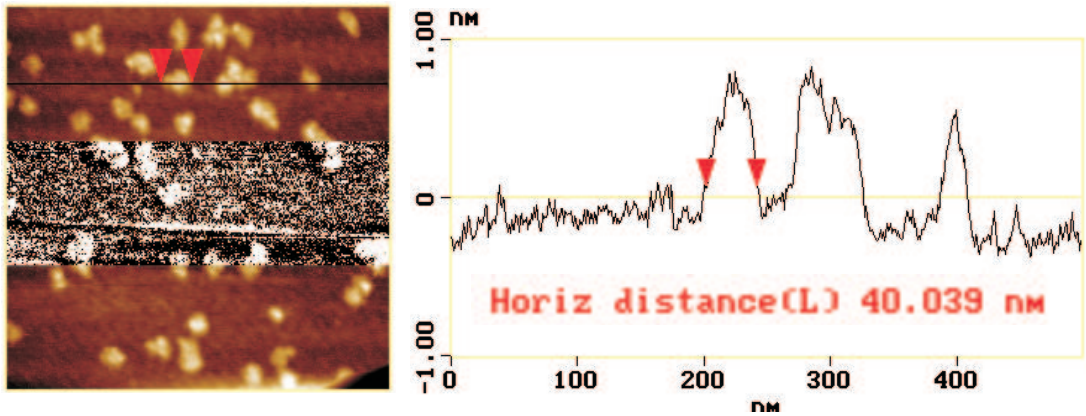

Figure 9.7: Line scan of the height of an IgG on mica in air.

radius of curvature of 50 nm[11]. This is a bit on the blunt side, but not unexpected for the cantilevers used here. The imaging is performed under ambient conditions which generally means that the proteins will be hydrated, a water layer will be felt around the protein.

Regarding the limited height, this is a characteristic feature from the imaging of proteins in air. The reason is not completely clear, but it is worth keeping

[11]The estimation is based on an assumed spherical tip and is roughly applicable for features of a height less than half the broadening: $r = 1/2h[(w/2)^2 + h^2]$, where r is the radius of curvature, w is the broadening and h is the height of the feature.

in mind that the contrast in the images is due to differences in the interaction between the tip and the sample. Imaging in ambient air some water will always be present, and if this water layer is thicker on the mica than over the IgG this will give rise to an apparent smaller height. The limited protein height is also seen in cryo-AFM [150]. Here the apparent height of the IgG was ∼2.5 nm and the reason expected to be residual water on the surface during freezing. It is tempting to think of the IgG in air as collapsed and dried out or denatured but considering the compact structure determined from X-ray crystallography (figure 9.5) it is hard to imagine that it would be possible to compress it to half the volume – after all it is seen with the CNT probes that the lateral dimensions are practically conserved [121]. Besides, if not specifically dried out and kept dry, proteins will be hydrated in air.

9.3.4 IgG on mica imaged in air with a CNT probe

Following the images above, of the IgG sample with the SiN probe, the sample was imaged with a MWCNT probe prepared in Tsukuba (section 8.6), figure 9.8.

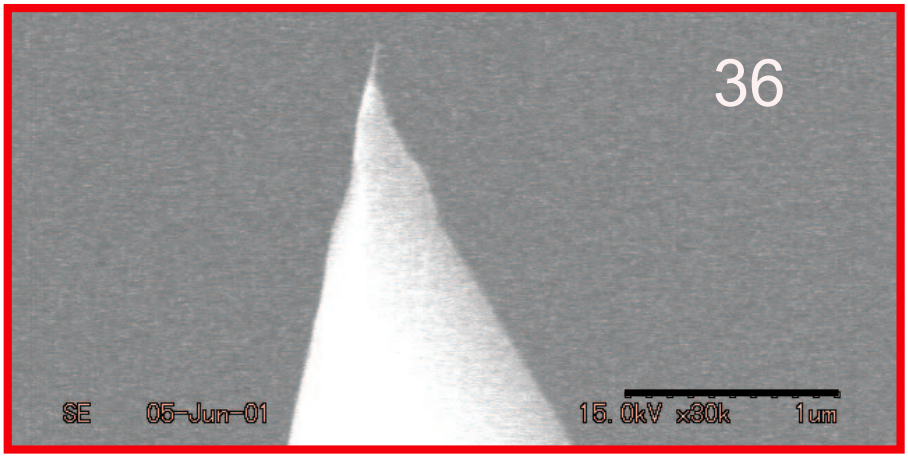

Figure 9.8: FE-SEM picture of the MWCNT tip used for the IgG images below (Figures 9.9 — 9.11). The CNT is about 15 nm wide and 150 nm long. The cantilever arm and chip are to the left. The scale bar is 1 μm.

In Figure 9.9 we see an IgG antibody in the centre of the image - and an aggregate of three or more to the left of it and perhaps one or two IgG, very close to one another, to the right. In the height image, the left panel, the mica surface seems full of little holes. It could also be that the CNT some times buckles, but some of the dark features recurred over several scans. In the line scan of the height, figure 9.10, we see that the resolution has indeed increased in comparison with the resolution achieved with the SiN probe. The substructure of the IgG is resolved in two distinct peaks and the separation of the peaks is comparable to the X-ray

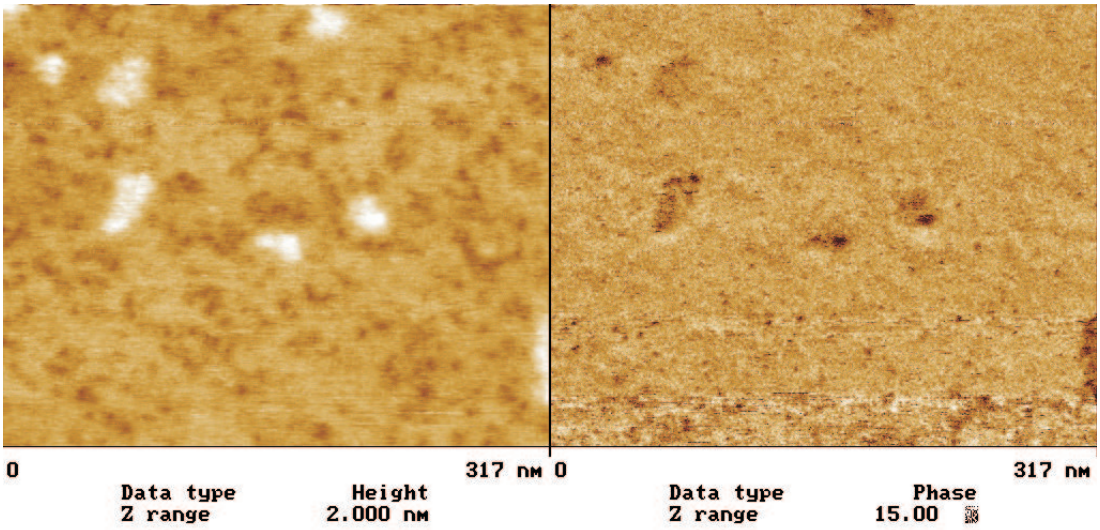

Figure 9.9: IgG on mica in air imaged with a CNT probe (250×250 nm). Tapping mode, height and phase image

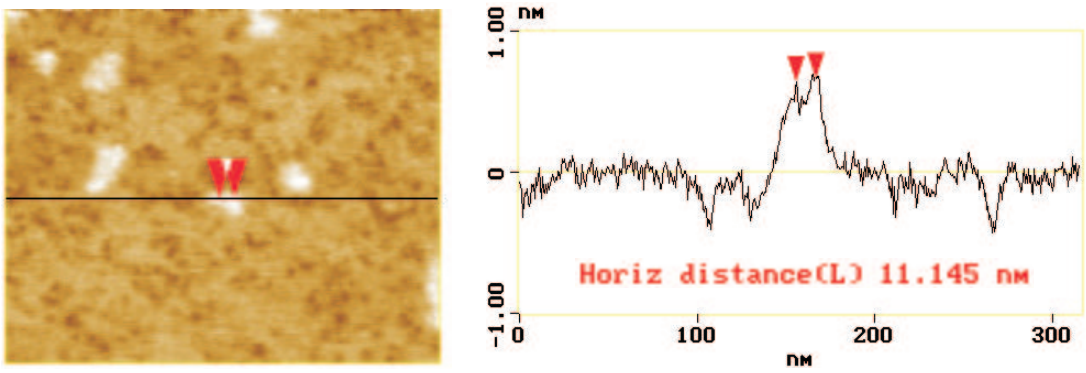

Figure 9.10: Line scan of the height of the IgG imaged with a CNT (figure 9.9).

crystal structure (figure 9.5). The apparent width of the IgG protein is now 30 nm, corresponding to an approximately 10 nm broadening. As the IgG still is an approximately 1 nm high feature this would correspond to a tip radius of curvature of ∼13 nm. This is a bit disappointing because we would expect that the probe used, even with no sharpening, is not more than 15 nm wide (figure 9.8)). Furthermore, we would expect the tip to have been sharpened while shortened. Of possible explanations the most probable seems to be the hydration of the protein, exposed to the ambient. The sharpness of the CNT probe should also minimise the effect of hydration because the capillary interaction with a high aspect ratio tip is much smaller than with the bulk of a pyramidal tip.

The phase image, figure 9.11, is very interesting because it shows a much larger and inverted contrast compared to the SiN tip (figure 9.6). Also, there seems to

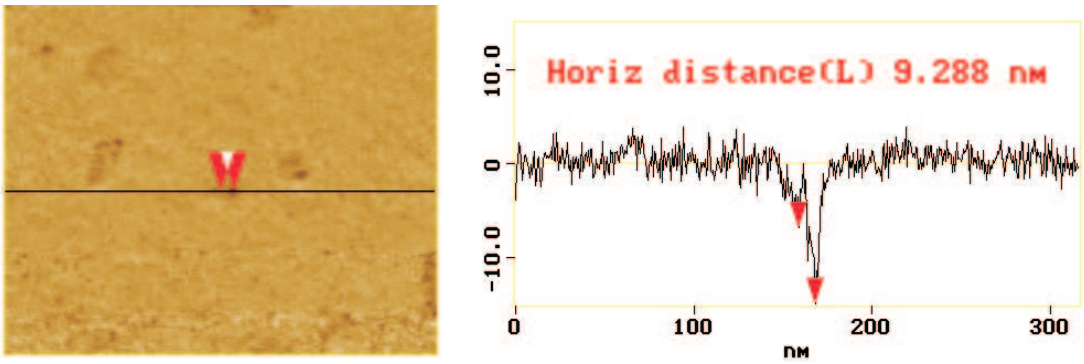

Figure 9.11: Line scan of the phase of the IgG imaged with a CNT (figure 9.9).

be a large intra molecular contrast and the phase contrast is not simply related to the topology. The point where the phase contrast is largest corresponds to a small change in height, which could indicate a change of domains. Measuring the peak-peak separations in hight and phase line scans respectively (figures 9.10 and 9.11), the distances between the phase peaks is smaller (∼8-10 nm) than the height peak distances (∼10-12 nm). There is often two distinct phase contrast points, one larger than the other. This is slightly confusing: Although the IgGs are most likely all different in specificity, within each one the two antigen recognising domains, the Fab, are exactly the same. Also the Fc part, the 'tail', of the IgG should be very similar on all the molecules. The random adsorption of the molecules makes it very likely that the two, highly mobile, Fab are oriented differently and this may be the reason we do not clearly see this symmetry.

Also, the energy dissipation is difficult to interpret because many different properties can contribute to it (section 7.2).

We have not yet seen any reports on intramolecular phase contrasts which are clearly distinct from the height differences. Recent measurements of IgG with SWNTs show less pronounced phase contrast and suggest that the phase contrast depends critically on the preparation of the tip[12].

9.3.5 IgG on mica imaged in liquid

The image of IgG in liquid, figure 9.12, was performed on the same samples as above, but one day later and with a different SiN probe. The IgG had had time to adsorb well onto the mica surface. A droplet of deionised water (DI)- large enough to fill the space between holder and sample but small enough not to spill onto the piezo elements below - was placed on the mica before the sample was mounted in the AFM. We used tapping mode to minimised the lateral force applied to the sample. However, it is clear that the proteins are still very mobile - too mobile for imaging. What we see in the line scan in figure 9.12 is that they

[12]Dionne Klein, private communication.

look both broader, 50 nm, and higher, 10 nm, than when imaged in air (figure 9.7), if indeed it is the same molecules at all.

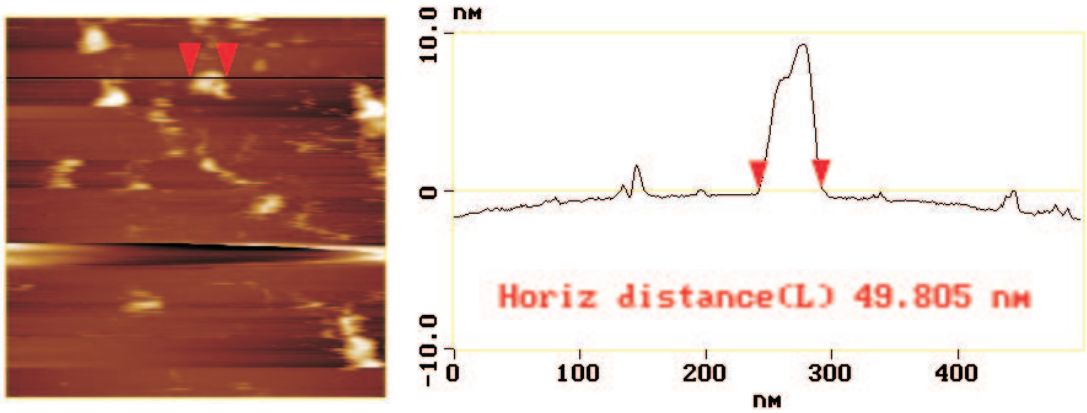

Figure 9.12: An IgG antibody on mica imaged in DI water. Scan area 500×500 nm. A scan along the indicated line show that the IgG looks both wider, ∼ 50 nm, and higher, ∼ 10 nm, than when imaged in air

While the broadening of the image could be due to tip convolutions[13] the difference in height is less obvious: As mentioned above, the low height observed in air can be due to a difference in the water layer adsorbed over the mica and the protein. This difference is no longer present when imaging in liquid. However, the molecule will also be surrounded by a cloud of ions attracted by the amine groups in the protein, which will be partly protonated in the DI water (pH 5.5). Also, the SiN of the tip might be positively charged at pH 5.5 [151]. The ion concentration in the DI water is low, so these double layer interactions will not be screened (compare with the carefully balanced situation in the purple membrane imaging section 9.2). Double layer interactions will naturally affect also the measured width of the protein by modifying the effective tip radius, the apparent width of the protein or any combinations of these.

Under phosphate buffer solutions IgG have successfully been imaged on mica with SWCNTs[14]. Although still very mobile the molecules could be resolved and the height measured to 4-5 nm in good agreement with the dimensions that would be expected from the crystal structure (figure 9.5). We may conclude that, as in the case of BR imaging, the ionic strength of the buffer is important to obtain high resolution.

Regarding the mobility of the IgG on the mica in DI water, we know from the Biosensor work, chapter 5, that antibodies adhere to and retain functionality on gold surfaces. Liquid imaging of antibodies adsorbed to Au could therefore be

[13]The observed broadening of approximately 30nm in a feature 10 nm high could be caused by a tip with a radius of curvature of 16 nm.

[14]T. Oosterkamp, private communication.

more successful.

9.3.6 IgG on gold

We used ultra flat Au surfaces prepared by Michael Wrang Mortensen at MIC [72]. Before use the surfaces were cleaned for 15 minutes in an ozon cleaner. There was very little contamination to be seen on the Au after the cleaning procedure.

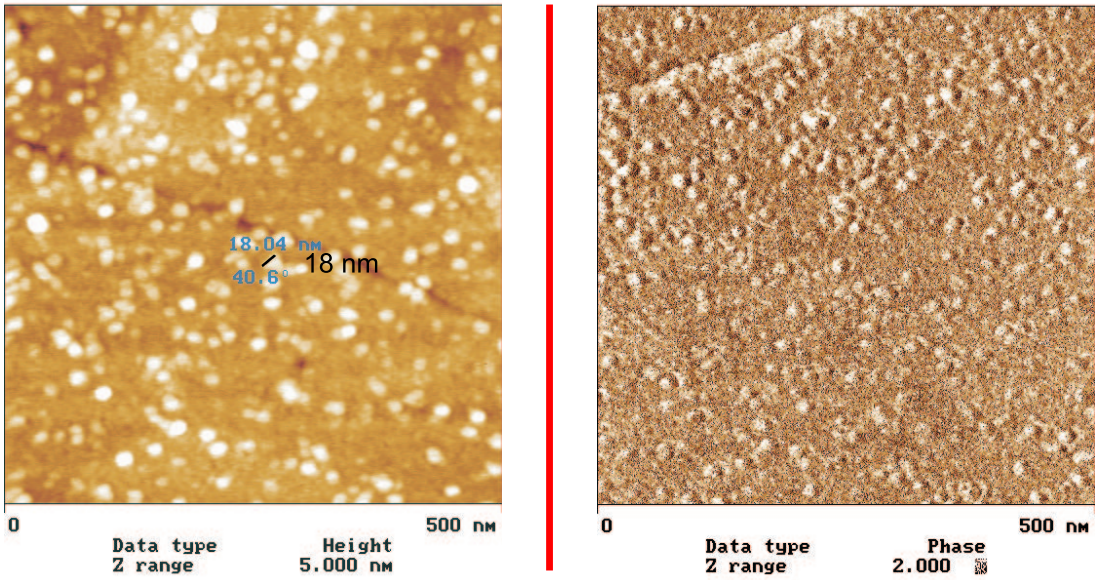

Figure 9.13: IgG antibody on gold in air. Tapping mode, left image is a hight scan and to the right a phase image — not simultaneous scans!

The IgG solution used in the mica preparations was also used for the gold. It was left to react on the surface three minutes longer before rinsing, which is probably a reason the surface became a bit crowded. Figure 9.13 shows a 500 × 500 nm scan with at SiN cantilever tip[15]. To the left is a hight scan and on the right hand side is a phase image — not simultaneous scans! A line originating from the (crystal) structure of the underlying gold is visible in both images, although not the same one. The observed phase contrast is comparable to the images on mica with SiN probe (figure 9.6). The high density notwithstanding, the individual particles are quite well defined in the height image and also some of them show characteristic IgG features. The lateral dimension is approximately 16-18 nm much smaller than the SiN imaged IgG on mica (figure 9.10). This could be due to a sharp tip. On the other hand the height, figure 9.14, is significantly larger

[15]Nanosensors FM Pointprobes $k = 2.8N/m$, $R = 5 - 10nm$.

than seen on mica with peak heights of 1.5 to 2 nm, more than twice the height on mica. Following the discussion for the imaging on mica, this is most probably due to different interactions between the tip and the mica respectively the gold. If we assume that the IgG in both cases is 4 nm high then the observed differences could be explained by the layer of water on the mica being approximately 3 nm thicker than over the IgG while on Au the water layer would be $\sim$ 1.5 nm thicker.

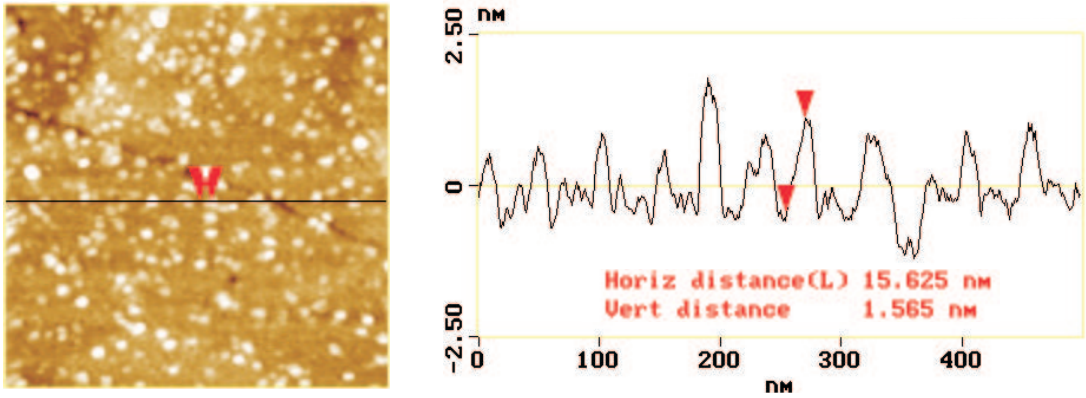

Figure 9.14: IgG antibody on gold in air, height scan from figure 9.13. The height of the molecules are more than twice as large as on mica.

We did not perform any more imaging on gold neither in air nor in liquid. In Leiden the work is however being continued.

In general it would be desirable to run more cross checks to unambiguously identify the particles we observed on the surface, for example using fluorescent labeled antibodies or a fluorescent sandwich assay. A combination of the AFM and a single molecule fluorescence microscope could in principle give simultaneous information about the structure and the identity of the molecule under investigation.

9.4 Conclusion on Bioimaging with AFM

Two different biological samples have been imaged with AFM. The purple membrane was an advanced test of the performance of the microscopes in contact mode liquid imaging. We succeeded in resolving the hexagonal structure of the BR lattice.

The IgG antibody was imaged under different conditions with both conventional tips and one of the MWCNT tips prepared in the previous chapter. The over all triangular shape of the molecule was observed in all cases. With the MWCNT the three lobed substructure was clearly resolved and the peak separations corresponded very well to the dimensions expected from crystallographic

studies.

The most interesting observation was not only the enhanced resolution of the height images using the CNT probes, but especially the strongly increased phase contrast, which showed distinct intramolecular variations that have not been reported before. In order to pursue the understanding of this phenomenon it would be advantageous to study monoclonal antibodies – that is antibodies which not only functionally, but also structurally and chemically are the same.

In liquid we did not manage to obtain stable imaging of the IgG on mica. Here one could work on both the surface and the buffer to stabilise the IgG for imaging. Especially, on could try imaging the IgG on gold.

The antibodies on a flat gold surface were observed to have smaller apparent lateral dimensions and larger height than on mica when imaged in air with a SiN tip.

Chapter 10

Non-Contact AFM with a Quartz Tuning Fork

The following chapter we change gears a bit, since we will no longer will be working with microscopic cantilevers, but rather millimeter sized quartz tuning forks (QTF). We will use carbon nanotube (CNT) tips mounted on QTFs to measure the interaction between the tip and a surface, down to the last molecular layers.

This work was conducted together with Masami Kageshima in Tsukuba, Japan. A paper has been accepted for publication in Applied Surface Science [152][1]. Not all experimental details will be discussed in this chapter, for which we refer to the paper.

10.1 Introduction

The direct contact with the sample is a continuous concern in the imaging of soft samples, where even small forces can deform the molecules. Tapping mode data are also not straight-forward to interpret quantitatively. This is partly because of the non-linearity of the motion of the cantilever and its dependence on factors such as contact deformation [153]. In non-contact atomic force microscopy (NC-AFM) the cantilever is oscillated at resonance with small amplitudes and it is the attractive part of the interaction between tip and sample which is probed. Using the soft microcantilevers common in AFM, the interactions are normally averaged over a distance of $\sim$ 10 nm. With a millimeter size quartz tuning fork (QTF) stable oscillations of a few Ångstrøm can be obtained. Further the high Q value of such a tuning fork, even in liquid, makes the resonance and the phase shift sufficiently sharp for the detection of changes in the weak attractive force. The

[1] A proof version is available on the web at `http://www.sciencedirect.com/` (*Applied Surface Science*, Articles in Press)

use of a CNT probe limits the influence of long range forces and hydrodynamic squeezing by the bulk of the tip.

10.1.1 Solvation Layers

At the interface between a solid and a liquid, between which there is an attraction, the last couple of molecular layers of the liquid become ordered[2]. When measuring interaction forces between two approaching surfaces in a liquid, this shows up as an oscillation of the interaction force at separations of a few molecular diameters. It is basically a geometric effect where ordering of the molecules near the surface cause a density variation. This is illustrated in figure 10.1: When the packing of

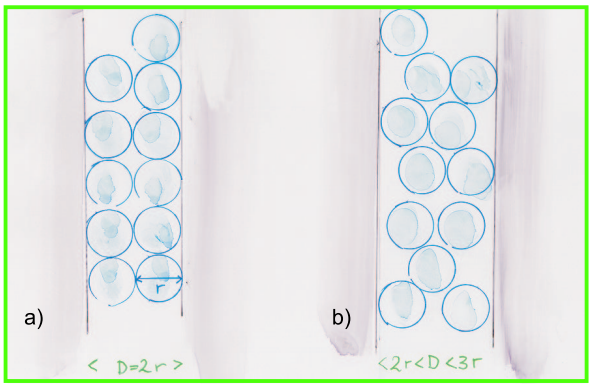

Figure 10.1: Sketch of solvation layers forming between two solid surfaces. a) shows the case where the liquid molecules have relatively large mobility and the density is quite low. In b) the separation between the solid surfaces closely corresponds to the packing of a couple of layers of molecules and the density is higher.

the molecules becomes dense the interaction is more repulsive and the interaction is softer at separations where close packing is not possible [70, chapter 13]. This phenomenon is sometimes called the solvation layer or, in the important case of water, the hydration layer effect. For biological molecules the molecular ordering of water around them is significant to the understanding of their behaviour.

On a macroscopic scale, oscillating interaction forces, attributed to the solvation layers, have been measured with the surface force apparatus (SFA) both for water between mica surfaces and other systems including organic solvents and liquid polymers[3]. The SFA is however limited in the choice of interaction

[2]If the liquid does not wet the surface there is actually a vapour layer between the surface and the liquid.

[3]The surface force apparatus consists of two crossed cylinders, with diameters of a few centimeters, one of the suspended by springs. The movement of the cylinders relative to each other is very accurately detected using interference techniques. With this technique many of the very first studies verifying surface interaction theories were performed in the late nineteen seventies. See for example [70, chapter 10] for details.

surfaces because these must be molecularly flat over a range of square microns. Consequently, measurements have largely been restricted to mica as the solid surface.

The atomic force microscope (AFM) has been used to investigate the solvation layers on a microscopic scale in a silicon oil (OMCTS)[4] [154] and water [155]. The hydration layers were measured by statistical analysis of the thermal vibrations of a static cantilever over half a second, which means that drift limits the local information. Recently it was possible to perform spatially resolved measurements of the hydration layers on mica [156], using carbon nanotube (CNT) probes. The CNTs were mounted on commercial AFM cantilevers modified with magnetic particles and refined actuation and detection techniques [157], .

However, using conventional silicon AFM cantilever probes it is very difficult to obtain stable oscillations with an amplitude of less than about 10 nanometers so the measurements of the oscillatory interaction due to the solvation layers are in fact averages over tens of molecular layers. It is therefore difficult to extract quantitative information about the interaction forces. In order to obtain quantitative force measurements one would need a probe with oscillations smaller than the expected thickness of the solvation layers. A quartz tuning fork (QTF), of the type used in quartz watches, is a high Q oscillator that is so stiff that the resonant amplitude can be less than an Ångstrøm.

10.1.2 Quartz Tuning Forks

Quartz tuning forks were introduced in scanning microscopy by Khaled Karrai and Robert Grober as a distance control device for near field scanning optical microscopy [158]. In this paper a basic model of the dynamics of the tuning fork was also presented. The QTF has since been developed for operation as a probe microscope with noise levels and scanning speeds comparable to the AFM [159]. The operation and vibrational modes in liquid have been studied and a QTF has been applied to imaging of soft biological samples in water [160]. The combination of a QTF and a CNT probe in a shear force image has been demonstrated in [123].

The high Q-factor of the tuning fork, compared to conventional AFM cantilevers, is mainly due to the large mass of the tuning fork. Due to the geometry, it is expected that the Q gain is significant compared to the loss by added drag. The stiffness of the QTF will also allow for continuous measurements in regimes where the force gradients are so large that conventional silicon cantilevers would snap to contact. For example in the study of non-wetting systems, where a vapour gap is expected between the solid an the liquid. Imagine investigating and perhaps modifying the structure of water over different domains of a hydrophbic/hydrophillic nano-patterned surface.

[4] Octamethylcyclotetrasiloxane

The QTF further offers significant advantages to conventional AFM as it exploits the piezo electric properties of the quartz: Both the activation and the detection can be achieved using the electrical leads on the prongs. This replaces both the optical readout system and the external excitation oscillator.

10.2 OMCTS measurements

We measured solvation layers of OMCTS (octamethylcyclotetrasiloxane) on an HOPG (highly oriented pyrolytic graphite) surface using a quartz tuning fork with a carbon nanotube probe tip. OMCTS, figure 10.2, is an inert silicon liquid of nonpolar quasi-spherical molecules, which have a mean diameter of approximately 9 Å at room temperature. These large, spherical, stable and largely inert molecules makes OMCTS a relatively simple liquid and therefore a 'physicist choice' of liquid [157]. OMCTS wets the HOPG. In our case it is also an advantage that the liquid is not conducting so we will not have to isolate the leads of the tuning fork.

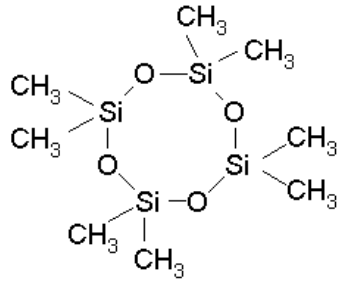

Figure 10.2: Structure (2d) of the OMCTS molecule (Octamethylcyclotetrasiloxane). From Sigma-Aldrich `www.sigma-aldrich.com`.

Gold tips were $CaCl_2$ etched and mounted on the quartz tuning forks, for detection of oscillations normal to the surface, by Martin Dienwiebel[5]. The etched wires typically had tip radii of a few hundred nanometers (figure 10.3).

To remove the background of long range interactions and hydrodynamic squeezing we used a CNT probe mounted on the Au wire. A MWCNT was mounted on the Au tip attached to the QTF, as shown in figure 10.3, using the 'direct manipulation' technique described in section 8.6.

A symmetric resonance peak was obtained in OMCTS using a finely tuned capacitance compensation to counter the effect of stray capacitances in the tuning fork (figure 3 of the manuscript). On the basis of the tuning fork properties and the driving voltage, the amplitude of the oscillation of the tuning fork prong was estimated to approximately 10 Å peak to peak.

[5]Kammerling Onnes Laboratory, Leiden Institute of Physics, Leiden University.

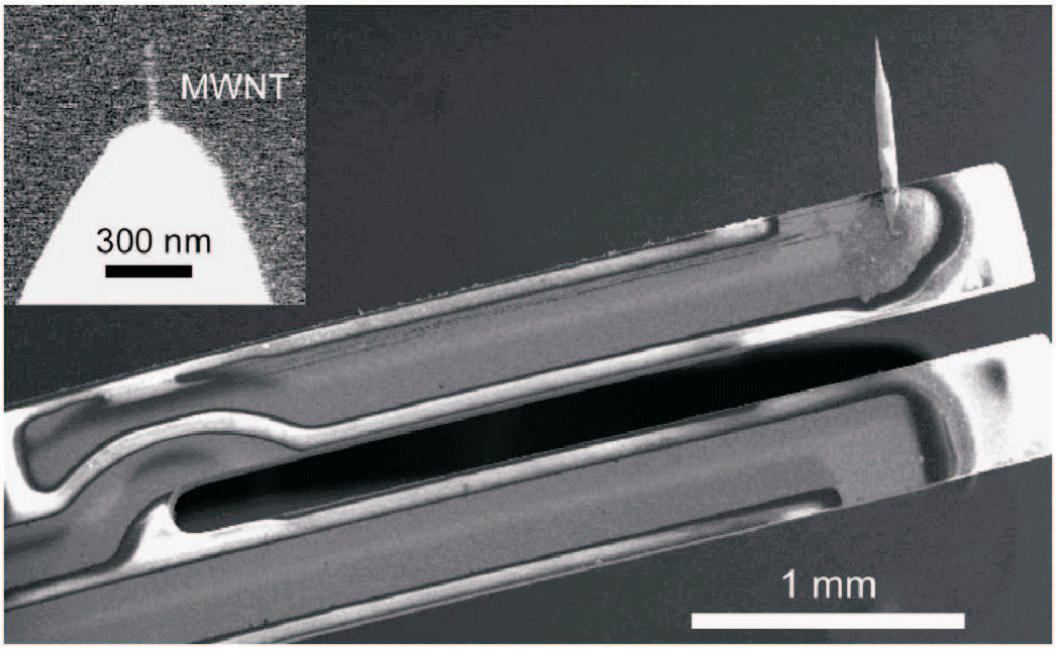

Figure 10.3: Optical micrograph of a QTF with an attached gold tip. The inset is a FE-SEM enlargement of the apex of the gold tip, where a MWCNT is attached. The dimensions of the prongs are approximately $3 \times 0.4 \times 0.35$ mm. [152].

In the frequency modulation technique the driving signal follows the changing resonance frequency of the tuning fork by locking to the 90° phase lag of the response relative to the driving frequency [161, 162]. With gain control a constant amplitude of the output is ensured. The energy needed to maintain the amplitude is then a measure of increased dissipation. This can be seen as the ultimate Q-enhancement as the driving frequency is always precisely at the resonance of the tuning fork.

Results of the measurements are seen in figure 10.4. An oscillatory behaviour with an periodicity of approximately 8-9 Å is observed, in both resonance frequency variation and dissipation, the dissipation being largest when the resonance frequency is lowest. This corresponds well to what is expected from the dimensions of the molecule and previous measurements with SFA [70, page 270] and AFM [154]. The periodicity is also very close to the estimated oscillation amplitude of 10 Å. This means that perhaps greater contrast could be obtained even by increasing the oscillation amplitude a bit.

It should be remembered that what is really being measured is the ordering of the OMCTS molecules due to the confinement by the CNT tip.

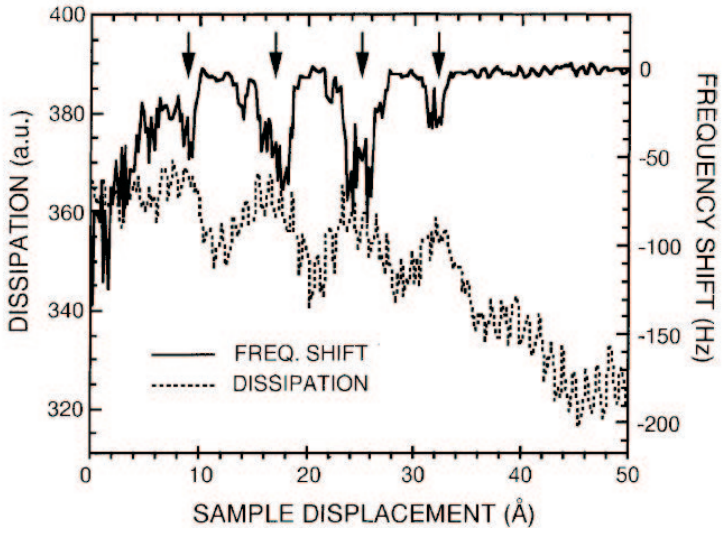

Figure 10.4: The frequency shift and the driving amplitude, needed to maintain constant response amplitude, recorded while reducing the spacing between the CNT probe and the HOPG surface. Zero height is arbirtary. Frequency minima, indicated by arrows, correspond to dissipation maxima, high driving amplitude [152].

10.3 Conclusion and Perspective on Solvation Layer Measurements

We measured the solvation layers of OMCTS on HOPG with a CNT tip on a QTF. It was seen that the CNT tip significantly reduced the long range interactions.

The high Q of the tuning fork, also in liquid, the small oscillation amplitudes and the resolution provided by the CNT could make it a usefull tool for non-contact imaging of soft biomolecules. Lightly brushing over the molecules in this way instead of banging into them with a tapping tip will reduce the doubts regarding mechanical deformation during imaging. The high resonance frequency makes also faster imaging possible.

Chapter 11

Perspectives on CNTs as Nanoprobes

We have especially seen the advantages of the high aspect ratio, both in bio imaging and in measurements on solvation layers. The chemical specificity of the electrically etched CNTs shows up in the phase images of the IgG molecules. Albeit not simple to interpret, the intramolecular contrast is clear, persistent over many scans and different molecules and not reported before. Chemical functionalisation for probing intramolecular contrasts in chemical adhesion, still seems one of the most exciting possibilities of the CNTs in bioimaging.

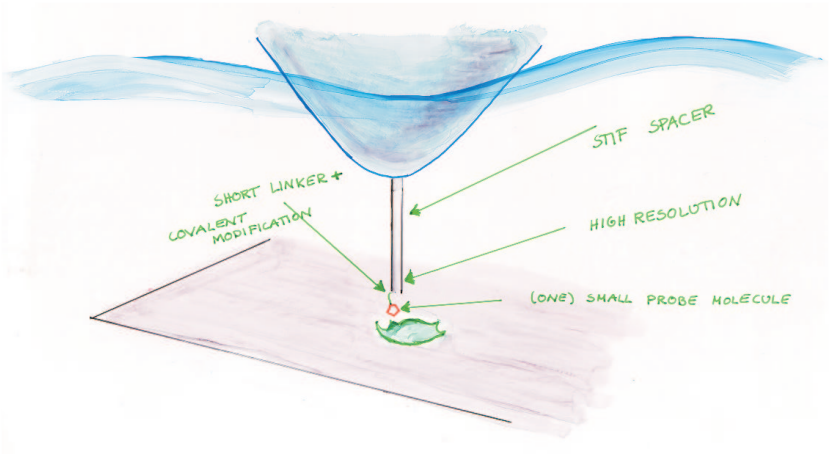

Figure 11.1: Illustrating of the main interests of using the CNT as a probe tip in the study of biomolecules

Figure 11.1 summarises the attractive features of the CNT as an AFM bioprobe. The small radius and high aspect ratio provide high resolution, also of deep features and isolated molecules, the length gives distance and shields the interactions between the sample and the bulk of the tip and the chemical properties of the end of the tube makes it possible to functionalise it with a large variety of

molecules. The length of the tube further provides a rigid spacer which increases the specificity of the interaction while retaining the spatial resolution.

With this tool it will be possible to study the functional sites within complex molecular structures and the dependence on environmental conditions. To mention a concrete example, using the amine coupling chemistry it is possible to functionalise the CNT with small carbohydrate structures, down to single sugar groups. The recognition of specific carbohydrates on the surface of microorganisms by specialised protein complexes is an alternative route to the activation of the immune system which currently is receiving much attention [163].

In other words, it will be possible to study large 'floppy' molecules in action – to "Feel Proteins at Work".

Chapter 12

Final Conclusions

In this thesis we have studied two different techniques using micromechanical cantilevers for the investigation of biomolecular systems.

First, a microelectromechanical cantilever chip, was developed into a biosensor (Part I). In chapter 2 this chip was used for laser power detection. By coating one of the two cantilevers on the chip with a polymer, the chip was made sensitive to vapour absorption; both humidity and vapours of different alcohols were detected. In the latter case the response was interpreted quantitatively in terms of the absolute alcohol vapour concentration. The method also proved to be a good tool for studying polymer properties (chapter 3).

The chip was made liquid-compatible with a wax coating. Temperature variations in water were measured with one gold coated cantilever and changes in the concentration of ethanol in water were detected using a polymer sensitised chip (chapter 4).

Applying the chip as a biosensor we detected the self-assembly of thiolated single-stranded DNA oligos, which was interpreted using Langmuir adsorption isotherms. We found indications that the bacterium E. coli can be detected with the chip, but further optimisation is needed (chapter 5).

In the second part of the thesis the use of carbon nanotubes (CNT) as probes tips in atomic force microscopy (AFM) was explored at the University of Leiden (part II). In order to test the performance of the AFM, purple membrane was imaged, with conventional tips, in contact mode in buffer and the characteristic hexagonal lattice was resolved (chapter 9).

CNT probes were assembled using two different strategies: a pick-up technique for single walled CNTs and a method of direct assembly for multiwalled CNTs (MWCNT) was used at AIST, Tsukuba, Japan (chapter 8).

Immunoglobulin G was imaged with conventional and MWCNT probes. The images with the MWCNT showed increased lateral resolution and a significant intra molecular phase contrast (chapter 9).

Finally, solvation layers in octamethylcyclotetrasiloxane were measured using a quartz tuning fork probe with a MWCNT tip.

Dansk resumé

I denne afhandling har vi studeret to forskellige teknikker, baseret på mikroskopiske bjælker (cantilevere), til at undersøge molekylærer biologiske systemer.

I afhandlingens første del blev en mikroelektromekanisk chip udviklet til en biosensor. I kapitel 2 blev denne chip brugt til måling af effekten af en laser. Ved at dække den ene af de to cantilevere med en polymer, blev chippen følsom overfor absorption af dampe. Der blev målt på både luftfugtighed og dampe fra forskellige alcoholer. Resposen på alkoholdampe blev tolket kvantitativt som den absolutte koncentration af alkoholdamp inde i målekammeret. Den metode kan også være nyttig til undesøgelse af polymerens egenskaber.

Chippen blev gjort væskekompatibel ved en voksning. Med en guldbelagt cantilever blev temperaturvariationer målt i vand og variationer i ethanol koncentrationer i vand kunne deteketers med en polymerbelagt cantilever (kapitel 4).

Brugt som biosensor detekterede vi adsorptionen af thiolerede enkeltstrengede DNA oligoer. Den tidslige respons kunne tolkes med Langmuir isotermer. Vi så tegn på at chippen vil kunne bruges som en immunosensor til detektering af E. coli, men optimering er nødvendig (kapitel 5).

I afhandlingens anden del ser vi på brugen af carbon nanorør (carbon nanotubes, CNT) som prober i atomar kraft mikroskopi (atomic force microscopy, AFM), på Leiden Universitet. For at afprøve mikroskopernes kvalitet i biomikroskopi, så vi først på 'purple membrane', et hexagonalt gitter, karakteristisk for membranens proteinstruktur, kunne opløses (kapitel 9).

CNT prober blev samlet ved brug af to forskellige strategier: en 'pick-up' teknik til enkeltvæg CNT og ved AIST, Tsukuba, Japan, blev der brugt direkte manipulation til at lave prober med multivæg CNT (MWCNT) (kapitel 8).

Immunoglobulin G blev afbildet med både konventionelle og MWCNT prober. Billederne taget med MWCNT udviste stor intramolkylær fasekontrast (kapitel 9).

Endelig blev der målt på solveringslag i octamethylcyclotetrasiloxane ved brug af en kvarts stemmegaffel med en MWCNT spids.

Bibliography

[1] Anja Boisen. *Passive and Active AFM Probes*. PhD thesis, MIC, DTU, Technical University of Denmark, Lyngby, Denmark, 1997.

[2] Jacob Thaysen. Nano-probe with integrated read-out. Master's thesis, MIC, DTU, Technical University of Denmark, Lyngby, Denmark, November 1998.

[3] G. Binnig, C. F. Quate, and Ch. Gerber. Atomic Force Microscope. *Physical Review Letters*, 56(9):930–933, March 1986.

[4] Marc Madou. *Fundamentals of Microfabrication*. CRC Press LLD, 1997.

[5] J. K. Gimzewski, Ch. Gerber, E. Meyer, and R. R. Schlittler. Observation of a chemical reaction using a micromechanical sensor. *Chemical Physics Letters*, 217(5,6):589–94, 1994.

[6] T. Thundat, R. J. Warmack, G. Y. Chen, and D. P. Allison. Thermal and ambient-induced deflections of scanning force microscope cantilevers. *Applied Physics Letters*, 64(21):2894–6, 1994.

[7] G.Y. Chen, T. Thundat, E.A. Wachter, and R.J. Warmack. Adsorption-induced surface stress and its effects on resonance frequency of microcantilevers. *Journal of Applied Physics*, 77(8):3618–22, 1995.

[8] T. Thundat, S.L. Sharp, W.G. Fisher, R.J. Warmack, and E.A. Wachter. Micromechanical radiation dosimeter. *Applied Physics Letters*, 66(12):1563–5, 1995.

[9] T. Thundat, E.A. Wachter, S.L. Sharp, and R.J. Warmack. Detection of mercury vapor using resonating microcantilevers. *Applied Physics Letters*, 66(13):1695–7, 1995.

[10] J.R. Barnes, R.J. Stephenson, M.E. Welland, C. Gerber, and J.K. Gimzewski. Photothermal spectroscopy with femtojoule sensitivity using a micromechanical device. *Nature*, 372(6501):79–81, 1994.

[11] J.R. Barnes, R.J. Stephenson, C.N. Woodburn, S.J. O'Shea, M.E. Welland, T. Rayment, J.K. Gimzewski, and C. Gerber. A femtojoule calorimeter using micromechanical sensors. *Review of Scientific Instruments*, 65(12):3793–8, 1994.

[12] Roberto Raiteri and Hans-Jürgen Butt. Measuring electrochemically induced surface stress with an atomic force microscope. *Journal of Physical Chemistry*, 99(43):15728–15732, 1995.

[13] Hans-Jürgen Butt. A sensitive method to measure changes in the surface stress of solids. *Journal of Colloid and Interface Science*, 180:251–60, 1996.

[14] Rüdiger Berger, Emmanuel Delamarche, Hans Peter Lang, Christoph Gerber, James K. Gimzewski, Ernst Meyer, and Hans-Joachim Günterodt. Surface stress in the self-assembly of alkanethiols on gold. *Science*, 276:2021–23, June 1997.

[15] R. Berger, H.P. Lang, Ch. Gerber, J.K. Gimzewski, J.H. Fabian, L. Scandella, E. Meyer, and H.-J. Güntherodt. Micromechanical thermogravimetry. *Chemical Physics Letters*, 294(4-5):363–369, 1998.

[16] H. P. Lang, R. Berger, F. Battiston, J. P. Ramseyer, E. Meyer, C. Andreoli, J. Brugger, P. Vettiger, M. Despont, T. Mezzacasa, L. Scandella, H. J. Güntherodt, Ch. Gerber, and J. K. Gimzewski. A chemical sensor based on a micromechanical cantilever array for the identification of gases and vapors. *Applied Physics A (Materials Science Processing)*, 66(1-2):61–64, 1998.

[17] D. Lange, A. Koll, O. Brand, and H. Baltes. Cmos chemical microsensors based on resonant cantilever beams. *Proceedings of the SPIE - The International Society for Optical Engineering*, 3328:233–43, 1998.

[18] C. Hagleitner, A. Hierlemann, D. Lange, A. Kummer, N. Kerness, O. Brand, and H. Baltes. Smart single-chip gas sensor microsystem. *Nature*, 414(6861):293–296, November 2001.

[19] David R. Baselt, Gil U. Lee, Karolyn M. Hansen, Linda A. Chrisey, and Richard J. Colton. A high-sensitivity micromachined biosensor. *Proceedings of the IEEE*, 85(4):672–79, 1997.

[20] Matthew D. Antonik, Neill P. D'Costa, and Jan H. Hoh. Biosensor based on micromechanical interrogation of living cells. *IEEE Engineering in Medicine and Biology*, 16(2):66–72, 1997.

[21] J. Fritz, M. K. Baller, H. P. Lang, H. Rothuizen, P. Vettiger, E. Meyer, H.-J. Günterodt, Ch. Gerber, and J. K. Gimzewski. Translating biomolecular recognition into nanomechanics. *Science*, 288(5464):316–18, April 2000.

[22] Karolyn M. Hansen, Hai-Feng Ji, Guanghua Wu, Ram Datar, Richard Cote, Arunava Majumdar, and Thomas Thundat. Cantilever-Based Optical Deflection Assay for Discrimination of DNA Single-Nucleotide Mismatches. *Analytical Chemistry*, 73(7):1567–1571, April 2001.

[23] Guanghua Wu, Ram H. Datar, Karolyn M. Hansen, Thomas Thundat, Richard J. Cote, and Arun Majumdar. Bioassay of prostate-specific antigen (PSA) using microcantilevers. *Nature Biotechnology*, 19:856–860, september 2001.

[24] Armelle Michelle Moulin. *Development of Microcantilever based Sensors*. PhD thesis, University of Cambridge, UK, October 1998.

[25] Hans-Jürgen Butt and Roberto Raiteri. *Measurement of the Surface Tension and Surface Stress of Solids*, volume Surface Characterization Methods, chapter 1, pages 1–36. Marcel Dekker Inc, andrew j. milling edition, 1999.

[26] Guanghua Wu, Haifeng Ji, Karolyn Hansen, Thomas Thundat, Ram Datar, Richard J. Cote, Michael F. Hagan, Arup K. Chakraborty, and Arun Majumdar. Origin of nanomechanical cantilever motion generated from biomolecular interactions. *Proceedings of the National Academy of Science*, 98(4):1560–1564, February 2001.

[27] Nickolay V. Lavrik, Christopher A. Tipple, Michael J. Sepaniak, and Panos G. Datskos. Gold nano-structures for transduction of biomolecular interactions into micrometer scale movements. *Biomedical Microdevices*, 3(1):35–44, 2001.

[28] S. J. O'Shea, M.E. Welland, T. A. Bunt, A. R. Ramadan, and T. Rayment. Atomic force microscopy stress sensors for studies in liquids. *Journal of Vacuum Science & Technology B (Microelectronics and Nanometer Structures)*, 14(2):1383–5, 1996.

[29] S. Prescesky, M. Parameswaran, A. Rawicz, R. F. B. Turner, and U. Reichl. Silicon micromachining technology for sub-nanogram discrete mass resonant biosensors. *Canadian Journal of Physics*, 70(10-11):1178–1183, 1992.

[30] Jianming Chen. Sub-nanogram mass sensor for in-liquid measurement. Master's thesis, School of Engineering Science, Simon Fraser University, December 1995.

[31] T. Thundat, D.P. Allison, R.J. Warmack, G.M. Brown, K.B. Jacobson, J.J. Shrick, and T.L. Ferrell. Atomic force microscopy of dna on mica and chemically modified mica. *Scanning Microscopy*, 6(4):911–18, 1992.

[32] B. Ilic, D. Czaplewski, M. Zalalutdinov, H.G. Craighead, P. Neuzil, C. Campagnolo, and C. Batt. Single cell detection with micromechanical oscillators. *Journal of Vacuum Science & Technology B (Microelectronics and Nanometer Structures)*, 19(6):2825–8, 2001.

[33] T. Thundat, P. I. Oden, and R. J. Wamack. Microcantilever sensors. *Microscale Thermophysical Engineering*, 1(3):185–199, July 1997.

[34] G. Meyer and N.M. Amer. Novel optical approach to atomic force microscopy. *Applied Physics Letters*, 53(12):1045–7, 1988.

[35] Jacob Thaysen. *Cantilever for Bio-Cemical Sensing Integrated in a Microliquid Handling System*. PhD thesis, MIC, DTU, Technical University of Denmark, Lyngby, Denmark, September 2001.

[36] Jacob Thaysen, Anja Boisen, Ole Hansen, and Siebe Bouwstra. Atomic force microscopy probe with piezoresistive read-out and highly symmetrical wheatstone bridge arrangement. *Sensors and Actuators A: Physical*, 83:47–53, 2000.

[37] Peter Rasmussen. Design, Fabrication and Characterisation of AFM Probes with Integrated Read-out. Master's thesis, MIC, DTU, Technical University of Denmark, Lyngby, Denmark, January 2001.

[38] J. Brugger, R.A. Buser, and N.F. de Rooij. Micromachined atomic force microprobe with integrated capacitive read-out. *Journal of Micromechanics and Microengineering*, 2(3):218–20, 1992.

[39] S. Akamine, T.R. Albrecht, M.J. Zdeblick, and C.F. Quate. Microfabricated scanning tunneling microscope. *IEEE Electron Device Letters*, 10(11):490–492, 1989.

[40] S. Watanabe and T. Fujii. Micro-fabricated piezoelectric cantilever for atomic force microscopy. *Review of Scientific Instruments*, 67(11):3898–903, 1996.

[41] M. Torotnese, H. Yamamda, R. C. Barret, and C. F. Quate. Atomic force microscopy using a piezoresistive cantilever. *TRANSDUCERS '91. 1991 International Conference on Solid-State Sensors and Actuators, Digest of Technical Papers*, pages 448–451, 1991.

[42] H. P. Lang, M. K. Baller, R. Berger, Ch. Gerber, J. K. Gimzewski, F. M. Battiston, P. Fornaro, J. P. Ramseyer, E. Meyer, and H. J. Güntherodt. An artificial nose based on a micromechanical cantilever array. *Analytica Chimica Acta*, 393(1-3):59–65, 1999.

[43] Ole Hansen and Anja Boisen. Noise in piezoresistive atomic force microscopy. *Nanotechnology*, 10:51–60, 1999.

[44] Rodolphe Marie. DNA hybridisation investigated by microcantilever-based sensor. Master's thesis, MIC, DTU, Technical University of Denmark, Lyngby, Denmark, September 2000.

[45] J. Thaysen, R. Marie, and A. Boisen. Cantilever-based bio-chemical sensor integrated in a microliquid handling system. *Micro Electro Mechanical Systems, 2001. MEMS 2001. The 14th IEEE International Conference on*, pages 401–404, 2001.

[46] Peter A. Rasmussen, Jacob Thaysen, Siebe Bouwstra, and Anja Boisen. Modular design of AFM probe with sputtered silicon tip. *Sensors and Actuators A*, 92:96–101, 2001.

[47] Steen Christian Eriksen. Improvement of the dna-chip's experimental set-up with focus on noise reduction. Technical report, MIC, DTU, Technical University of Denmark, Lyngby, Denmark, September 2001.

[48] R. Berger, Ch. Gerber, J. K. Gimzewski, E. Meyer, and H. J. Güntherodt. Thermal analysis using a micromechanical calorimeter. *Applied Physics Letters*, 69(1):40–42, July 1996.

[49] Allan G. Hansen, Michael W. Mortensen, Jens E. T. Andersen, Jens Ulstrup, Anders Kühle, Jørgen Garnaes, and Anja Boisen. Stress formation during self-assembly of alkanethiols on differently pre-treated gold surfaces. *Probe Microscopy*, 2(2):139–150, 2001.

[50] Anja Boisen, Jacob Thaysen, Henriette Jensenius, and Ole Hansen. Environmental sensors based on micromashined cantilevers with integrated read-out. *Ultramicroscopy*, 82(1-4):11–16, 2000.

[51] Lars Helt Veje. Funktionalisering af cantilevers med antistof. Master's thesis, MIC, DTU, Technical University of Denmark, Lyngby, Denmark, September 2000.

[52] Rodolphe Marie, Henriette Jensenius, Jacob Thaysen, Claus B. Christensen, and Anja Boisen. Adsorption kinetics and mechanical properties of thiol-modified DNA-oligos on gold investigated by microcantilever sensors, 2001.

[53] Henriette Jensenius, Jacob Thaysen, Anette A. Rasmussen, Lars H. Veje, Ole Hansen, and Anja Boisen. A microcantilever-based alcohol vapour sensor — application and response model. *Applied Physics Letters*, 76(18):2615–17, 2000.

[54] H. P. Lang, R. Berger, C. Andreoli, J. Brugger, M. Despont, P. Vettiger, J. P. Ramseyer, E. Meyer, P. Vettiger, Ch. Gerber, and J. K. Gimzewski. Sequential position readout from arrays of micromechanical cantilever sensors. *Applied Physics Letters*, 72(3):383–385, 1998.

[55] M. K. Baller, H. P. Lang, J. Fritz, Ch. Gerber, J. K. Gimzewski, U. Drechsler, H. Rothuizen, M. Despont, P. Vettiger, F. M. Battistion, J. P. Ramseyer, P. Fornaro, E. Meyer, and H.-J. Günterodt. A cantilever array-based artificial nose. *Ultramicroscopy*, 82(1-4):1–9, 2000.

[56] Carl Nordling and Jonny Österman. *Physics Handbook*. Studentlitteratur, Box 141, S-221 00 Lund, Sweden, 4 edition, 1987.

[57] H. P. Lang, M. K. Baller, F. M. Battiston, J. Fritz, R. Berger, J. P. Ramseyer, P. Fornaro, E. Meyer, H. J. Güntherodt, J. Brugger, U. Drechsler, H. Rothuizen, M. Despont, P. Vettiger, Ch. Gerber, and J. K. Gimzewski. The nanomechanical NOSE. *Technical Digest. IEEE International MEMS 99 Conference. Twelfth IEEE International Conference on Micro Electro Mechanical Systems (Cat. No.99CH36291)*, pages 9–13, 1999.

[58] F. M. Battiston, J. P. Ramseyer, H. P. Lang, M. K. Baller, Ch. Gerber, J. K. Gimzewski, E. Meyer, and H. J. Güntherodt. A chemical sensor based on a microfabricated cantilever array with simultaneous resonance-frequency and bending readout. *Sensors and Actuators B (Chemical)*, B77(1-2):122–131, 2001.

[59] Irving Lngmuir. Evaporation of small spheres. *Physical Review*, 12(5):368–370, 1918.

[60] R.K. Traeger. Hermeticity of polymeric lid sealants. *26th Electronics Components Conference, IEEE, San Fransisco, California*, pages 361–367, 1976.

[61] Louise Nygaard Christensen. Applications of a micromechanical alcohol vapour sensor. Master's thesis, MIC/University of Copenhagen, 2000.

[62] Thomas A. Betts, Christopher A. Tipple, Michael J. Sepaniak, and Panos G. Datskos. Selectivity of chemical sensors based on micro-cantilevers coated with thin polymer films. *Analytica Chimica Acta*, 422(1):89–99, 2000.

[63] B.H. Kim, F.E. Prins, D.P. Kern, S. Raible, and U. Weimar. Multicomponent analysis and prediction with a cantilever array based gas sensor. *Sensors and Actuators B (Chemical)*, B78(1-3):12–18, 2001.

[64] T. L. Porter, M. P. Eastman, D. L. Pace, and M. Bradley. Sensor based on piezoresistive microcantilever technology. *Sensors and Actuators A*, 88:47–51, 2001.

[65] Esben Friis. *Scanning Probe Investigations of Adsorbed Proteins on Metal Surfaces*. PhD thesis, Department of Chemistry, DTU, Technical University of Denmark, Lyngby, Denmark, July 1999.

[66] Michael Riepl, Vladimir M Mirsky, and Otto S Wolfbeis. Electrical control of alkanethiols self-assembly on a gold surface as an approach for preparation of microelectrode arrays. *Mikrochimica Acta*, 131(1-2):29–34, 1999.

[67] H. Sigrist, A. Collioud, J.-F. Clemence, Hui Gao, R. Luginbuhl, M. Sanger, and G. Sundarababu. Surface immobilization of biomolecules by light. *Optical Engineering*, 34(8):2339–48, 1995.

[68] E. Delamarche, G. Sundarababu, H. Biebuyck, B. Michel, Ch. Gerber, H. Sigrist, H. Wolf, H. Ringsdorf, N. Xanthopoulos, and H. J. Mathieu. Immobilization of antibodies on a photoactive self-assembled monolayer on gold. *Langmuir*, 12:1997–2006, 1996.

[69] Irving Lngmuir. The adsorption of gases on plane surfaces of glass, mica and platinum. *Journal of the American Chemical Society*, 40:1361–1403, 1918.

[70] Jacob Israelachvili. *Intermolecular and Surface Forces*. Academic Press, 2 edition, 1992.

[71] Joseph B Schlenoff, Ming Li, and Hiep Ly. Stability and self-exchange in alkanethiol monolayers. *Journal of the American Chemical Society*, 117(50):12528–12536, 1995.

[72] Micheal Wrang Mortensen. Biological sensor surfaces investigated by Atomic Force Microscopy. Master's thesis, MIC, DTU, Technical University of Denmark, Lyngby, Denmark, February 2001.

[73] J. D. Watson and F. Crick. Molecular Structure of Nucleic Acids. *Nature*, 171:738, April 1953.

[74] Gavin MacBeath and Stuart L. Schreiber. Printing proteins as microarrays for high-throughput function determination. *Science*, 289(5485):1760–1763, September 2000.

[75] Ernst-Ludwig Florin, Vincent T. Moy, and Hermann E. Gaub. Adhesion forces between individual ligand-receptor pairs. *Science*, 264:415–417, April 1994.

[76] A Roda, M Guardigli, C Russo, P Pasini, and M Baraldini. Short technical reports - protein microdeposition using a conventional ink-jet printer. *Biotechniques*, 28(3):492–497, 2000.

[77] Wolfgang Knoll, Manfred Zizlsperger, Thorsten Liebermann, Stefan Arnold, Antonella Badia, Martha liley, Darko Piscevic, Franz-Josef Schmidt, and Jürgen Spinke. Streptavidin arrays as supramolecular architectures in surface-plasmon optical sensor formats. *Colloids and Surfaces A (Physicochemical and Engineering Aspects)*, 161:115–37, 2000.

[78] Mengsu Yang, Hellas C. M. Yau, and Hing Leung Chan. Adsorption kinetics and ligand-binding properties of thiol-modified double-stranded dna on a gold surface. *Langmuir*, 14(21):6121–6129, 1998.

[79] R. Berger, E. Delamarche, H.P. Lang, C. Gerber, J.K. Gimzewski, E. Meyer, and H.J. Guentherodt. Surface stress in the self-assembly of alkanethiols on gold probed by a force microscopy technique. *Applied Physics A (Materials Science Processing)*, 66(1-2):S55–9, 1998.

[80] B. Ilic, D. Czaplewski, and H. G. Craighead. Mechanical resonant immunospecific biological detector. *Applied Physics Letters*, 77(3):450–52, 2000.

[81] Vladimir Haldy and Jos Buijs. Protein adsorption on solid surfaces. *Current Opinion in Biotechnology*, 7:72–77, 1996.

[82] A. M. Moulin, S. J. O'Shea, R. A. Badley, P. Doyle, and M. E. Welland. Measuring surface-induced conformational changes in proteins. *Langmuir*, 15:8776–9, 1999.

[83] A. M. Moulin, S. J. O'Shea, and M. E. Welland. Microcantilever-based biosensors. *Ultramicroscopy*, 82:23–31, 2000.

[84] Roberto Raiteri, Gabriele Nelles, Hans-Jürgen Butt, Wolfgang Knoll, and Petr Skládal. Sensing of biological substances based on the bending of microfabricated cantilevers. *Sensors and Actuators B*, 61:213–17, 1999.

[85] Roberto Raiteri, Massimo Grattarola, Hans-Jurgen Butt, and Petr Skládal. Micromechanical cantilever-based biosensors. *Sensors and Actuators B: Chemical*, 79(2-3):115–126, 2001.

[86] Robert Ros, Falk Schwesinger, Dario Anselmetti, Martina Kubon, Rolf Schafer, Andreas Pluckthun, and Louis Tiefenauer. Antigen binding forces of individually addressed single-chain Fv antibody molecules. *Proceedings of the National Academy of Sciences of the USA - Paper Edition*, 95(13):7402–7405, 1998.

[87] Janese C O'Brien, Vivian W Jones, Marc D Porter, Curtis L Mosher, and Eric Henderson. Immunosensing platforms using spontaneously adsorbed antibody fragments on gold. *Analytical Chemistry - Columbus*, 72(4):703–710, 2000.

[88] Stanley Brown. Metal-recognition by repeating polypeptides. *Nature Biotechnology*, 15(3):269–272, 1997.

[89] Robert Ros, Falk Schmesinger, Celestino Padeste, Andreas Pluckthun, Dario Anselmetti, Hans-Joachim Güntherodt, and Louis Tiefenauer. SPM for functional identification of individual biomolecules. *Proceedings of SPIE - The International Society for Optical Engineering*, 3607:84–89, January 1999.

[90] S. Iijima. Helical microtubules of graphitic carbon. *Nature*, 354(6348):56–8, 1991.

[91] Hongjie Dai, Jason H. Hafner, Andrew G. Rinzler, Daniel T. Colbert, and Richard E. Smalley. Nanotubes as nanoprobes in scanning probe microscopy. *Nature*, 384:147–150, November 1996.

[92] J.H. Hafner, C.-L. Cheung, A.T. Woolley, and C.M. Lieber. Structural and functional imaging with carbon nanotube AFM probes. *Progress in Biophysics and Molecular Biology*, 77(1):73–110, 2001.

[93] Carlos Bustamante and David Keller. Scanning Force Microscopy in Biology. *Physics Today*, pages 32–38, December 1995.

[94] A.L. Weisenhorn, M. Egger, F. Ohnesorge, S.A.C. Gould, S.-P. Heyn, H.G. Hansma, R.L. Sinsheimer, H.E. Gaub, and P.K. Hansma. Molecular-resolution images of langmuir-blodgett films and dna by atomic force microscopy. *Langmuir*, 7(1):8–12, 1991.

[95] H.G. Hansma, J. Vesenka, C. Siegerist, G. Kelderman, H. Morrett, R.L. Sinsheimer, V. Elings, C. Bustamante, and P.K. Hansma. Reproducible imaging and dissection of plasmid dna under liquid with the atomic force microscope. *Science*, 256(5060):1180–4, 1992.

[96] M. Radmacher, M. Fritz, H.G. Hansma, and P.K. Hansma. Direct observation of enzyme activity with the atomic force microscope. *Science*, 265(5178):1577–9, 1994.

[97] Franz J. Giessibl. Atomic Resolution of the Silicon $(111) - (7 \times 7)$ Surface by Atomic Force Microscopy. *Science*, 267:68–71, January 1995.

[98] J. P. Cleveland, B. Anczykowski, A. E. Schmidt, and V. B. Elings. Energy dissipation in tapping-mode atomic force microscopy. *Applied Physics Letters*, 72(20):2613–2615, May 1998.

[99] Andreas Engel and Daniel J. Müller. Observing single biomolecules at work with the atomic force microscope. *Nature Structural Biology*, 7(9):715–718, September 2000.

[100] Hajime Takano, Jeremy R. Kenseth, Sze-Shun Wong, Janese C. O'Brien, and Marc D. Porter. Chemical and Biochemical Analysis Using Scanning Force Microscopy. *Chemical Reviews*, 99:2845–2890, 1999.

[101] M. Rief, M. Gautel, F. Oesterhelt, J.M. Fernandez, and H.E. Gaub. Reversible unfolding of individual titin immunoglobulin domains by afm. *Science*, 276(5315):1109–12, 1997.

[102] Vincent T. Moy, Ernst-Ludwig Florin, and Hermann E. Gaub. Intermolecular forces and energies between ligands and receptors. *Science*, 266:257–259, October 1994.

[103] G.U. Lee, D.A. Kidwell, and R.J. Colton. Sensing discrete streptavidin-biotin interactions with atomic force microscopy. *Langmuir*, 10:354–357, 1994.

[104] G.U. Lee, L.A. Chrisey, and R.J. Colton. Direct measurement of the forces between complementary strands of DNA. *Science*, 266(5186):771–3, 1994.

[105] O.H. Willemsen, M.M.E. Snel, A. Cambi, J. Greve, B.G. De Gooth, and C.G. Figdor. Biomolecular interactions measured by atomic force microscopy. *Biophysical Journal*, 79(6):3267–81, 2000.

[106] M. Guthold, R. Superfine, and R.M. Taylor. The rules are changing: force measurements on single molecules and how they relate to bulk reaction kinetics and energies. *Biomedical Microdevices*, 3(1):9–18, 2001.

[107] Peter Hinterdorfer, Werener Baumgartner, Herman J. Gruber, Kurt Schilcher, and Hansgeorg Schindler. Deterction and localization of individual antibody-antigen recognition events by atiomic force microscopy. *Proceedings of the National Academy of Sciences of the USA*, 93:3477–3481, April 1996.

[108] Anneliese Raab, Wenhai Han, Dirk Badt, Sandra J Smith-Gill, Stuart M Lindsay, Hansgeorg Schindler, and Peter Hinterdorfer. Research articles - antibody recognition imaging by force microscopy. *Nature Biotechnology*, 17(9):902–905, 1999.

[109] Philip Ball. Roll up for the revolution. *Nature*, 414:142–144, November 2001.

[110] A. Krishnan, E. Dujardin, T.W. Ebbesen, P.N. Yianilos, and M.M.J. Treacy. Young's modulus of single-walled nanotubes. *Physical Review B (Condensed Matter)*, 58(20):14013–19, 1998.

[111] C. Dekker. Carbon nanotubes as molecular quantum wires. *Physics Today*, 52(5):22–8, 1999.

[112] P.G. Collins and P. Avouris. Nanotubes for electronics. *Scientific American (International Edition)*, 283(6):62–9, 2000.

[113] S.J. Tans, R.M. Verschueren, and C. Dekker. Room temperature transistor based on a single carbon nanotube. *Nature*, 393(6680):49–52, 1998.

[114] W.B. Choi, D.S. Chung, J.H. Kang, H.Y. Kim, Y.W. Jin, I.T. Han, Y.H. Lee, J.E. Jung, N.S. Lee, G.S. Park, and J.M. Kim. Fully sealed, high-brightness carbon-nanotube field-emission display. *Applied Physics Letters*, 75(20):3129–31, 1999.

[115] S. Iijima and T. Ichihashi. Single-shell carbon nanotubes of 1-nm diameter. *Nature*, 363(6430):603–15, 1993.

[116] D.S. Bethune, C.H. Kiang, M.S. deVries, G. Gorman, R. Savoy, J. Vazquez, and R. Beyers. Cobalt-catalysed growth of carbon nanotubes with single-atomic-layer walls. *Nature*, 363(6430):605–7, 1993.

[117] T. W. Ebbesen and P. M. Ajayan. Large-scale synthesis of carbon nanotubes. *Nature*, 358:220–222, July 1992.

[118] Jason H. Hafner, Bobak R. Azamian, Andrew G. Rinzler, and Ken A. Smith. Catalytic growth of single-wall carbon nanotubes from metal particles. *Chemical Physics Letters*, 296(1-2):195–202, 1998.

[119] Jason H. Hafner, Chin Li Cheung, and Charles M. Lieber. Growth of nanotubes for probe microscopy tips. *Nature*, 398:761–762, April 1999.

[120] Jason H Hafner, Chin Li Cheung, and Charles M Lieber. Communications to the editor - direct growth of single-walled carbon nanotube scanning probe microscopy tips. *Journal of the American Chemical Society*, 121(41):9750–9751, 1999.

[121] Chin Li Cheung, Jason H. Hafner, and Charles M. Lieber. Carbon nanotube atomic force microscopy tips: Direct growth by chemical vapor deposition and application to high-resolution imaging. *Proceedings of the National Academy of Science*, 97(8):3809–3813, April 2000.

[122] M. Ishigami, John Cumings, A. Zettl, and S. Chen. A simple method for the continuous production of carbon nanotubes. *Chemical Physics Letters*, 319(5-6):457–459, 2000.

[123] K. Moloni, A. Lal, and M.G. Lagally. Sharpened carbon nanotube probes. *Proceedings of the SPIE - The International Society for Optical Engineering*, 4098:76–83, 2000.

[124] J.H. Hafner, Chin-Li Cheung, T.H. Oosterkamp, and C.M. Lieber. High-yield assembly of individual single-walled carbon nanotube tips for scanning probe microscopies. *Journal of Physical Chemistry B*, 105(4):743–6, 2001.

[125] S. Akita, H. Nishijima, and Y. Nakayama. Influence of stiffness of carbon-nanotube probes in atomic force microscopy. *Journal of Physics D (Applied Physics)*, 33(21):2673–7, 2000.

[126] Stanislaus S. Wong, Adam T. Woolley, Ernesto Joselevich, and Charles M. Lieber. Functionalisation of carbon nanotube AFM probes using tip-activated gases. *Chemical Physics Letters*, 306:219–225, June 1999.

[127] S.S. Wong, E. Joselevich, A.T. Woolley, Chin Li Cheung, and C.M. Lieber. Covalently functionalized nanotubes as nanometer-sized probes in chemistry and biology. *Nature*, 394(6688):52–5, 1998.

[128] H. Hiura, T.W. Ebbesen, and K. Tanigaki. Opening and purification of carbon nanotubes in high yields. *Advanced Materials*, 7(3):275–83, 1995.

[129] S. Akita, H. Nishijima, Y. Nakayama, F. Tokumasu, and K. Takeyasu. Carbon nanotube tips for a scanning probe microscope: their fabrication and properties. *Journal of Physics D (Applied Physics)*, 32(9):1044–8, 1999.

[130] N. Choi, T. Uchihashi, H. Nishijima, T. Ishida, W. Mizutani, S. Akita, Y. Nakayama, M. Ishikawa, and H. Tokumoto. Atomic force microscopy of single-walled carbon nanotubes using carbon nanotube tip. *Japanese Journal of Applied Physics, Part 1*, 39(6B):3707–10, 2000.

[131] H. Nishijima, S. Kamo, S. Akita, Y. Nakayamaa, K.I. Hohmura, S.H. Yoshimura, and K. Takeyasu. Carbon-nanotube tips for scanning probe microscopy: Preparation by a controlled process and observation of deoxyribonucleic acid. *Applied Physics Letters*, 74(26):4061–3, 1999.

[132] Chin Li Cheung, J.H. Hafner, T.W. Odom, K. Kim, and C.M. Lieber. Growth and fabrication with single-walled carbon nanotube probe microscopy tips. *Applied Physics Letters*, 76(21):3136–8, 2000.

[133] K. Yamamoto, S. Akita, and Y. Nakayama. Orientation and purification of carbon nanotubes using ac electrophoresis. *Journal of Physics D (Applied Physics)*, 31(8):L34–6, 1998.

[134] Daniel M. Czajkowsky and Zhifeng Shao. Submolecular resolution of single macromolecules with atomic force microscopy. *FEBS Letters*, 430(1-2):51–54, 1998.

[135] Werner Kuhlbrandt and Karen A Williams. Analysis of macromolecular structure and dynamics by electron cryo-microscopy. *Current Opinion in Chemical Biology*, 3(5):537–543, 1999.

[136] D.J. Müller, F.A. Schabert, G. Buldt, and A. Engel. Imaging purple membranes in aqueous solutions at sub-nanometer resolution by atomic force microscopy. *Biophysical Journal*, 68(5):1681–6, 1995.

[137] Daniel J. Müller, J. Bernard Heymann, Filipp Oesterhelt, Clemens Moller, Hermann Gaub, Georg Buldt, and Andreas Engel. Atomic force microscopy of native purple membrane. *Biochimica et Biophysica Acta (BBA)/Bioenergetics*, 1460(1):27–38, 2000.

[138] Daniel J. Müller, Dimitios Fotiadis, Simon Scheuring, Shirley A. Müller, and Andreas Engel. Electrostatically Balanced Subnanometer Imaging of Biological Specimens by Atomic Force Microscope. *Biophysical Journal*, 76:1101–1111, February 1999.

[139] M. Stark, C. Moller, D.J. Müller, and R. Guckenberger. From images to interactions: high-resolution phase imaging in tapping-mode atomic force microscopy. *Biophysical Journal*, 80(6):3009–18, 2001.

[140] D.M. Czajkowsky, H. Iwamoto, and Zhifeng Shao. Atomic force microscopy in structural biology: from the subcellular to the submolecular. *Journal of Electron Microscopy*, 49(3):395–406, 2000.

[141] Stanislaus S Wong, James D Harper, Peter T Lansbury Jr, and Charles M Lieber. Carbon nanotube tips: High-resolution probes for imaging biological systems. *Journal of the American Chemical Society*, 120(3):603–604, 1998.

[142] S.S. Wong, A.T. Woolley, T. Wang Odom, Jin-Lin Huang, P. Kim, D.V. Vezenov, and C.M. Lieber. Single-walled carbon nanotube probes for high-resolution nanostructure imaging. *Applied Physics Letters*, 73(23):3465–7, 1998.

[143] J Li, A M Cassell, and H Dai. Biomaterials and composite materials - carbon nanotubes as afm tips: Measuring dna molecules at the liquid/solid interface. *Surface and Interface Analysis*, 28(1):8–11, 1999.

[144] Dieter Oesterhelt and walther Stoeckenius. *Isolation of the Cell membrane of Halobacterium halobium and Its Fractionation into Red and Purple Membrane*, volume 31, A of *Methods in Enzymology*, chapter 5, pages 667–678. Academic Press, 1974.

[145] Bruce Alberts, Dennis Bray, Julian Lewis, Martin Raff, Keith Roberts, and James D. Watson. *Molecular Biology of The Cell*. Garland Publishing, Inc, 3 edition, 1994.

[146] Lisa J Harris, Steven B Larson, Karl W Hasel, and Alexander McPherson. Refined structure of an intact IgG2a monoclonal antibody. *Biochemistry - Columbus*, 36(7):1581–1597, 1997.

[147] Alfred Nisonoff, John E. Hopper, and Susan B. Spring. *The Antibody Molecule*. Immunology. Academic Press, 111 Fifth Avenune, NY, NY 100003, USA, 1975.

[148] Jürgen Fritz, Dario Anselmetti, Janina Jarchow, and Xavier Fernandez-Busquets. Probing single biomolecules with atomic force microscopy. *Journal of Structural Biology*, 119(2):165–171, 1997.

[149] Magnus Bergkvist, Jan Carlsson, Torbjorn Karlsson, and Sven Oscarsson. TM-AFM Threshold Analysis of Macromolecular Orientation: A Study of the Orientation of IgG and IgE on Mica Surfaces. *Journal of Colloid and Interface Science*, 206(2):475–481, 1998.

[150] Yiyi Zhang, Sitong Sheng, and Zhifeng Shao. Imaging biological structures with the cryo atomic force microscope. *Biophysical Journal*, 71(4):2168–76, 1996.

[151] Roberto Raiteri, Sergio Martinoia, and Massimo Grattarola. ph-dependent charge density at the insulator-electrolyte interface probed by a scanning force microscope. *Biosensors and Bioelectronics*, 11(10):1009–1017, 1996.

[152] Masami Kageshima, Henriette Jensenius, Martin Dienwiebel, Yoshikazu Nakayama, Hiroshi Tokumoto, Suzanne P. Jarvis, and Tjerk H. Oosterkamp. Noncontact Atomic Force Microscopy in Liquid Environment with Quartz Tuning Fork and Carbon Nanotube Probe. *Applied Surface Science*, 2002. in press.

[153] N.A. Burnham, O.P. Behrend, F. Oulevey, G. Gremaudi, P.-J. Gallo, D. Gourdon, E. Dupas, A.J. Kulik, H.M. Pollock, and G.A.D. Briggs. How does a tip tap? *Nanotechnology*, 8(2):67–75, 1997.

[154] S.J. O'Shea, M.E. Welland, and J.B. Pethica. Atomic force microscopy of local compliance at solid-liquid interfaces. *Chemical Physics Letters*, 223(4):336–40, 1994.

[155] J.P. Cleveland, T.E. Schaffer, and P.K. Hansma. Probing oscillatory hydration potentials using thermal-mechanical noise in an atomic-force microscope. *Physical Review B (Condensed Matter)*, 52(12):R8692–5, 1995.

[156] Suzanne P Jarvis, Takayuki Uchihashi, Takao Ishida, Hiroshi Tokumoto, and Yoshikazu Nakayama. Local solvation shell measurement in water using a carbon nanotube probe. *Journal of Physical Chemistry B - Condensed Phase*, 104(26):6091–6094, 2000.

[157] S. P. Jarvis, T. Ishida, T. Uchihashi, Y. Nakayama, and H. Tokumoto. Frequency modulation detection atomic force microscopy in the liquid environment. *Applied Physics A*, 72(Suppl.):S129–S132, 2001.

[158] Kahled Karrai and Robert D. Grober. Piezoelectric tip-sample distance control for near field optical microscopes. *Applied Physics Letters*, 66(14):1842–44, 1995.

[159] H. Edwards, L. Taylor, W. Duncan, and A.J. Melmed. Fast, high-resolution atomic force microscopy using a quartz tuning fork as actuator and sensor. *Journal of Applied Physics*, 82(3):980–4, 1997.

[160] W. H. J. Rensen, N. F. van Hulst, and S. B. Kämmer. Imaging soft samples in liquid with tuning fork based shear force microscopy. *Applied Physics Letters*, 77(10):1557–9, September 2000.

[161] T.R. Albrecht, P. Grutter, D. Horne, and D. Rugar. Frequency modulation detection using high-q cantilevers for enhanced force microscope sensitivity. *Journal of Applied Physics*, 69(2):668–73, 1991.

[162] U. Durig, H.R. Steinauer, and N. Blanc. Dynamic force microscopy by means of the phase-controlled oscillator method. *Journal of Applied Physics*, 82(8):3641–51, 1997.

[163] Steen Vang Petersen, Steffen Thiel, and Jens Christian Jensenius. The mannan-binding lectin pathway of complement activation: biology and disease association. *Molecular Immunology*, 38(2-3):133 – 149, 2001.

List of Figures

Abbreviations

Ab : Antibody. Highly specialised molecules that recognise foreign elements in the body and can trigger an immunereaction.
1Ab/1Ab* : Primary antibody, here antibody against E.coli. The star designates that it has been fluorescent labeled.
2Ab* : Secondary antibody: Fluorescent labeled antibody against 1Ab.
AFM: Atomic force microscope.
Ag : Here, unless otherwise stated, used not in the meaning silver but antigen. The element recognised as foreign by an antibody.
Aqua Regia : A gold etching solution of hydrochloric acid (HCl, 37%) and nitric acid (HNO_3, 69%), 3:1 v/v (dansk: Kongevand).
BBSA: Biotinylated BSA, that is BSA with biotin molecules attached.
BR : Bacteriorhodopsin, the protein pump in the purple membrane of the bacterium Halobacterium Halobium. **BSA** : Bovine serum albumin.
CNT : Carbon nanotube. Carbon macromolecule, with amazing properties, made of one or more sheets of carbon rolled up to form a tube. More sheets wrap around each other to from multiwalled CNTs.
Da; Dalton : Mass unit used in biochemistry, identical to the atomic mass unit ($1.66 \cdot 10^{-24}$ g).
DI : Deionised water MilliQ
DLU : Digital light units; the units of the fluorescence scanner.
DNA : Deoxyribonuclease. The macromolecule encoding the inherited information in all living creatures. The ability to duplicate DNA is a central part of some definitions of life itself.
E. coli : Escherichia coli, O157:H7.
FE-SEM : Field emission scanning electron microscope.
HOPG : Highly Ordered Pyrolytic Graphite.
IgG : Immunoglobulin G or gamma globulin. The most common form of antibody in a secondary immuneresponse. Characteristic Y shape.
MIC : Mikroelektronik Centret, Technical University of Denmark, 2800 Lyngby, Denmark
MWCNT : Multiwalled carbon nanotubes.
OMCTS : Octamethylcyclotetrasiloxane.
PBS : Phosphate buffered saline: 10mM sodium phosphate, 0.9% NaCl, pH 7.4

Piranha : Sulphuric acid (H_2SO_4) and hydrogen peroxide (H_2O_2), 4:1 v/v. The mixing releases quite a lot of heat
PMT : Photo multiplier tube; the detecting unit in the laser scanner instrument.
QCR : Quartz crystal resonator, also called quartz microbalance (QMB). Measures mass changes piezoelectrically by the change in resonance frequency. **QTF** : Quartz tuning fork.
SDS : Sodium dodecyl sulphate.
SEM : Scanning electron microscope
SMP : Skimmed milk powder, an efficient and cheap blocking agent against (other) proteins.
SPM : Scanning probe microscope. A collective term sometimes used for all types of microscopes that use a tiny tip to sense properties at a surface while scanning over it. Includes for example scanning nearfield optical microscopy (SNOM), AFM and STM.
SPR : Surface plasmon resonance.
SSC : Purchased as 20×SSC: a solution of sodium (3M) and sodium citrate (0.3M). Diluted and used in buffer solution in DNA hybridisation experiments.
ss-DNA : Single stranded DNA.
STM : Scanning Tunneling Microscope.
SWCNT: Single walled carbon nanotube.
TEM : Transmission electron microscope
Tween20 : A non-ionic detergent: polyoxyethylene(20) sorbitan monolaurate, Sigma-Aldrich: 9005-64-5; product number 274348

List of Publications

Masami Kageshima, **Henriette Jensenius**, Martin Dienwiebel, Yoshikazu Nakayama, Hiroshi Tokumoto, Suzanne P. Jarvis, Tjerk H. Oosterkamp, "Noncontact Atomic Force Microscopy in Liquid Environment with Quartz Tuning Fork and Carbon Nanotube Probe", *Applied Surface Science*, in press, (2002).

Rodolphe Marie, **Henriette Jensenius**, Jacob Thaysen, Claus B. Christensen and Anja Boisen, "Adsorption kinetics and mechanical properties of thiol-modified DNA-oligos on gold investigated by microcantilever sensors", accepted for publication in Ultramicroscopy, 2002.

H. Jensenius, J. Thaysen, A. A. Rasmussen, L.H. Veje, O. Hansen and A. Boisen, "A microcantilever-based alcohol vapor sensor - Application and response model", *Appl. Phys. Lett.*, **76**, pp. 2615-2617(2000).

A. Boisen, J. Thaysen, **H. Jensenius** and O. Hansen, "Environmental sensors based on micromachined cantilevers with integrated read-out", *Ultramicroscopy*, **82**, pp. 11-16 (2000).

H. Jensenius, J. Thaysen, A.A. Rasmussen, L.H. Veje, O. Hansen and A. Boisen, "Gas sensor based on micromachined cantilevers with integrated read-out", Preliminary proceedings of STM99, pp 586-587, (Seoul 1999).

J.E.T. Andersen, J.D. Zhang, Q. Chi, A.G. Hansen, J.U. Nielsen, E. P. Friis, J. Ulstrup, A. Boisen and **H. Jensenius**, "In situ scanning probe microscopy and new perspectives in analytical chemistry", *Trends in analytical chemistry*, **18(11)**, pp. 665-674 (1999).

Patent: A. Boisen, F. Grey, **H. Jensenius** and J. Thaysen "Transducer for microfluid handling systems" 1: Danish Patent application PA 1999 0060. 2: American Patent application US 60/133,240.